Delft University of Technology

Underwater separation of gravel from sand in hydraulic dredging ships

Author:
G. T. Kayadibi
Student number: 4577957

Supervisor:
Dr. Ir. R.L.J. Helmons

Committee:
Dr. Ir. G.H. Keetels

May 3, 2024

TU Delft Delft University of Technology

Abstract

Gravel is a material with multiple purposes in construction and infrastructure. Its usage ranges from construction of roads, building navigational channels to land reclaimation. Gravel can be obtained through multiple methods, such as dredging with ships. One of such dredging ship is the trailing suction hopper dredger (TSHD).

However, in the seabed the gravel is thoroughly mixed with sand, thus during the collection process the unwanted sand is pumped up with the gravel. It is not uncommon to receive up to 80% sand and only 20% gravel. In order to use the storage of the ship more efficiently, the gravel is separated from the sand through an on board sieve installation. The sand is released back into the water and the gravel is collected in the hopper. This has several disadvantages, such as wasting energy by pumping unwanted sand which is returned back to the seabed. The turbidity in the seabed that occurs by releasing the fine sand which settles slowly to the seabed. And the requirement of a large sieve installation to separate the gravel from the sand, which reduces the already limited space of a ship. In order to limit the mentioned disadvantages, it would be favourable to bring the separation process at or near the seafloor. Through a literature study the best underwater separator has been selected. From this it is concluded that the usage of a jet that pushes fine sediment out is the best for underwater separation. The fine sediment is pushed to the upper part of the pipe, whilst the coarse particles resist the jet and remain at the lower part of the pipe. The fine particles at the top are sucked in by a retour pipe, which guides them down to the seabed where it is released with a lowered environmental impact.

Further research on this concept is done through the use of computer simulations which models the conditions using a drift-flux solver. The concept has been tested with different configurations to determine the influence of several input variables. The chosen variables are the inlet velocity, jet velocity, sediment size and sediment concentration. For these configurations the separation efficiency of the system is determined by analysing the retained gravel and the filtered sand. The containment of gravel is generally over 90% and highly satisfactory. The maximum separation of sand is 50%. These results indicate the viability of the system and thus research on improvements are recommended to further increase the systems effectiveness and efficiency.

Contents

List of Figures

List of Tables

Nomenclature

Physics Constants		**Unit**
ρ_f	Density of fluid	$1025\,\mathrm{kg\,m^{-3}}$
ρ_s	Density of solids	$2650\,\mathrm{kg\,m^{-3}}$
g	Gravitational acceleration	$9.81\,\mathrm{m\,s^{-1}}$
Symbols		
α	Volumetric concentration	%
δ_{ij}	Kronecker delta	–
ϵ	Error	–
ϵ	Turbulent energy dissipation	$\mathrm{m^2\,s^{-1}}$
μ	Dynamic viscosity	$\mathrm{Pa\,s}$
ν	Kinematic viscosity	$\mathrm{m^2\,s^{-1}}$
ν_k	Kolmogorov vortex length	m
ν_t	Eddy viscosity	$\mathrm{m^2\,s^{-1}}$
ϕ	Conserved quantity	–
$_k$	Kolmogorov vortex time scale	s
k	Turbulent energy	$\mathrm{m^2\,s^{-2}}$
w_0	Particle settling velocity	$\mathrm{m\,s^{-1}}$
w_s	Particle hindered settling velocity	$\mathrm{m\,s^{-1}}$
$\dot{M}$	Massflow	$\mathrm{kg\,s^{-1}}$
A	Area	$\mathrm{m^2}$
a	Acceleration	$\mathrm{m\,s^{-2}}$
c	Volumetric concentration	%
C_D	Drag coefficient	–
Co	Courant number	–
D	Pipe diameter	m
d_p	Particle diameter	m
F	Force	N
h	Height	m
I	Initial turbulence intensity	%
L	Pipe length	m
n	Richardson Zaki constant	–
P	Pitch	m
p	Pressure	Pa
Q	Volume flow	$\mathrm{m^3\,s^{-1}}$
R	Pipe radius	m

Re	Reynolds number	–
S_{ij}	Strain rate	s^{-1}
t	Time	s
u	Flow velocity	$m\,s^{-1}$
V	Volume	m^3
v	Flow velocity	$m\,s^{-1}$

1 Introduction

1.1 Background

Gravel is material with multiple purposes in construction and infrastructure. Its usage ranges from construction of roads, navigational channels to land reclaimation. Gravel can be obtained through multiple methods, such as dredging with ships. One of such dredging ship is the trailing suction hopper dredger (TSHD). The TSHD operates both mechanically and hydraulically and is self propelling (figure 1a). Gravel is obtained from the seabed by lowering a suction pipe. At the end of this pipe there is a draghead which loosens the soil through the use of mechanical teeth and hydraulic jets, which is visualised in figure 1b. The loosened soil is sucked up to the ship where it is stored in the hopper. Abundant water in the system is discharged through the overflow system. TSHDs commonly have a suction pipe with a diameter of 1 meter and a flow velocity of 7 m/s.

Once the storage is full, the stored soil can be released in two ways. It can be released by opening a door placed under the storage, this will drop all the soil under the ship. Or it can be shot to a certain location, this is called rainbowing.

When simply dredging unselectively, this method works fast. When dredging gravel the ship moves to a gravel deposit to gather gravel. However, gravel in these deposits is not easily distinguished as it is mixed with sand which is what these deposits majorly consist of. It not not uncommon that 80% of the extracted soil is too fine to use. Since the soil at the seabed is thoroughly mixed, it is not possible to mostly extract the wanted gravel. Thus the mixed sand and gravel are both transported to the ship. Usable material is separated through the use of a sieve installation on board which leads to the majority of the material returning back overboard, while a smaller portion remains in the hopper. In practise the definition of fine or coarse is determined by the cutoff diameter of 6mm. Anything smaller than this is considered fine, and anything larger than this is considered coarse.

The current method of gravel collection has multiple disadvantages such as energy loss from pumping unwanted sediment, the creation of a fine and slowly settling sediment plume when discharging the sand back into the water, covering the gravel on the seabed with the discharged sand and the requirement of a large sieve installation on board. The sediment plume is discharged overboard, which lands on top of the sea life and reduces their vision. In order to prevent some of the disadvantages mentioned above, it would be favourable to separate the gravel from the sand part at or near the seafloor. In this way the energy demand for the vertical transport, the turbidity effect, and the required dimensions of the sieve installations would reduce. (W.Vlasbom 2007) [37] (C. van Rhee 2016) [32].

(a) A Trailing suction hopper dredge (Qincy, 2022)[30]

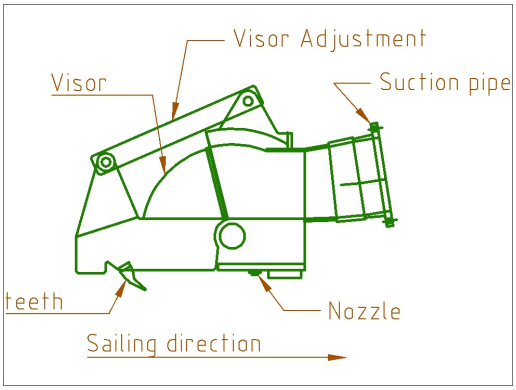

(b) A schematic view of a draghead (Dredge drag head, 2022)[36]

Figure 1: Trailing suction hopper dredge

1.2 Research objective

The following objective and questions are defined in this research:

Research objective:

- Develop a method for TSHD ships that can separate fine sediment from coarse sediment underwater

Sub questions:

- What methods for separating fine and coarse sediment exist
- Which separation method seems most adaptable for underwater application
- How effective is the separation method

1.3 Method of research

The method of research majorly consists of desk research additionally dredging companies and researchers were approached for specific questions. Most of the papers were accessed through google scholar and Scopus and information about OpenFOAM was obtained from papers, OpenFOAMs manual pages and the forum in cfd-online. During the simulations the structure in the OpenFOAM tutorials was used as a base for the simulations. Of the simulations the flow fields were visually inspected and the condition at the boundaries were numerically inspected.

2 Separation

There are many ways to separate two or more elements from each other. However, two main methods are commonly used, which is mechanical separation and separation through inertia. Mechanical separation is separating elements by using physical parts, such as a sieve. And separation through inertia is more focused on the forces that occur in a system, such as gravity.

2.1 Mechanical separation

Sieving is a mechanical separation mechanism that makes use of a medium with gaps. This can be achieved by drilling holes into a plate or using the pores inside a cloth for example. When the medium is put inside a flow, the flow will be forced through these openings, this will disturb the flow and cause a pressure drop. Sediment, dust or other forms of particles in the flow will be unable to pass through if they are larger than the holes in the sieve. Over time these particles will accumulate and create a layer of particles called a cake. A cake will increase the effectiveness of separation since the flow will be forced through a "thicker" sieve, but this will also increase the pressure drop and reduce the flow rate through the medium as shown in figure 2. It is important for many sieving processes to deal with the formation of a cake. This can be done by preventing the formation of a cakes, removing the cake or to replace the sieve with a clean one (T.Sparks & G.Chase 2016) [35].

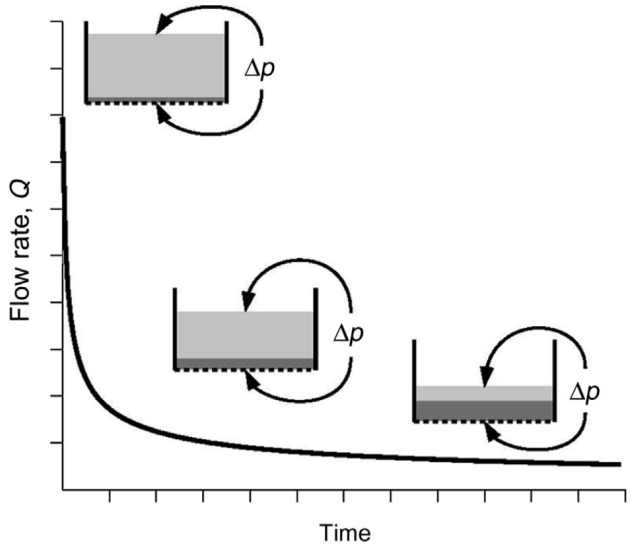

Figure 2: Influence of filter cake size on flow rate, light grey is the fluid, dark grey is the accumulated particles (T.Sparks & G.Chase 2016) [35]

2.1.1 Dead end filtration

One method of sieving is the dead end filtration. A sieve is placed perpendicular to the flow. This is called dead end because the captured particles cannot move further, thus come to a dead end as shown in figure 3. The particles start accumulating and form a filter cake. This form of separation is generally used to gather the particles in a liquid or gas by accumulating them on the sieve and collecting them afterwards. This is a discontinuous process since the system needs to be stopped in order to collect the filter cake (T.Sparks & G.Chase 2016) [35].

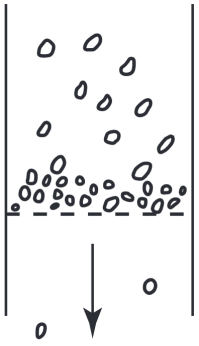

Figure 3: Dead end filtration (T.Sparks & G.Chase 2016)[35]

2.1.2 Cross flow

A cross flow is a sieve that is placed parallel to the flow as shown in figure 4. This does not force the entire flow through the sieve. Since the flow is parallel to the sieve, big particles that cannot pass the sieve will not accumulate on it, but rather wash off by the shear force of the flow. The part of the fluid or gas that passes the sieve is called the permeate and the part that does not pass the sieve is called retentate. Since the flow is not forced through the sieve, it is inefficient at separating, thus it is a common practise to collect the retentate and return it to the cross flow multiple times (T.Sparks & G.Chase 2016) [35].

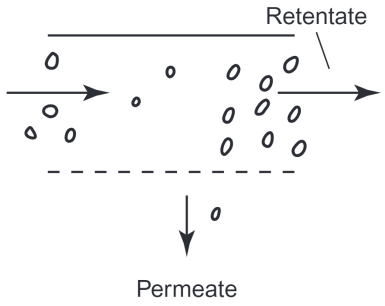

Figure 4: Influence of filter cake size on flow rate (T.Sparks & G.Chase 2016)[35]

2.1.3 Coandă-effect screen

A coandă-effect screen is a curved sieve. The filtration is done by making the slurry flow over the screen (figure 5a). The slurry flows over the sieve, but is also guided into it. The flow is guided into the bars because of multiple mechanics. Firstly, the coandă screen has a curved shape, this creates a centrifugal force that pushes the fluid into the screen. Secondly, the bars of the sieve have an angle ϕ that pushes a part of the flow into the sieve, this is illustrated in figure 5b. Lastly, the holes of the sieve have a convex shape which enhances the flow through the use of the coandă-effect. The coandă-effect occurs when a fluid or gas flows over a curvature. The curvature will pull the flow towards it. This is caused by the pressure differences and the details are explained in (D.Camuffo 2019). [5]
From its working principle it can be concluded that the coandă-effect screen has mechanisms that both pushes the flow through the sieve and over the sieve. This makes a coandă-effect screen effective as it is a sieve with the ability to reduce cake formation whilst operating (L.Tony & P.E.Wahl 2001) [39] (L.Tony & P.E.Wahl 2003) [38].

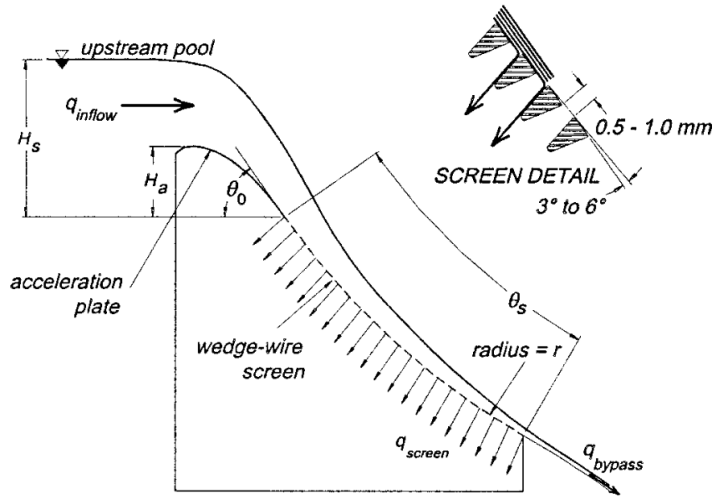

(a) Coandă screen schematic

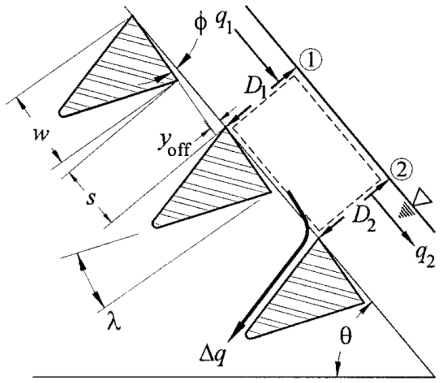

(b) Geometry of the wires in the coandă screen and flow analysis

Figure 5: Coandă Screen (L.Tony & P.E.Wahl 2001)[38]

2.1.4 Screw press

In a screw press the slurry enters a pipe with a rotating screw, which is shown in figure 6. The screw rotates to exert a radial and axial force on the slurry. Fluid and fine particles will go through the sieve while the coarse particles will be pushed forward by the screw. This separation method prevents clogging by mechanically scraping the sediment cake off the sieve with the screw. However, it also requires high forces which accelerates the sanding of the sieve and the screw. Thus these need to be replaced over a set period of time (G.Lyons et al 2021) [23] (B.E.Idrissi et al 2019) [19] .

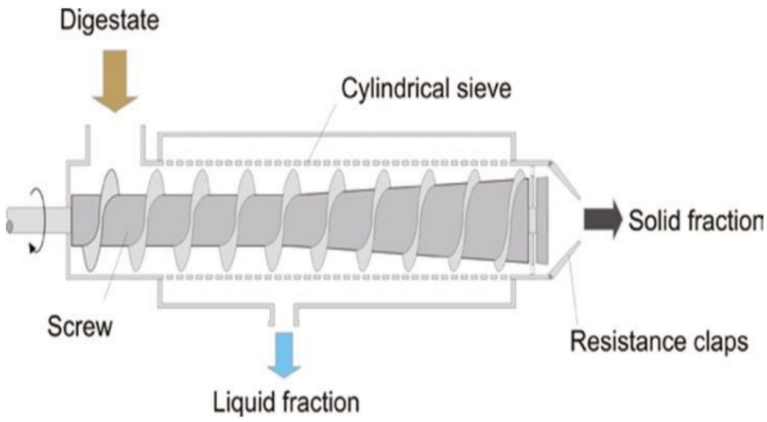

Figure 6: Screw press (G.Lyons et al 2021)[23]

2.1.5 Rotary vacuum drum filter

A rotary vacuum drum filter consists of a rotating drum that is partly submerged into a slurry. The drum is covered with a cloth or a wire mesh that prevent big particles from entering. A pump inside the drum will suck in the slurry and pump it out at another location. Since the drum prevents big particles from entering, they will start to pile up. The piled up particles will form a cake and are scraped off by a knife while the drum rotates (figure 7) (T.Sparks and G.Chase 2016) [35] (T.Burt & C.Fletcher 1999) [4].

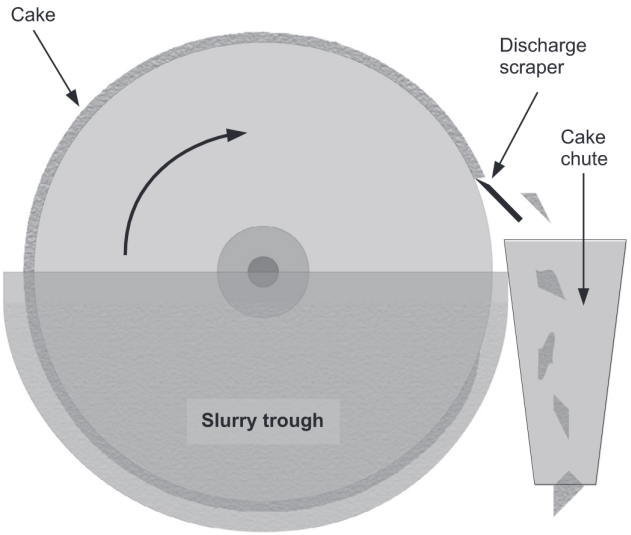

Figure 7: Rotary Vacuum Drum filter (T.Sparks and G.Chase 2016)[35]

2.2 Inertial separation

Inertial separation is a separation technique that utilises inertia. Inertia is the resistance of a body against forces that are applied on it (Inertia, 2022) [20]. An aspect that increases the resistances is its weight, which is directly related to the size of a particle. This way the behaviour of particles are different depending on their sizes, thus some will resist moving a certain direction more than others. This phenomenon can be used to separate elements from each other. The relevant forces will be mentioned and explained for each concept that uses this principle.

2.2.1 Hydrocyclone

Hydrocyclones work with inertial forces generated by the flow. Through the feed the flow enters a cone which makes the flow twist (figure 8a). Particles that are introduced into the system will follow the twisting flow. As these particles move in a circular motion, a centrifugal force will be applied on them. The heavy and coarse particles experience stronger inertial and centrifugal forced and thus are pushed towards the wall. Here they lose their velocity and start to drop down to the underflow. The finer and lighter particles receive a smaller centrifugal force and are dominated by the drag force. Thus they follow the flow and are removed from the system through the overflow. This is illustrated in figure 8b. When extremely big particles are introduced to the system these will completely resist the flow and immediately by pulled down to the underflow through the force of gravity.

Whilst the capital and operation costs are low, this method for separation causes high pressure loss since the flow twists many times and has a lot of friction with the surface (T.Sparks and G.Chase 2016) [35]. The maximum grain size that can enter the hydrocyclone is equal to one fourth of the inlet diameter to prevent damage. A hydrocyclone generally works with very fine particles, which have a diameter between 40 to 400 μm, but it also works for particles of 1000 μm. It is mostly used at capacities below 0.225 m^3/s (T.Burt & C.Fetcher 1999) [4].

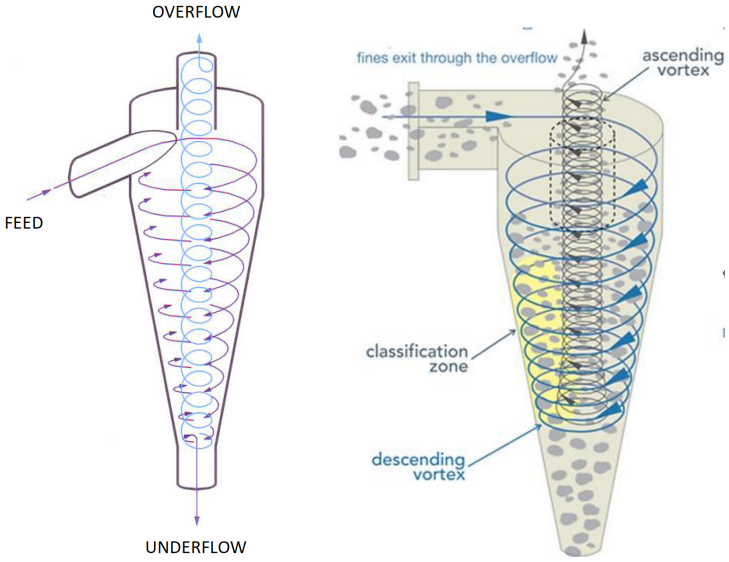

(a) Hydrocyclone flow visualisation (Hydrocyclone, 2022)[18]

(b) Particle route in hydrocyclone (S.Razavi Alavi et al 2018)[31]

Figure 8: Hydrocyclone

2.2.2 Vortex tube

A vortex tube makes use a of static helix which is placed after a pump as shown in figure 9. The helix will swirl the flow which applies a centrifugal force onto the particles. Just like the hydrocyclone, the centrifugal force pushes the particle towards the wall, which is resisted more by the heavier particles. At the end of the pipe there are two tubes, the inner and outer tube. The coarser particles will flow to the outer tube, while the finer sediment will flow into the inner tube. This system is used in helicopters to make the air for the cooling system dust free (A.Filippone 2017) [9] (A.Filippone & N.Bojdo 2010) [10] (N.Bojdo & A.Filippone 2012) [3].

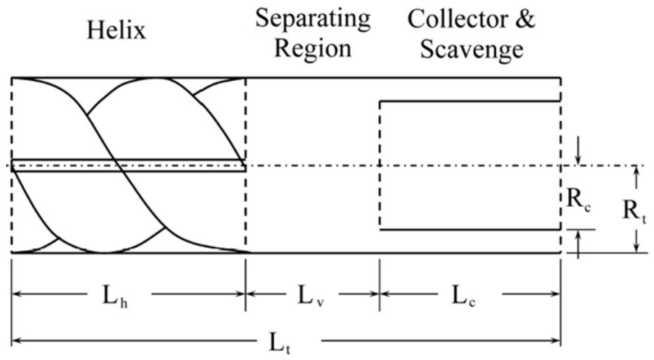

Figure 9: Vortex tube (A.Filippone 2017)[9]

2.2.3 Sedimentation

Separation through sedimentation makes use of the difference in settling velocity of particles. As the size of a particle increases, so does their settling velocity. Whilst it is possible to separate by purely using the natural settling velocity of the particles. It is also possible to introduce an upward flow. This upward flow pushes the sediment up if its velocity is higher than the settling velocity. Through this mechanism it is possible to selectively choose which sediments should float and which are allowed to settle. It should be noted that this process is time consuming as it reduces the speed at which the coarse particles settle.

A method to obtain the separated particles is to use a spiral classifier. This method uses jets that add water to the system and induce an upward flow. As the amount of liquid increases, this will start to fill the area and when the system is full the liquid will be discharged through the overflow. The fine particles will be pushed up and leave the system through the overflow. The coarse particles withstand the upward flow and settle onto the ground where a rotating spiral will push them out of the fluid and discharge them at the underflow (figure 10). (A. Gupta and D.S. Yan 2016) [14] (A.Müller & I.Martins 2022) [25].

The main working area is with solids concentrations below 50% and the particle sizes are generally between 50 to 1500 μm (T.Burt & C.Fletcher 1999) [4].

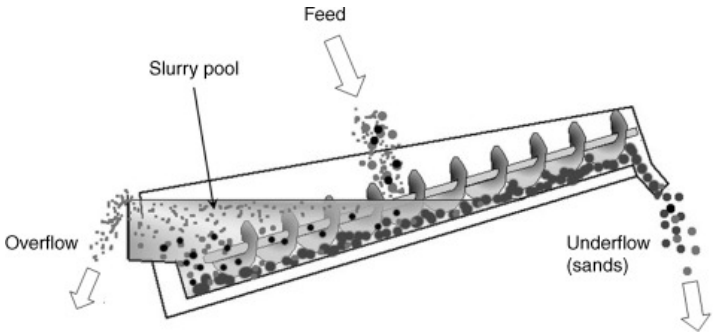

Figure 10: Spiral classifier (A. Gupta and D.S. Yan 2016)[14]

2.2.4 Flow separator

The flow separator functions by using a counter flow which pushes fine sediment up. The counter flow velocity can be adjusted, allowing this system to control the sediment size that will be pushed up. This concept functions like an "inverse" sieve which lets through big particles and pushes away small partices (M.Shapiro & V.Galperin 2005) [34].

A process in dredging that resembles a flow separator is a bubble curtain. The bubble curtain is used to prevent sediment from leaving a region by inducing bubbles which rise up in the fluid and create a flow. This flow will push away fine sediment, but heavier sediment or sealife such as fishes will pass the bubble curtain. With the current technology, it is not realistic to use a bubble curtain to separate fine and coarse sediment since the energy usage of a bubble curtain is extremely high. But if this was not the case, then a bubble curtain could have been considered as a separation method using an "inverse" sieve (Y.Cheng et al 2021) [6].

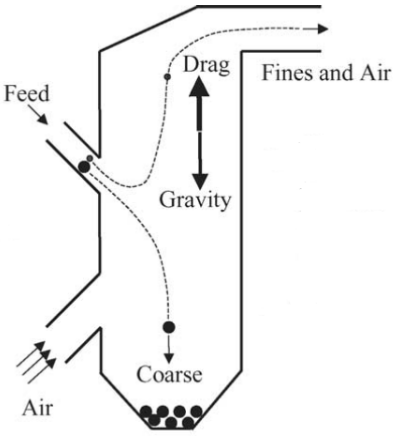

Figure 11: Flow separator (M.Shapiro & V.Galperin 2005)[34]

2.2.5 Bend separator

When a flow bends in a pipe such as figure 12, the pressure differences create a secondary flow in the radial direction which flows towards the inner bend as shown in figure 13. Because of this, three main forces are applied on the slurry. Firstly, the centrifugal force that pushes particles to the outer bend. Secondly the drag force of the secondary flow which pulls particles to the inner bend. And lastly, the pressure gradient which also pulls the particles to the inner bend. Coarse particles have a higher mass, thus their centrifugal force exceeds the drag force and pressure gradient. This causes them to get pushed to the outer bend. Fine particles have a lower mass, thus the drag force and pressure gradient exceeds the centrifugal force, causing them to be pulled to the inner bend (H.Gao et al 2002) [12]. By creating two exits, where one is located at the outer bend and the other at the inner bend, it is possible to separate the coarse and fine particles. Efficiency of this system can be further improved by adding multiple bends, changing the bend radius, adjusting the spiral pitch and by changing the shape of the pipe. It has been shown that a square pipe has stronger secondary flows than a round pipe and that it is directly effected by the Reynolds number because the separation efficiency is reduced when turbulence occurs (H.C.Cuming 1995) [7] (A.K.Pukella et al 2019) [28] (Pukella et al 2019) [29].

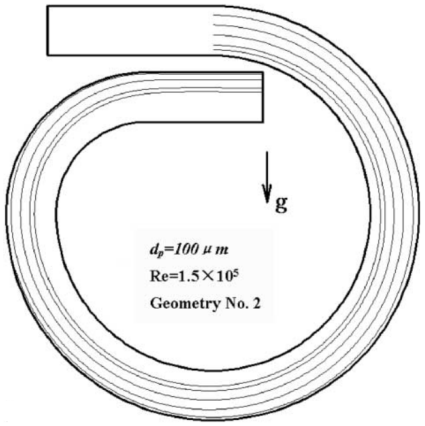

Figure 12: Sediment path in bend pipe (H.Gao et al 2002)[12]

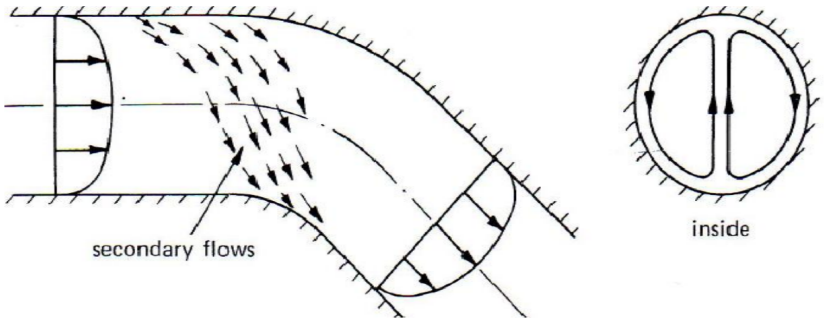

Figure 13: Secondary flow in pipe (M.M. Muhammadua et al 2013) [24]

2.2.6 Inertial separator

An inertial separator makes use of a rapid change in curvature. Whilst the flow will be able to follow the curvature, the particles with a high inertia will not. The coarser a particle is, the higher its inertia. This will make the inflow push the coarse particles into the scavenge flow, while the fine particles follow the core flow. This can be seen in figure 14. However, this system can also operate inversely if the flow velocity is low. This will cause the coarse particles to fall into the core flow and the fine particles will follow the scavenge flow. The efficiency of an inertial separator is defined by two variables. The amount of particles in the system and the flow velocity (D.Barone et al 2015) [1] (D.Barone et al 2017) [2].

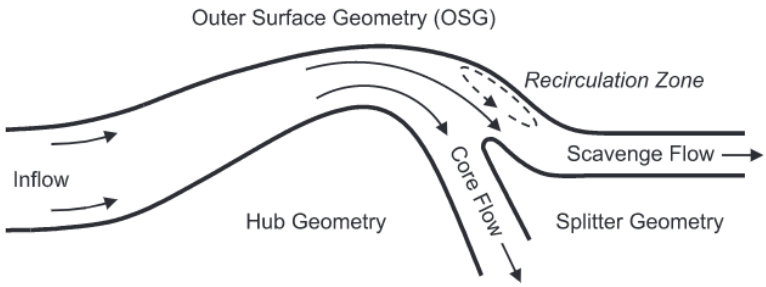

Figure 14: Inertial particle separator (D.Barone et al 2015)[1]

2.3 Summary

All the mentioned separation methods and techniques can be categorised into two main categories, mechanical and inertia separation. The concepts are visually categorised in figure 15.

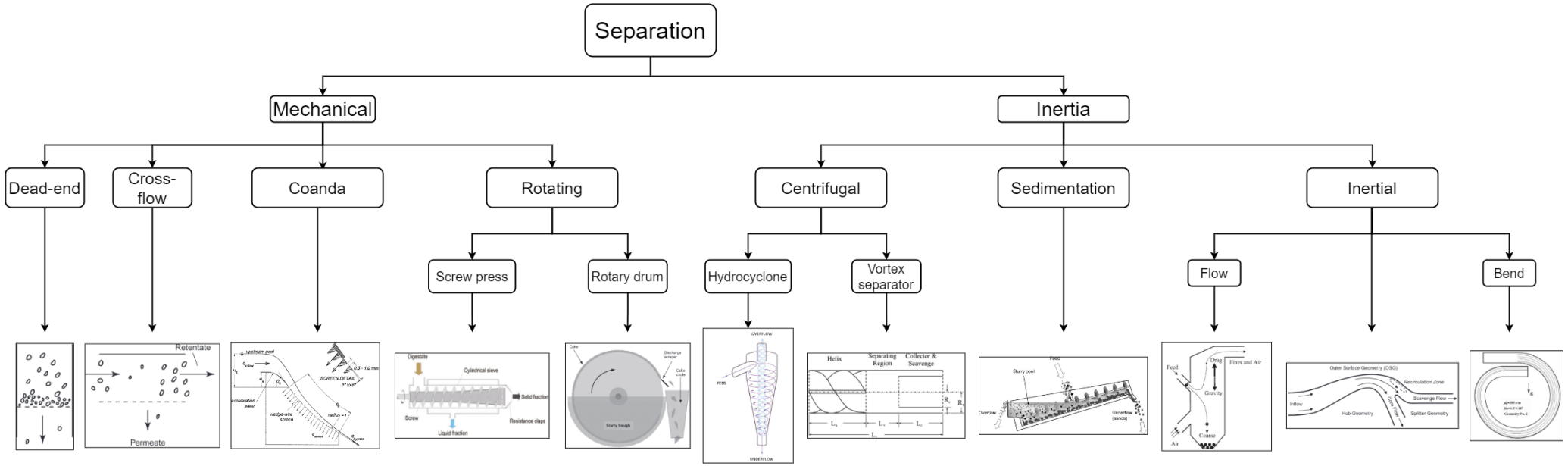

Figure 15: Diagram showing all separation methods

3 Criteria analysis

3.1 Criteria

In the criteria analysis the concepts will be rated on several criteria. However, to reduce the amount of work done the criteria analysis is split into two parts. Firstly, the concepts are checked with the literature and simple calculations whether it would work in dredging. In these calculations the dimensions, flow rate or other relevant parameters are estimated, then these are compared to parameters that occur in dredging to see whether the system could be applied in dredging. From these results the concepts that cannot be applied in dredging will be removed and a smaller group of concepts are left that will be ranked on several parameters. This way all concepts do not need to be ranked but only those that can be applied in dredging. Once the ranking has been done through a multi-criteria analysis the best concept will be clear. Afterwards the concept is further improved to a finalised system.

3.2 First check

As mentioned above, the applicability of the separation methods will be checked through literature or simple calculations. The goal of these calculations is to have an estimation for their size, flow rates, forces or other relevant information that can determine whether it is suited for dredging. All calculations will have the following assumptions:

- All particles in the slurry are considered to be spherical.
- At the sieve, a cake of maximum three times the grain size can grow before the sieve is clogged.
- Particles with a diameter below 6mm are considered fine and it is assumed that all of them will be separated out of the system. Thus calculations are generally done for the cutoff diameter of the particles, which is 6mm.

The variables in table 1 are based on information provided by (C.Pretorius 2012) [27] and the supervisors:

Quantity	Variable	Value and unit
Gravitational acceleration	g	9.81 m/s^2
Diameter pipe	D	1 m
Average flow velocity	v	7 m/s
Volumetric concentration	c	30%
Concentration sand in solids	$c_{sand,s}$	80%
Density gravel	ρ_s	2650 kg/m^3
Density water	ρ_w	1025 kg/m^3

Table 1: Advantages and disadvantages of first set of concepts

With this information the flow rate of the slurry in the pipe can be calculated. This is done by multiplying the average flow rate with the area of the pipe:

$$Q = v * \frac{\pi * D^2}{4} = 5.50 m^3/s$$

3.2.1 Dead end

To test the applicability of dead end filtration, the time it takes for the filter to clog will be calculated. For this calculation it will be assumed that fine particles will flow freely and will not get clogged at the sieve, even when the sediment cake starts to form. In order to calculate how long it takes for the system to clog, the maximum cake volume for particles of 6mm have to be calculated first. The area of the pipe multiplied by the thickness of the maximum cake size will give the volume:

$$V = 3d_{gravel} * \frac{\pi * D^2}{4} = 0.014 m^3$$

Next the flow rate of gravel will be calculated by multiplying the flow rate of the slurry with the concentration of gravel. The concentration of gravel is calculated by multiplying the concentration of solids in the slurry, which is 30%, with the concentration of gravel in the solids of 20%. Combining these gives the following equation:

$$Q_{gravel} = c_{solids} * c_{gravel,s} * Q = 0.33m^3/s$$

The flow rate for gravel will also be used for other separation methods when it is relevant. Finally, the time for the system to clog can be calculated by dividing the volume of the cake with the flow rate of gravel :

$$t = \frac{V}{Q_{gravel}} = 0.04s$$

This means that it takes 0.04 seconds for the system to clog, making it extremely unreliable in dredging application.

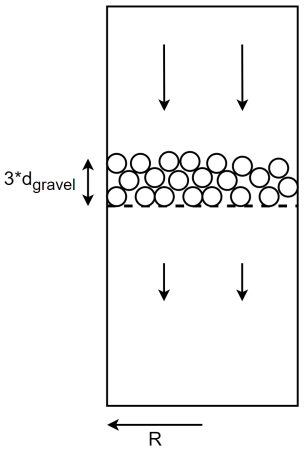

Figure 16: Schematic of a dead end

3.2.2 Cross flow

In a cross flow it will be assumed that the separation is purely done through the settling velocity of the particles. The fine particles are able to pass through the sieve while settling, whereas coarse particles are stopped by the sieve. For the cross flow it is important to calculate how long it would take for a particle at the top to settle onto the sieve, this is also illustrated in figure 17.

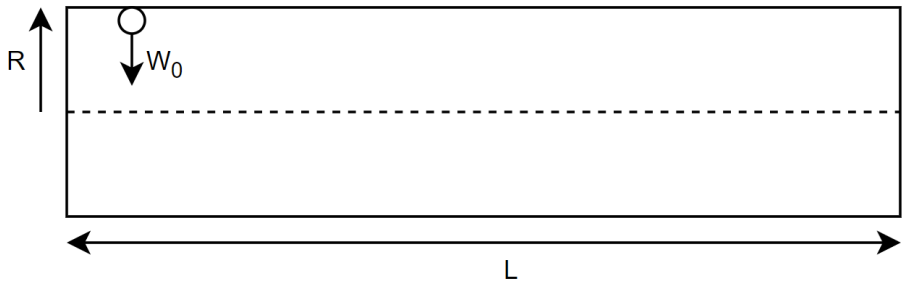

Figure 17: Schematic of a cross flow

To simplify the settling, it is assumed that unhindered settling occurs. For particles with a diameter of 6mm, the formula for unhindered settling velocity is:

$$w_0 = \sqrt{\frac{4 * (\rho_s - \rho_w)gd}{3\rho_w C_D}} = 0.52m/s$$

Since the diameter of the pipe is 1 meter, the radius is 0.5 meter. This is equal to the maximum distance that a particle needs to travel to reach the sieve. By dividing the distance by the settling velocity, the time it takes for a particle to pass the sieve can be calculated:

$$t = \frac{R}{w_0} = 0.95s$$

The required length L of the sieve can be calculated by multiplying the forward velocity of the particles with the time it takes to reach the sieve. Here it is assumed that the particles forward velocity is equal to that of the fluid:

$$L = t * v = 6.67m$$

This is a fairly long horizontal pipe, thus the efficiency of the method is very low. The calculation was done with a particle of 6mm, smaller particles will have a lower settling velocity and thus take even longer to reach the sieve. This means that the calculated length L is has to be even longer. Phenomena that apply in reality, such as hindered settling and turbulence effects are not taken into account. These would reduce the settling velocity even more. Thus this method of separation is not fitting.

3.2.3 Coandă-effect screen

The Coandă-effect screen is assumed to function as follows: at the inflow, there will be a slurry containing sand and gravel. When the slurry reaches the screen, water and sand will pass through it, it is assumed that all the sand in the slurry passes through the screen. Thus there will only be water and gravel in the bypass, this will be the slurry that is pumped up by the dredging ship. At the inflow, which can be seen in figure 18, the total flow rate is 5.50 m^3/s and the flow rate of gravel is 0.33 m^3/s. It is assumed that no gravel passes through the screen, thus the flow rate of gravel is also 0.33 m^3/s at the bypass. Another assumption is that the volumetric concentration of gravel will be 30% at the bypass as this is commonly the concentration of solids in dredging. This means that the total flow rate at the bypass should be 1.1 m^3/s.

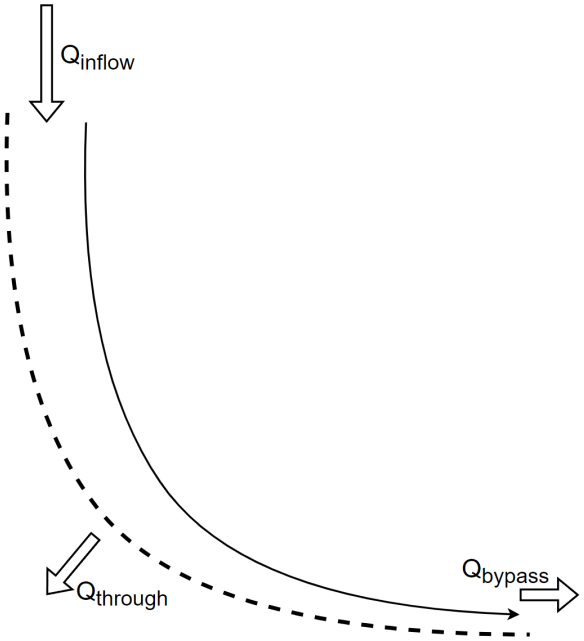

Figure 18: Schematic of a coandă screen

Now that the required bypass flow rate is known, calculations can be done to see whether this is reachable with a coandă-effect screen that has tolerable dimensions. However, it is hard to do calculations with the coandă-effect screen because it makes use of multiple phenomena. Because of this a tool designed by the Bureau of Reclamation of the United States will be used to calculate the flow rate. The tool makes use of a numerical model of the coandă-effect screen which is developed by Wahl (2001)[38]. Wahls model is based off of the energy equation in fluid dynamics. The flow through the sieve depends on the flow pressure and streamline curvature of the sieve which pushes the fluid through the sieve. The only major difference with dredging is that the coandă-effect screen is used in open flows and not inside a pipe.

To calculate the flow rate with the Coandă tool, the dimensions of the coandă-effect screen and the flow conditions are required, the following dimensions are used.
A screen length of 2.75 meters, width of 1 meter and a radius of 3 meters. The screen slot size and wire width is 6mm. The tilt angle of the wires is 5 degrees. And there is an inflow of 5.50 m^3/s.
The width, length and radius of the screen are based on dimensions that could fit in an inflow pipe of a dredging ship. The slot size is based on the particle cut off diameter of 6mm, and the wire width is equal to the slot size for consistency. A wire tilt angle of 5 degrees is chosen since this is often used in coandă-effect screens (Wahl 2001) [38]. Filling this into the tool gives a bypass of 1.06 m^3/s as seen below in figure 19. This is quite close to the required flow rate of 1.1 m^3/s and thus possible to use in dredging applications.

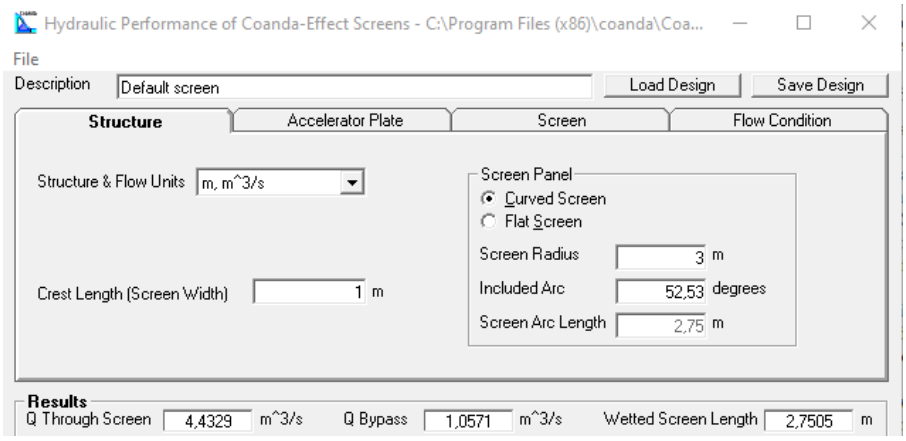

Figure 19: Screenshot of the coandă tool

3.2.4 Screw press

A screw press takes in a slurry which first enters the inner chamber. A screw presses the slurry onto a sieve, which allows the fluid and fine sediment to pass through and enter the outer chamber, this is illustrated in figure 20.

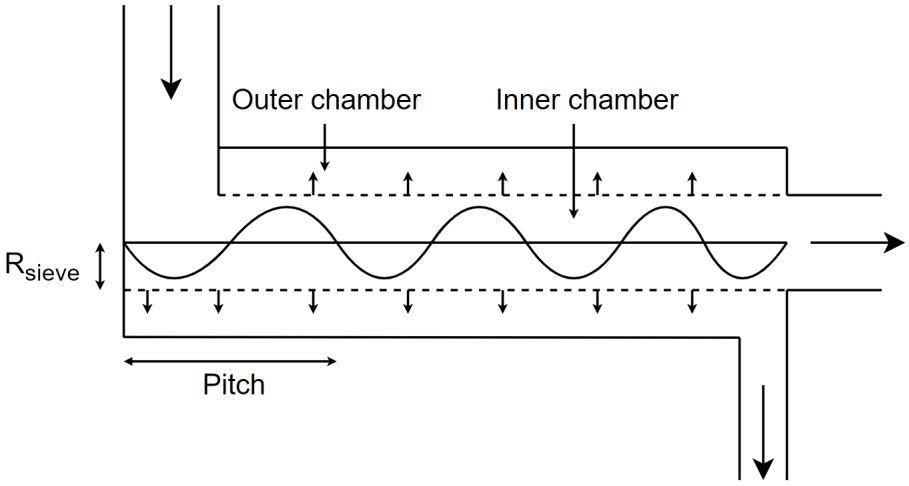

Figure 20: Schematic of a screw press

For the calculations it is assumed that sand with some water passes through the sieve. This causes the slurry in the inner chamber to consist of water and gravel, where 30% of the slurry is gravel. The diameter of the inner chamber is taken equal to the pipe diameter of 1m. It is also assumed that gravel in the system moves along with the screw, thus the forward velocity of a particle will be the pitch times the screws rotational velocity n. The pitch P is assumed to be 1m, which is equal to the diameter of the screw as that is commonly done (K.Mahendra 2018)[21]. In order to calculate the flow rate caused by the rotating screw at the inner chamber, the area, pitch size and rotational velocity are required:

$$Q_{inner} = \pi * R_{sieve}^2 * P * n = \frac{Q_{gravel}}{c_{inner}}$$

Everything except for the rotational velocity is known, thus the equation is rewritten and filled in:

$$n = \frac{Q_{gravel}}{\pi * R_{sieve}^2 * P * c_{inner}} = 1.4rps$$

The calculated rotational velocity is quite high, in K.Mahendra (2018) the screw had a rotational velocity of 0.13 rps and that screw had a diameter almost 10 times smaller than the one used in the calculation. A

low rotational velocity is needed in order to allow fine sediment to pass through the sieve. In order to move a big screw with a high velocity through a slurry an extremely strong engine would be required, which is high impractical. If an engine was able to do this, then the screw would most likely wear down quickly, including the sieve. If the system worked with a screw radius of 1.5m instead, the required rotational velocity would be around 0.13 rps. Whilst this reduces the velocity to a more acceptable degree, it will also increase the required power for the engine exponentially since the radius of the screw is exponentially related to the area that is being pushed. Thus this method is not applicable.

3.2.5 Hydrocyclone

Since a hydrocyclone has a fairly complex process, it is not possible to make a simple calculation. Instead, data will be researched about the feasability of a hydrocyclone. The capacity of a hydrocyclone with an inlet diameter close to that of a hopper dredge is researched. According to Heibel et al (1994) [15], a hydrocyclone with an inlet of 0.914m has a capcity of 0.252 m^3/s. It should be noted that this is a slightly old paper and the performance of a hydrocycle has been improved since then. Thus this will be considered in the result of the calculation. The desired flow rate is around 5.50 m^3/s, dividing the desired flow rate by the flow rate a hydrocyclone gives $5.50/0.252 = 21.8$. This means that the desired flow rate is far too high for a hydrocyclone.

3.2.6 Vortex tube

In T.Dziubak et al (2020) [8] and A.Filippone and N.Bodjo (2012) [3], it shows the required calculations to determine the cut off diameter of the particles. The dimension of the vortex tube can be determined through these equations. It should be noted that vortex tubes are not used for slurry but rather for gasses that contains particles. However, for the calculations it is assumed that the slurry will act like a gas with particles in it. By looking at the result of the calculations, it is possible to see whether the vortex tube is possible in dredging.
In a vortex tube there are three forces applied on the particles, the centrifugal force F_C, aerodynamic force D_P and buoyancy force B. The formula of the three forces are the following:

$$F_C = m_p * \frac{u_s^2}{r} = \frac{1}{6}\pi\rho_p d_p^3 \frac{V_\theta^2}{r}$$

$$D_P = 3\pi d_p \mu U_r$$

$$B = -\frac{1}{6}\pi\rho_g d_p^3 \frac{V_{\theta^2}}{r}$$

Here ρ_p and ρ_g are the particle and gas density respectively, V_θ is the tangential velocity, r is the radius of the static helix, μ is the kinematic viscosity, d_p is the diameter of the particle, which is assumed to be a sphere. And U_r is the radial velocity of the gas. When these three forces cancel each other out the radial velocity can be found:

$$V_{pr} = -U_r = \frac{\rho_p - \rho_g}{18\mu} d_p^2 \frac{V_\theta^2}{r}$$

The cut off diameter can be determined by solving the mass balance of a infinitesimal slice of length dL of a cylinder and then calculating the diameter of a particle that is pushed onto the collector tube. This is done by filling in the radius of the collector R_c for r into the formula:

$$d_{50} = \sqrt{\frac{18ln(2)R_c^2 P^2 \mu}{8\pi\rho_p Q_g L_v}}$$

The following variables are assumed for the calculation, $R_c = 0.25$m, P = 1m, $\mu = 8.9*10^{-4}$ Pa*s, $\rho_p = 2650$ kg/m^3, Q_g= 5.5 m^3/s. Some of these variables are visualised in figure 9 It is known already that particles with a diameter below 6mm are not wanted, thus the equation can be rewritten to solve the required length L_v:

$$L_v = \frac{18ln(2)R_c^2 P^2 \mu}{8\pi\rho_p Q_g d_{50}^2} = 5.26 * 10^{-5} m$$

This is extremely low. When looking in (A.Filippone & N.Bodjo 2010) [10], it is seen that the vortex separator has a diameter of only 18mm. Thus the strange length that has been calculated possibly stems from the fact that it is generally designed to be much smaller than the required dimension at dredging. Furthermore, the shown flow rate in the same paper is 4.4 g/sec, which would be 0.0037 m^3/s. The intended flow rate thus is far less than in dredging. All these significant differences in parameters could be the cause for the strange length and thus making it unlikely that this can be used in dredging. (T.Dzuibak et al 2020) [8] (N.Bodjo & A.Filippone 2012) [3].

3.2.7 Sedimentation

An upward flow is required to prevent sedimentation of fine particles. This way coarse and fine particles can be separated. The required upward flow v_{jet} can be found by calculating the settling velocity of particle with the desired cut off diameter, which is 6 mm. This calculation was done already at the cross flow calculation:

$$v_{jet} = w_0 = \sqrt{\frac{4 * (\rho_s - \rho_w) g d}{3 \rho_w C_D}} = 0.52 m/s$$

It is assumed that the vertical velocity of a particle will be equal to the sum of the settling velocity and the upward flow of 0.52 m/s. The vertical velocity of a particle with a diameter of 10mm will be calculated in order to find out how fast it settles. First the settling velocity is calculated, which is 0.68 m/s. Then by adding the upward flow from the jets the vertical velocity can be calculated:

$$v_{d=10} = w_0 - v_{jet} = 0.68 - 0.52 = 0.16 m/s$$

Whilst the required jet velocity is low and easy to achieve, gravel with a particle of 10mm would settle with a velocity of 0.16m/s, which would be even lower when including particle interaction and hindered settling. Since the particle settles fairly slow, collection of the coarse particles will also be slow. With an expected flow rate of 5.50 m^3/s where the average flow velocity is 7 m/s, this process is simply far too slow to separate particles.

3.2.8 Rotary vacuum drum filter

A rotary drum filter causes a cake formation on the drum by blocking coarse sediment that tries to flow in. It will be assumed that the maximum cake thickness of three times the grain size will be present all over the drum. The production of the system can be determined through the volume of the cake and the rotational velocity of the drum. The volume of the cake will be the width times the area it covers, which is seen in figure 21. Here the coloured circle is the sediment cake which covers the drum.

$$V_{cake} = \pi((R+h)^2 - (R)^2) * W = 0.17 m^3$$

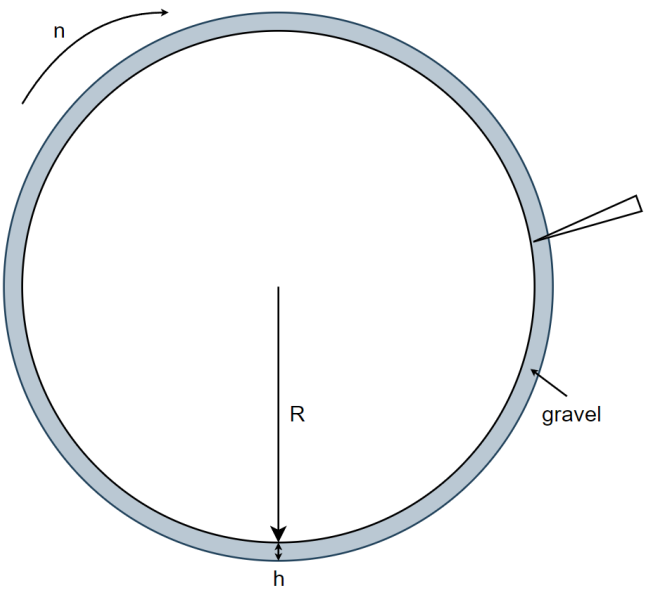

Figure 21: Schematic of rotary drum filter

The expected flow rate of gravel is 0.33 m^3/s. And by dividing the volume by the flow rate, the rotational velocity can be calculated, which is:

$$n = \frac{V_{cake}}{Q_{gravel}} = 1.9 rps$$

This is quite high and has three problems. Firstly, the high rotational velocity will not give particles time to accumulate. Secondly, it is highly likely that the particles get rotated out of the drum by the centrifugal

force. Lastly, the required energy for rotating such a big drum will be high. Thus it can be concluded that this method is too inefficient to be viable for dredging.

3.2.9 Flow separator

A flow separator makes use of inertia and settling velocity to separate particles by introducing a counter flow which affects smaller particles more than bigger particles. An estimate can be made of the required counter flow velocity by using the settling velocity and the flow velocity. Looking at figure 22, the two pipes on the left show the flow velocity v1, which consists of a slurry and the counter flow velocity v2, which is pure water. On the center of the image a particle can be seen that is affected by three forces, these forces are from the flow velocity v1', the counter flow velocity v2' and the gravitational force. The velocities are being called v1' and v2' instead of v1 and v2 because they have been changed as it now is in a pipe with a different diameter. It is assumed that the velocity of the particle is equal to the flow velocity which it is in. The particle velocity in the center of the flow separator can thus be calculated by taking the sum of the flow velocities and the settling velocity:

$$v_{particle} = v_2' * sin(\theta) - v_1' * sin(\theta) - w_0$$

Where the unhindered settling velocity is the following:

$$w_0 = \sqrt{\frac{4 * (\rho_s - \rho_w) g d}{3 \rho_w C_D}} = 0.52 \frac{m}{s}$$

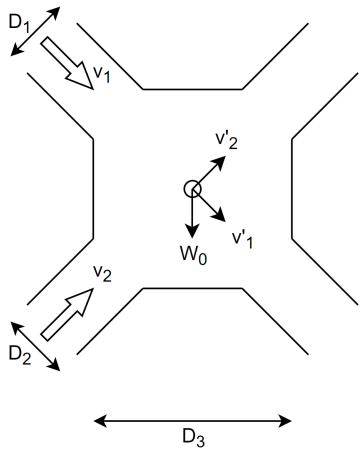

Figure 22: Schematic flow separator

To make the upper formula work another assumption is made, when the flow moves to a pipe with a different area, then the flow velocity will change immediately. But in reality the velocity gradually decreases when the area of the pipe changes. The required counter flow can be determined by calculating it for particle that has a vertical velocity of zero. The pipes in this system have an angle of 45 degrees, and the relation between both v1, v'1 v2 and v'2 can be found through the conservation of mass:

$$v_1 A_1 = v_1' A_3$$

$$v_2 A_2 = v_2' A_3$$

$$A = \pi * \frac{D^2}{4}$$

$$v_1 D_1^2 = v_1' D_3^2$$

$$v_2 D_2^2 = v_2' D_3^2$$

Now by combining, rewriting and filling in the previous two equations the following is gained:

$$v_2 (\frac{D_2}{D_3})^2 * sin(\theta) - v_1 (\frac{D_1}{D_3})^2 * sin(\theta) - w_0 = 0$$

$$v_2 = \frac{v_1(\frac{D_1}{D_3})^2 * sin(\theta) + w_0}{(\frac{D_2}{D_3})^2 * sin(\theta)} = 13.62m/s$$

This counter flow is feasible and thus possible as a method to use for separation.

3.2.10 Bend separator

Calculation of the forces of particles in bends is too difficult. While the centrifugal forces can be calculated easily, the drag force cannot. This is because a pipe with a bend creates a secondary flow, this flow spirals back and forth from the inner bend to the outer bend. Since it is not possible to calculate flow velocity of the secondary flow, experiments and simulations will be investigated in order to check the feasibility in dredging application.

H.Gao et al (2002) [12] show the effects of bends on the particles through an experiment. The experiments were done with a pipe that has a diameter of 41mm, the flow velocity is between 2 and 7m/s, the particles have a diameter between 50 to 400 μm and the volumetric concentration of particles is 0.1%. In figure 23, the effect of radial acceleration is measured for the parameters that were mentioned above and a flow velocity of 3.5 m/s. Here it is seen that the main forces on the particle are the centrifugal force, drag force and the pressure gradient.

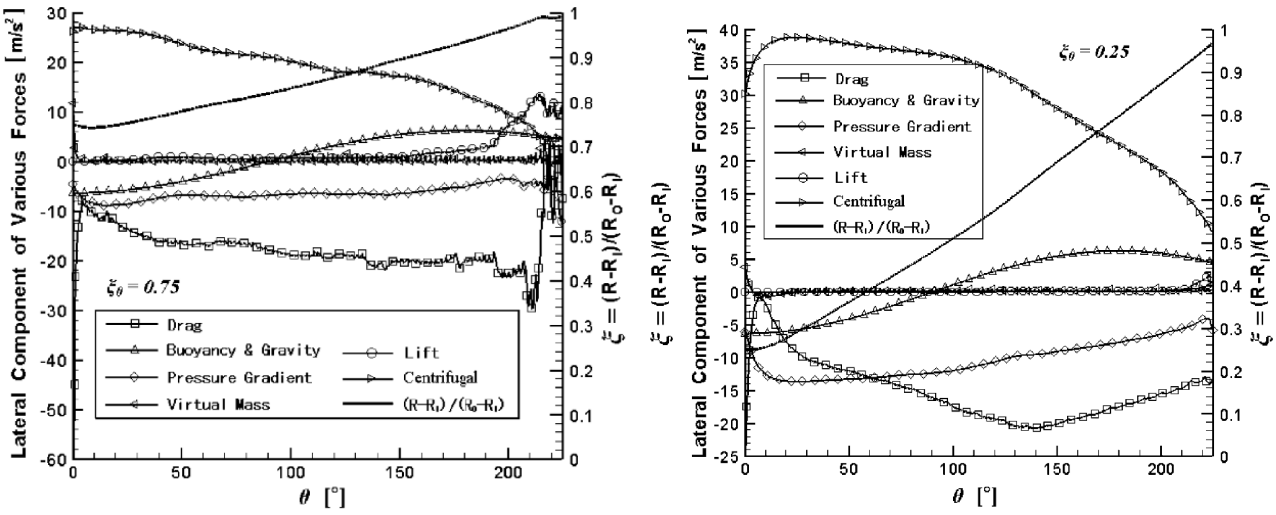

(a) Acceleration of 100μm particle over a bend

(b) Acceleration of 250μm particle over a bend

Figure 23: Particle-subjected forces (H.Gao et al 2002)[12]

Furthermore, Gao documented the effect on the separation of certain parameters. Firstly, the flow rate was increased to see whether this would cause more particles to reach the outer bend, however when the average flow rate was doubled from 3.5 to 7m/s, the amount of particles reaching the outer bend only increased by 7.5% which means that the increase of velocity has a slight effect on the particle trajectory. Turbulence causes the trajectory of the particles to be more irregular, thus has a negative impact on the efficiency. The ratio between the height and width of the pipe plays a role on the intensity of the secondary flow, when this ratio is low, the secondary flow will be weakened. This reduces the drag force on the particles that push it towards the inner bend. Finally the analysis result show that the centrifugal force is the main force that pushes particles to the outer bend, and the main forces that pull particles to the inner bend are the drag force and the pressure gradient (H.Gao et al 2002)[12].

Whilst the results from Gao were valuable, it must be noted that the research was done on a pipe with a volumetric concentration of 0.1%. This is very low compared to dredging application, thus another research was found that tested on higher concentration.

This research is done by A.Pukella et al (2019)[28][29]. The setup has a rectangular cross section of 2cm and 0.5cm, the flow velocity is 5m/s and the volumetric concentration is 5%. These will be the parameters of the setup unless a change is mentioned. One interesting point of this research is the use of a rectangular pipe. According to H.Cuming et al (1955)[7] secondary flow in curved pipes is more intense for rectangular pipes than for circular ones, this is taken into consideration when looking at the test results.

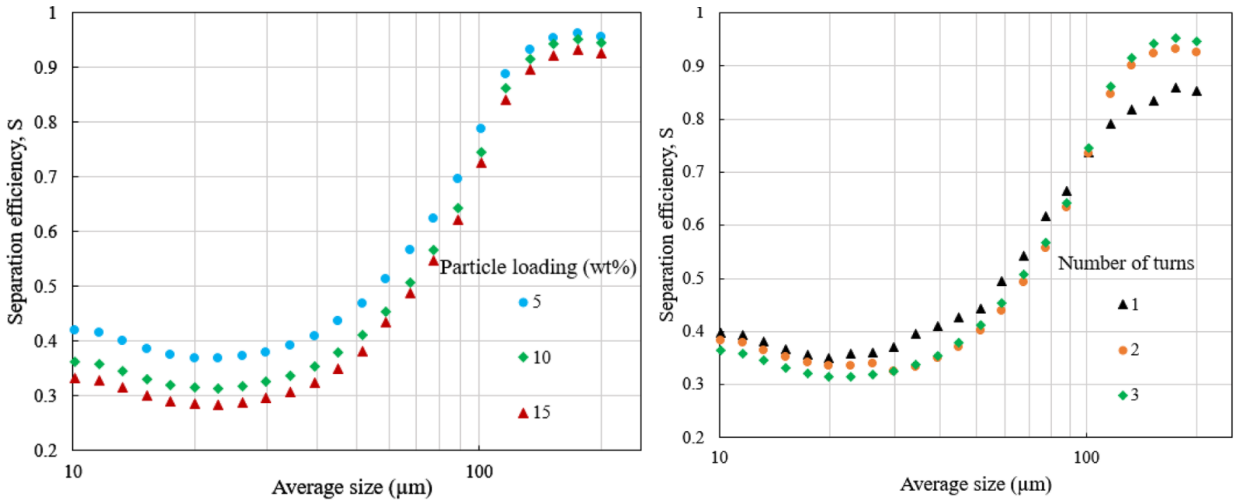

(a) Percentage of particles collected depending on concentration of particles

(b) Percentage of particles collected depending on the amount of bends

Figure 24: Experiments done by A.Pukkella et al (2019)[28]

For the first experiment the change of volumetric concentration is investigated. Here the concentration of the particles in the fluid varies between 5% to 15%. Changing the concentration of particles gives an interesting result. Increasing the concentration reduces the amount of fines that are retained, which is good. But there is also a reduction in coarse particles that are retained. When the concentration increases, the reduction of fines is greater than the reduction of coarse particles. This can be seen in figure 24a.

Another test was done where the amount of bends was tested. When the amount of bends goes from one to two, the separation efficiency increases greatly. Increasing the amount of bends to three has a minor increase on the efficiency, thus it seems that the improvement is limited to three turns. The data can be seen in figure 24. The combination of these papers show that using a bend separation works well, even when the flow velocity and solids concentration is high. Thus it is possible to use bend separation in dredging application.

3.2.11 Inertial separator

The calculation for inertial separator will use three forces, the centrifugal force, drag force and gravitational force. A schematic of the situation is shown in figure 25. The figure shows the inertial separator, the radius R of the bend, the path of the flow and a particle with the three forces applied on it.

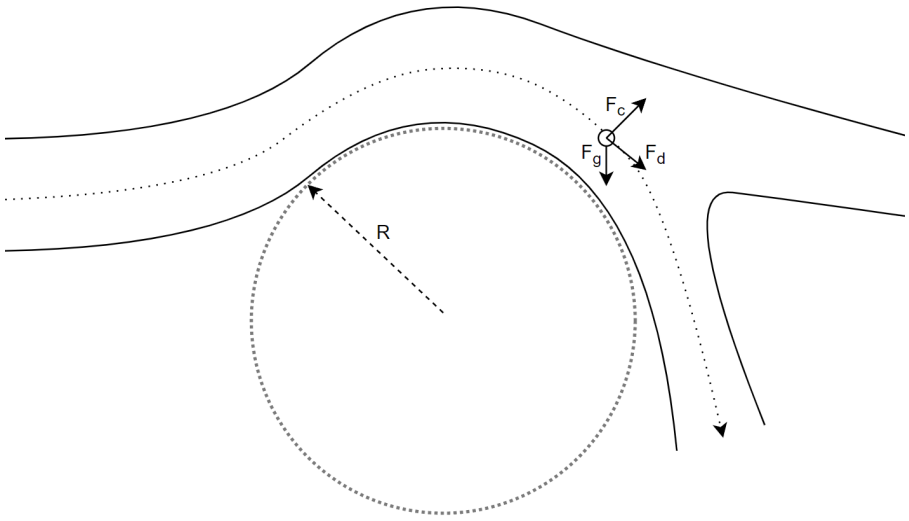

Figure 25: Schematic inertial separator

Calculation will be done at the part where the centrifugal force and drag force have an angle of 45 degrees. To determine how likely it is for a particle to go in the scavenge or core flow, the vertical force applied on the particle will be determined. Calculating the sum of vertical forces gives:

$$\sum F_y = F_{cy} - F_{dy} - F_g$$

Where:

$$F_{cy} = \frac{m * v^2}{R} * sin(45)$$

$$F_{dy} = \frac{\pi}{4} d_{gravel}^2 C_D * 0.5 \rho_w (v * sin(45))^2$$

$$F_g = \frac{\pi}{6} d_{gravel}^3 g(\rho_s - \rho_w)$$

$$m = \frac{4}{3} \pi r_{gravel}^3 * \rho_s$$

In this formula the unknown variables are the drag coefficient C_D and the radius of the bend. Since it is assumed that particles have a spherical shape, the drag coefficient will be 0.47. Furthermore a bend radius of 1m is assumed as this is equal to the pipe radius. Thus by filling this in for a particle of 4 and 8mm the vertical force on the particle is:

$$F_{4mm} = -0.070N$$

$$F_{8mm} = -0.269N$$

The vertical acceleration of the particles can be gained by filling in the formula F=ma:

$$a_{4mm} = -786 m/s^2$$

$$a_{8mm} = -378.8 m/s^2$$

These accelerations are enormous. Looking at the current application for inertial separations, it is seen that it is applied on gas with particles (D.Barone et al 2017) [2]. Thus this calculation will be redone for air with a density of $\rho = 1.185$ kg/m^3, the new accelerations will be:

$$a_{4mm} = -23.9 m/s^2$$

$$a_{8mm} = -3.04 m/s^2$$

These values for acceleration are far more realistic. Thus the application of the inertial separator is not possible for dredging application since the drag force of water is far stronger than that of air, which pulls in too much sediment to the core flow.

3.2.12 Conclusion first criteria

A large amount of information has been processed in order to assess the feasibility of each concept. This has been condensed into table 2 which summarises the advantages and disadvantages of each concept, whilst also showing whether a concept is applicable for dredging application or not.

Concept	Advantage	Disadvantage	Applicable
Dead end	Very simple design, hard cut off	Clogs extremely fast	No
Cross flow	Very simple design, low turbidity effects	Low efficiency	No
Coandă screen	Hard cut off, control dewatering	Complex structure	Yes
Screw separator	Hard cut off, high separation efficiency	High wearability, limited productivity	No
Hydrocyclone	Low capital costs	High pressure loss, inefficiency at high concentration	No
Vortex separator	Low capital costs	High wearability, not applicable with water	No
RVDS	Effective at removal of fines	Low production, gravel will not stick	No
Flow separator	Suspends sediment, adjustable jet velocity	Reduces solids concentration, jet requires energy	Yes
Bend separator	Very simple design	Low efficiency in turbulent systems	Yes
Inertia	Simple design	Designed for gasses, not fluids	No

Table 2: Advantages and disadvantages of first set of concepts

3.3 Multi-criteria analysis

Now that the first part is done, a multi criteria analysis can be made in order to determine the effectiveness of remaining concepts. The goal is to find a concept that is both technically and economically favourable by checking the following criteria.

- Simplicity
- Size
- Adjustability
- Wear resistance
- Separation efficiency
- Selectivity
- Reliability
- Pressure loss

Since no exact data can be found of each concepts performance, a relative comparison is made. When a concept scores a 1 then it performs worse on that criteria than the rest. And if it scores a 5, then it scores better than the other concepts. A 3 means that it not the best nor the worst at that criteria. A 2 or 4 is given when it is slightly worse or better than the other concepts. The following analysis and argumentation is done for each concept in order to determine their rank.

Coandă:

- **Simplicity:** The structure of a coandă screen is fairly complex, the flow rate through the sieve depends on many variables, such as length, width, curvature, wire thickness, wire angle, etc. The wires will have a specific curvature that might not even be constant.
- **Size:** Assuming the parameters used in the calculation, a width of 1 meter and length of less than 3 meter would be sufficient.
- **Adjustability:** For the Coanda screen it is not possible to adjust the selectivity of the system during operations, it would be required to halt the operation and replace the Coanda screen with one that has larger or smaller gaps.
- **Wear resistance:** The geometry of a coandă screen allows water to be guided through the sieve, this also occurs with sediment. This mechanism will make particles collide with the sieve and damage it over time. Since particles have a high velocity, which is around 7m/s, the screen will wear down over time and need to be replaced.
- **Separation efficiency:** The coandă screen separates most fines that pass through it. However, whilst the coandă screen guides most of the flow through the sieve, there is still a certain amount that does not go through the screen. Thus the sediment that does not pass the screen will not be separated. According to the calculation for the coandă screen, around 20% of the flow at the inlet will not pass through the screen and thus roughly 20% of the fines will not be separated when excluding the fact that some particles will hit and bounce off the coandă screen.
- **Selectivity:** Since a coandă screen works like a sieve, only particles below 6mm will leave the system. This hard cut off makes its selectivity highly efficient.
- **Reliability:** Clogging could occur over time since particles collide with a high velocity against the coandă screen, which makes it possible for them to get stuck in it. Furthermore, clogging will also occur when there is insufficient flow to erode the sediment that got stuck on the screen. The second issue can be solved by increasing the power of the pump or by pumping purely water. But that will also increase its complexity.
- **Pressure loss:** The sieve is an obstacle which the flow is forced through, this will have relatively high pressure losses.

Flow separator

- **Simplicity:** Whilst the structure is not mechanically complex, the flow condition and fluid dynamics are. The jet directly affect how much fluid goes to the ship and how much fluid is used to guide fines out of the system. Sensors that measure these flow rates are likely required in order to operate the pumps.
- **Size:** The jet need a certain amount of room in order to work. If the pipe diameter is too small, the jetted water will hit the wall, rebound and push the particles down. However, the standard pipe diameter of 1 meter is likely sufficient.
- **Adjustability:** The flow separator has excellent adjustability. The cutoff diameter is directly related to the jet velocity, the higher this becomes, the higher the cutoff diameter becomes. Thus the cutoff diameter can be adjusted by increasing or reducing the pump power.
- **Wear resistance:** A jet will be placed in such a way that sediment does not collide with it, thus making it impossible for the jet to wear. Furthermore, the interaction between the jet and the sediment will suspend the sediment and prevent beds from locally occurring. Since a moving bed normally occurs when dredging gravel, this means this will get suspended and the wearing at the bottom of the pipe will be reduced.
- **Separation efficiency:** Turbidity and particle interaction will allow a certain amount of fines to pass through. Furthermore, the flow rate of the jet are affected by the flow rate of the main pump. Which is important since the main force that is used to separate is the flow rate of the jet. And inconsistencies during dredging, for example the concentration of solids, will cause an inconsistent flow rate and thus make the force of the jet also inconsistent.

- **Selectivity:** Unlike a sieve, there is no hard cut off diameter with the flow separator. This is because a flow does not have a constant velocity over the area, but it is high in the center, and it is low near the walls of the pipe. Furthermore, inconsistency of the flow rate of the main pump, turbidity effects and particle interactions add another element of irregularity. These effects reduce the selectivity of the flow separator. Thus the lower the diameter of a particle is, the higher the chance of separation. And the higher the diameter is, the lower the chance of separation.
- **Reliability:** The dredging system now also depends on the jet pumps. If these get damaged or break down two major issues happen. If the power of the jet is reduced, then the separation process becomes less efficient. And if the jet pump completely stops working then this will not only halt the separation process, but the main pump will also push the slurry into the jets.
- **Pressure loss:** The jet will disrupt the flow and cause recirculation which acts like an obstacle. This creates a resistance that causes pressure loss.

Bend separator

- **Simplicity:** Very simple, just a curved pipe with two exists.
- **Size:** Assuming realistic values means having a bend with a radius of 2 meters, a pipe diameter of 1 meter and 3 bends of 360 degrees. This means that the dimensions will be around 4x3m, which is considerably big.
- **Adjustability:** The bend separator has a bad adjustability just like the Coanda screen. The process needs to be halted to change the bend with another one that has a smaller or larger bend radius. The bend separator is a larger part than the Coanda screen, thus it is more of a challenge to change this. In H. Gao et al (2002) [12] it was mentioned that increasing the flow velocity only has a slight effect on the separation mechanism.
- **Wear resistance:** The forces push sediment to both the inner and outer bend, local wear will increase at those two locations.
- **Separation efficiency:** In the experiments of Pukella et al (2019) [28] it has been shown that it is not possible to filter out all fines in the system, no matter how much you change and improve the variables or design. In figure 24 the results show that between 20% to 50% of the fines still remain.
- **Selectivity:** In experiments at figure 24 it has already been shown that there will always be some coarse sediment filtered out of the system. An increase of concentration and turbidity will increase this effect even more. In Pukella et al (2019) this was around 5% to 20%.
- **Reliability:** Barely any new parts are added to the dredging system thus the reliability is as high as it was before adding the separator.
- **Pressure loss:** The bends cause an increase in pressure loss. But this is relatively low compared to the other two concepts which add an obstacle.

Based on the analysis, a table with scores for each criteria has been created. Table 3 is taken and each criteria has been coloured depending on how high they scored. The colours are green, orange and red for high, medium and low respectively. This way the strengths and weaknesses are visualised in a clear way.

Concept	Simplicity	Size	Adjustability	Wear resistance	Separation efficiency	Selectivity	Reliability	Pressure loss	sum
Coandă effect screen	3	3	2	1	4	5	3	3	24
Flow separator	3	4	5	5	3	3	4	3	30
Bend separator	5	1	2	3	2	3	5	4	25

Table 3: Multi-criteria analysis coloured

Looking at the multi-criteria analysis, it is seen that the flow separator performs the best in general. However, whilst it has scored the highest out of all concepts, it score is close to the other concepts. Thus further examination will be done.

At the coandă-effect screen it is seen that it has the highest at separation efficiency and selectivity. The flow separator has high scores in general and performs the best for size and wear resistance. Lastly, the bend separator shows to be mostly simple, reliable and has the least pressure loss. Whilst the flow separator is shown to be the best option, the other concepts can be better for certain criteria. If the need arises to improve its performance, the flow separator can be combined with the other concepts. In the case of selectivity, a sieve can be added if a higher selectivity is required.

However, combining the flow separator with the bend separator will not gain its benefits. The bend separators benefits are based on its simplicity, thus combining this with another concept will take away its simplicity.

Currently the flow separator will be implemented into the dredging system. A jet will be placed inside the pipe that push the drag dominated fines upwards, which the coarse sediment will resist. An opening will be placed where the fines are guided to in order to remove them from the system. The general shape of the concept is shown in figure 26. In this figure the jet are visualised as a physical cylinder inside the pipe, however, this is purely done for visual clearance. The jet do not stick into the pipe as shown in the figure but instead are simply holes where water comes from.

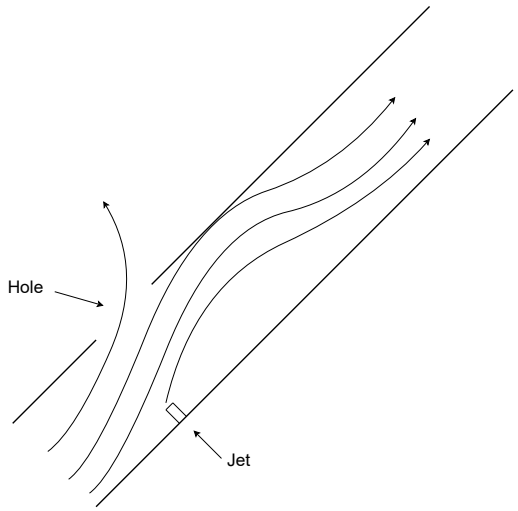

Figure 26: Schematic of gravel dredging with flow lines showing the direction of the flow

The working principle is the following. A slurry is introduced to the system. These particles will travel a certain distance, this will give coarse particles time to settle, whilst the fine particles are still high up in the pipe. Next the slurry will reach the jet and a hole. The jet will push the fine sediment upwards through the hole, whilst the coarse sediment will retain in the system. The goal of the hole is for it to function as an outlet, thus water needs to exit from it. However, the pump in the ship will try to suck in water through the hole. However, the jet is placed below the hole prevent this. These will increase the local pressure which causes the water to flow out from the hole.

3.4 Environmental impact

Unlike coarse particles which immediately start to settle onto the seabed, the fine particles suspends when released and create a plume (N.H. Kim et al 2018)[22]. When a sediment plume is created during the releasing of fines, the sight of nearby sealife is hindered and they are covered with the sand. Thus these sand plumes have a negative environmental impact, which can be reduced through the use of underwater separation. When separating underwater, the fine sediment is released at a lower location. This reduces the time for it to reach the seabed and thus the local sealife will have its vision hindered for a shorter duration. However when looking at the final concept, it can be seen that the fine sediment is pushed upwards when it leaves the system, which is visualised in figure 27a. Giving the fine sediment an upward momentum will increase the time for the sediment cloud to settle. In order to prevent this a pipe will be added at the hole which guides the fines down to the seabed. This will make sure that the fines are always released at the seabed. This has been visualised with figure 27b where the released fluid and fine sand are guided down to the seabed through another pipe.

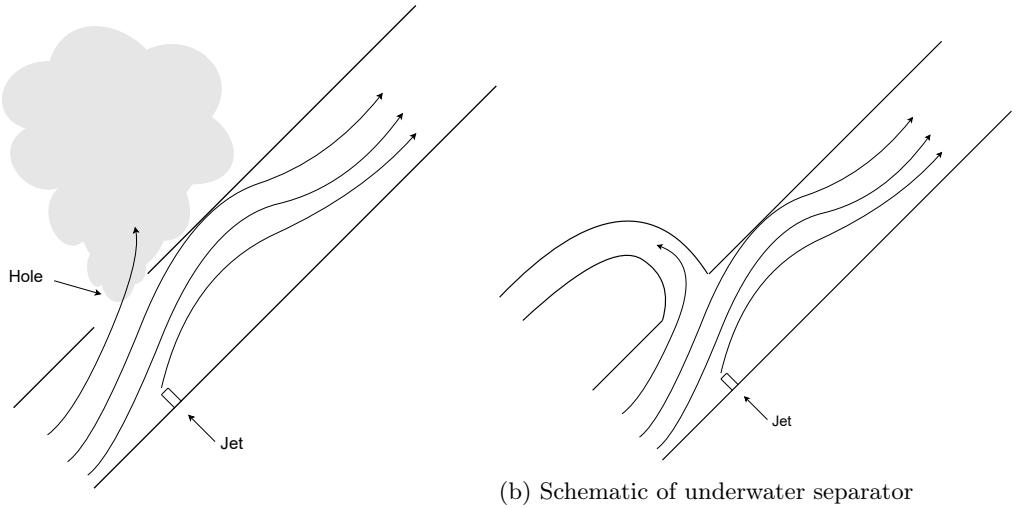

(a) Sediment plume caused by current concept

(b) Schematic of underwater separator with second pipe

Figure 27: Sediment discharge guiding

This pipe, which returns a part of the flow, will be placed over the draghead. This way the fines will be released behind the draghead and thus cannot return into the system. Since the draghead is capable of rotating through its visor, the return pipe should be made flexible or partially flexible so that it can move along. This will make it possible to always release the fines parallel to the seabed so that no seabed erosion can occur.

It should be noted that through this method, a sediment plume will still occur and thus its negative environmental impact is still present. However, since it has been guided down to the seabed, the required time for it to settle onto the seabed is reduced. This will cause the sediment plume to hinder vision for a shorter amount of time.

This part of the research could be expanded further by looking at methods which reduce the size of the sediment plume. However, the goal of the current research is to determine if a method exists that can separate coarse sediment from fines underwater. Reducing the impact from sediment plumes does not help with answering this. For this reason, no further research is done about this topic.

3.5 Schematics of entire system

The general process of the system will be the following:

1. 70% seawater, 24% sand and 6% gravel pass through the draghead
2. The slurry reaches the separation mechanism
3. The jet pushes the fluid and fines towards the return flow
4. The fines are released on the seabed
5. The retained gravel and water continue through the system
6. The gravel and water slurry reaches the hopper and the gravel is stored

A sketch of this process has been made in figure 28. It should be noted that the sizes shown in this sketch are not representative of the reality as it visualises a simplified system.

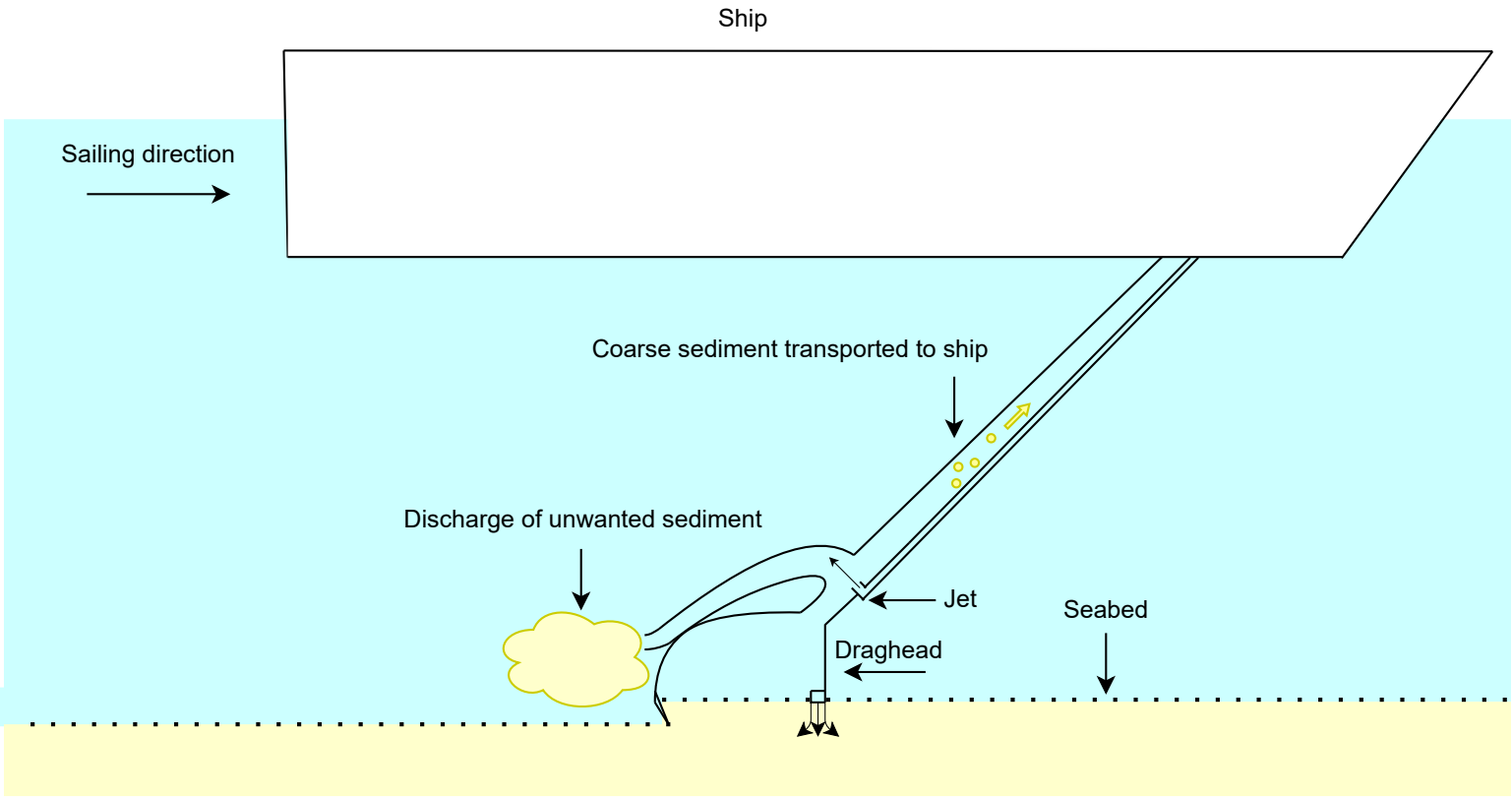

Figure 28: Schematic of gravel dredging with underwater separation

3.6 Conclusion of literature research

Underwater separation methods have been researched for a TSHD in this research. During the research multiple concepts were considered and researched. After consideration only the coandă-effect screen, flow separator and bend separator were found to be applicable in dredging. Through the multi-criteria analysis it was concluded that the flow separator is the most suitable concept. However, it is known that the jet will affect the flow field of the pipe, thus further research will be done on this through computational fluid dynamics (CFD) simulations to better determine the local flow conditions and to further improve the design.

4 Simulation

To further improve the researched separation technique, a CFD simulation will be made. CFD is tool that predicts the movement and interaction of fluids based on the given conditions.

CFD can be done through the use of computer programs, for this research the open source tool OpenFOAM will be used. OpenFOAM is considered to be a reliable and accurate CFD tool and is able to simulate particles through different methods. It makes use of solvers, which is a method to simulate a situation by using certain equations and assumptions. However, the accuracy of the simulation depends on various factors such as the quality of the mesh, the choice of turbulence model, and the appropriateness of the boundary conditions. Thus these parameters will be carefully considered when creating the simulation. This will be further described in the convergence test.

The simulation has the following goals:

- Analyse base design and conduct a sensitivity analysis
- Analysis whether the chosen solution/design principle gives sufficient confidence to develop further

4.1 Approach

In order to ensure that the simulation of the chosen concept is thrustworthy, the setup will be split into multiple steps which increase the complexity. This will be done by making the geometry more complex over time and by adding more complexity to the solver. The solver will first work with purely a fluid. As the simulations run successfully, particles concentration will be increased slowly till it reaches the desired concentration.

As for the geometry, it will go through the following steps:

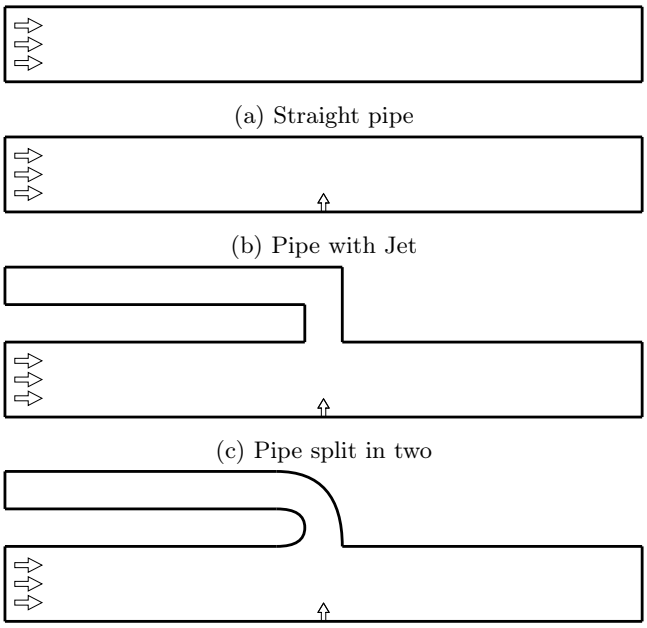

(a) Straight pipe

(b) Pipe with Jet

(c) Pipe split in two

(d) Pipe with a curved split

Figure 29: Pipes geometry for CFD simulation

As seen in figure 29, this research will make use of 2D geometries since these require a far shorter simulation time. The reason why the complexity is increased with little steps is to ensure values remain realistic. As the complexity increases, it is harder to deduct this. Thus at each complexity step the result is compared with the previous step in order to see if the system is comparable. Additional information of this process is found in appendix A.

4.2 Choice of solver

For the solver, it is of importance that it is able to simulate the effect of particles in a slurry. There are two main methods to simulate a slurry: the Euler-Lagrange and Euler-Euler approach.

In the Euler-Lagrange approach the system is considered to have one continuous phase with trackable particles. For each particle the particle interactions are calculated. Through this method it is possible to determine the path each particle takes and how it changes when conditions differ. Furthermore it is plausible to simulate a mixture of particles with different sizes. However, the high volume flow in combination with high particle percentage of 30% makes it far too computationally demanding to use this method.

And in the Euler-Euler approach the system consist of two phases, which are the solid and liquid phase. This method works faster than the Euler-Lagrange since all the particles are considered to be a pseudo-fluid. Based on the chosen pseudo-fluid, the interaction between fluid and solids is determined. However, since this method considers all particles to be one pseudo-fluid, it lacks the capability to accurately calculate the effects of the individual particles (B.Nieuwboer 2022) [26] (J.Goeree 2022) [13].

As the system will have a high concentration, the Euler-Euler approach will be used for its computational efficiency. This will be done by making use of the driftFluxFoam solver in OpenFOAM. This solver simplifies the Euler-Euler approach by combining the fluid and particles into one mixture. This solver fits the requirements the most as it can take the settling velocity of the sediment into consideration, even including the effect of hindered settling (G.Holzinger 2020)[17]. A limitation of this solver is that only one particle size can be simulated at a time. It would be favourable to simulate the real situation where the solids fraction consists of 80% fines and 20% coarse sediment. However, this is not possible with driftFluxFoam and instead the solids fraction will consist of particles with the same diameter.

4.2.1 Governing equations

In driftFluxFoam the system is considered to consist of a mixture with a certain concentration. Thus the solver sums each momentum equation, which creating a single momentum equation. The original continuity equation changes to the following in the two-fluid model (J.Goeree 2018) [13].

$$\frac{\partial \rho}{\partial t} + \nabla(\rho u) = 0$$

$$\frac{\partial \alpha_k \rho_k}{\partial t} + \nabla(\alpha_k \rho_k u_k) = 0$$

With the specified relations.

$$\rho_m = \alpha_1 \rho_1 + \alpha_2 \rho_2$$

$$\rho_m u_m = \alpha_1 \rho_1 u_1 + \alpha_2 \rho_2 u_2$$

The following can be gained.

$$\frac{\partial \rho_m}{\partial t} + \nabla(\rho_m u_m) = 0$$

For the mixture momentum equation the following diffusion stress is used.

$$\tau_{dm} = \rho_m \frac{\alpha_2 \rho_2}{\alpha_1 \rho_1} u_{2m}^2$$

And the relative velocity between the diffusion velocity and the drift velocity (G.Holzinger 2020)[17] is:

$$u_{dm} = \frac{\rho_1}{\rho_m} u_{dj}$$

The unhindered settling velocity of the particles is calculated with the following formula:

$$w_0 = \sqrt{\frac{4 * (\rho_s - \rho_w) g d}{3 \rho_w C_D}}$$

Each particle will have a velocity profile around it. As the concentration increases, it is possible that these profiles overlap each other. Thus at high particle concentrations the unhindered settling velocity is no longer accurate and a correction must be made. The new velocity will be called the hindered settling velocity and it is calculated using the Richardson-Zaki equation, which is formulated below.

$$w_s = w_0 (1 - c)^n$$

$$n = \frac{4.7 + 0.41 Re_p^{0.75}}{1 + 0.175 Re_p^{0.75}}$$

$$Re_p = \frac{w_0 d}{\nu}$$

Here w_s is the hindered settling velocity in m/s, c is the volume concentration of particles, n is the exponent which is a function of the particles Reynolds number and Re_p is the particles Reynolds number (C. van Rhee 2018) [33].

Figure 30 shows the effect of concentration and particle size on the ratio between hindered and unhindered settling $\frac{w_s}{w_0}$. This shows that the hindered settling can be as low as 10% of the unhindered settling and thus its effect is significant and needs to be included.

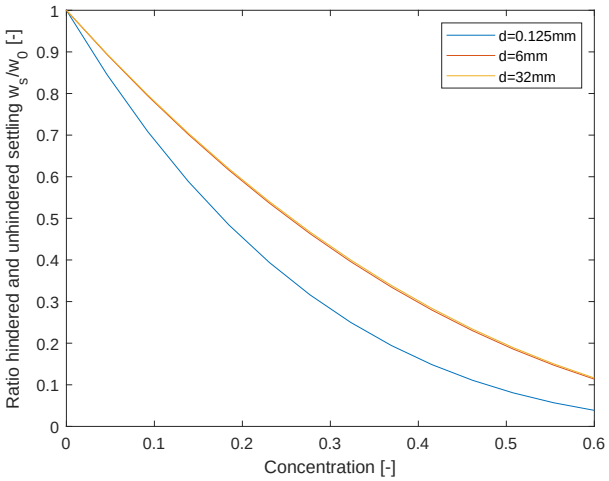

Figure 30: Richardson ratio of hindered and unhindered settling

DriftFluxfoam will model the mixture through the use of its slurry model. This model applies a correction on the Newtonian viscosity with the use of Thomas' equation (G.Holzinger 2020)[17].

$$\mu = \mu_c(1 + 2.5\alpha_d + 10.05\alpha_d^2 + 0.00273e^{16.6\alpha})$$

Here μ_c is the viscosity of the continuous phase. And α is the solids concentration

4.2.2 Turbulence model

A flow can have two situations, laminar or turbulent. This depends on the Reynolds number, once this is higher than 2000, the situation is considered turbulent. The Reynolds number can be calculated with the following formula.

$$Re = \frac{\rho u L}{\mu}$$

Filling this in gives a value for the Reynolds number of 7175000 which is far above 2000, meaning that the situation is highly turbulent and that the turbulence should be modelled.

Unlike laminar flows, turbulent flows are irregular and chaotic, this is because the streamlines mix and vortices appear. There are three approaches to simulating turbulence. Direct Numerical Simulation (DNS), Large Eddy Simulation (LES) and Reynolds Averaged Navies Stokes (RANS). DNS can be considered to be the "exact" solution in theory. A DNS simulation captures even the smallest vortices that occur through its calculation. This makes it highly time consuming and thus it is not applied.

LES is a method that shares similarities with DNS. By partially modelling the structure of turbulence scales it is possible to work with bigger spacial steps and time steps. Where small turbulence scales are modelled as these are relatively homogeneous. However, to have an accurate simulation it is still required to have a relatively fine mesh, especially at the wall where the shear rate is high. Whilst it is possible to partially model the simulation, it is still too computationally demanding.

RANS is a method that takes the original Navier-Stokes equations and applies an averaging operator on it. Here all the vortices are modelled instead of being resolved or partly resolved. It makes use of turbulent kinematic energy to model the turbulence, which is characterised by the velocity fluctuation. Since this method resolves none of the turbulence, it can have the biggest spacial and time steps, making it the fastest methods out of all three turbulence models. For this reason the RANS method is chosen as its low computational load allows for more tests to be created. Once the best configuration is decided, it is would be of interest to apply a different turbulence model such as LES in order to more precisely determine the data.

In RANS simulations the velocity the velocity is split a mean value and fluctuation. This is shown in the formula below.

$$u = \overline{u} + u'$$

Original Navier-Stokes

$$\frac{\delta u}{\delta t} + \nabla(uu) + \frac{1}{\rho}\nabla p - \frac{1}{Re}\nabla * \nabla u = 0$$
$$\nabla u = 0$$

Averaged Navier-Stokes

$$\frac{\delta \overline{u}}{\delta t} + \nabla((\overline{u})(\overline{u})) + \frac{1}{\rho}\nabla p - \frac{1}{Re}\nabla * \nabla \overline{u} = -\nabla \overline{u'u'}$$
$$\nabla \overline{u} = 0$$

$$\tau_{ij} = -\overline{u_i' u_j'}$$

When taking the average of the Navier-Stokes equation, the right side of the equation gets a new variable which is written as τ. This is called the Reynolds stress tensor. The Reynolds stress tensor is the average of the velocity fluctuation product. This is an unknown value and cannot be changed into a solvable form using Reynolds decomposition. Instead a transport equation can be used to calculate the Reynolds stress tensor. The transport equation is shown in the formula below, details on how to achieve this formula can be found in (S.Hickel 2021)[16].

$$\frac{\partial \overline{u_i' u_j'}}{\partial t} + \overline{u_k}\frac{\partial \overline{u_i' u_j'}}{\partial x_k} = -(\overline{u_i' u_k'}\frac{\partial \overline{u_j}}{\partial x_k} + \overline{u_j' u_k'}\frac{\partial \overline{u_i}}{\partial x_k}) + \frac{\partial \overline{u_i' u_j' u_k'}}{\partial x_k} + \frac{1}{Re}\frac{\partial^2 \overline{u_i' u_j'}}{\partial x_k \partial x_k} - \frac{1}{\rho}(\frac{\partial \overline{u_j' p'}}{\partial x_i} + \frac{\partial \overline{u_i' p'}}{\partial x_j}) + \overline{\frac{p'}{\rho}(\frac{\partial u_j'}{\partial x_i} + \frac{\partial u_i'}{\partial x_j})} - \frac{2}{Re}\overline{\frac{\partial u_j'}{\partial x_i}\frac{\partial u_i'}{\partial x_j}}$$

The transport equation of the Reynolds stress tensor consists of more unknowns than the averaged Navier-Stokes equation, thus this method does not provide a solution and modelling is required. This will be explained in the next chapter.

4.2.3 Reynolds stress tensor calculation

The Reynolds stress tensor can be solved through two methods, eddy viscosity models and Reynolds stress models. The eddy viscosity model was proposed by Boussinesq in 1877. The following formula was used for that.

$$\tau = 2\nu_t S_{ij} - \frac{2}{3}\delta_{ij} k$$
$$S_{ij} = \frac{1}{2}(\frac{\partial u_i}{\partial x_j} + \frac{\partial u_j}{\partial x_i}) - \frac{1}{3}\delta_{ij}\frac{\partial u_k}{\partial x_k}$$
$$k = \frac{1}{2}\overline{u_i' u_i'}$$
$$\delta_{ij} = \begin{cases} 1 & \text{, if } i = j, \\ 0 & \text{, if } i \neq j \end{cases}$$

Where ν_t is the eddy viscosity S_{ij} is the strain rate, δ_{ij} is the kronecker delta and k is the turbulence kinetic energy.

ν_t can be modelled using multiple ways, which is done best by using two equation models. There are two variants of the two equation model, the Jones & Launder k-ϵ model and then Wilcox k-ω model. The k-ϵ model is the most used model and the only one available to use with driftFluxFoam. It solves the equation for the turbulent kinetic energy k and the dissipation of the turbulent kinetic energy ϵ. It assumes isotropic turbulence and an equilibrium between the production and dissipation of turbulence. With these assumptions it creates the following formula:

$$\nu_t = C_D \frac{k^2}{\epsilon}$$

The exact equations for k and ϵ contain multiple unknowns, so this is modelled instead. This reduces the unknowns whilst still being applicable in many turbulent flows. The formulas become the following:

$$\frac{\partial k}{\partial t} + \overline{u_j}\frac{\partial k}{\partial x_j} = \tau_{ij}\frac{\partial \overline{u_i}}{\partial x_j} + \frac{\partial}{\partial x_j}([\frac{1}{Re} + \nu_t]\frac{\partial k}{\partial x_j}) - \epsilon$$

$$\frac{\partial \epsilon}{\partial t} + \overline{u_j}\frac{\partial \epsilon}{\partial x_j} = C_{\epsilon 1}\frac{\epsilon}{k}\tau_{ij}\frac{\partial \overline{u_i}}{\partial x_j} + \frac{\partial}{\partial x_j}([\frac{1}{Re} + \frac{\nu_t}{Pr_\epsilon}]\frac{\partial \epsilon}{\partial x_j}) - C_{\epsilon 2}\frac{\epsilon}{k}\epsilon$$

The values for the constants are the following. $C_D = 0.09$, $Pr_\epsilon = 1.3$, $C_{\epsilon 1} = 1.44$ and $C_{\epsilon 2} = 1.92$. These values are determined by using data fitting at numerous turbulent flows where many terms of the transport equation cancel each other out. That way the isolated parameter can be determined. This method has a relatively low computational time since it uses two transport equations (S.Hickel 2022) [16].

4.3 Simulation setup

4.3.1 Mesh design

Mesh designs for a CFD simulation is of high importance as a good solver is unable to converge to a stable and correct result if the mesh has shortcomings. In the design of the mesh there are two main elements that are of importance to consider. Firstly the grid that the mesh consists of, which is either structured or unstructured. And secondly, the general design of the mesh will be checked on multiple phenomena that can occur which reduce the accuracy or stability of the simulation.
Like mentioned before, the mesh of the system can be build by two types of grids, structured and unstructured grids. Structured grids consist of rectangles or hexahedrons. And unstructured grids consist of triangles or tetrahedrons. Structured grids are more space efficient, computationally efficient and can have a lower error from numerical viscosity when placed orthogonal to the flow. However, these grids do not have a straightforward method to apply local refinement. In simple geometries it is straightforward to apply structured meshes however, as the complexity increases of the geometry, so does the complexity of applying a structured grid. But that is of no high importance as the geometry is relatively simple (S. Hickel 2022) [16]. Thus for these reasons the structured grids will be used.

As for the design of the mesh, certain negative aspects are monitored in order to reduce their inaccuracies or instabilities. An aspect that is of importance is the mesh non-orthogonality. This is caused by the orthogonality of the faces of a grid cell. This is visualised in 31 by making a line between two cell centers and then checking whether this is orthogonal to the cell face.

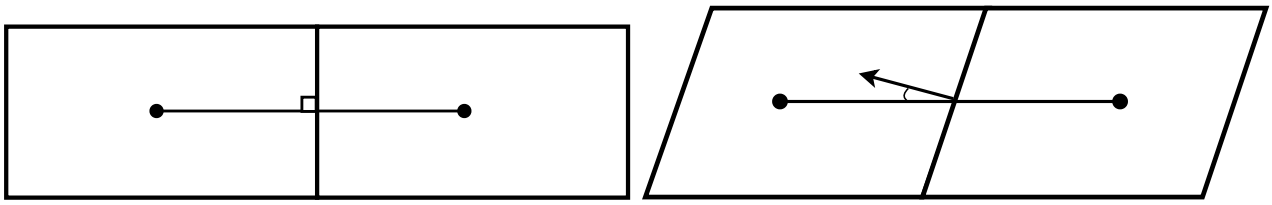

(a) Orthogonal cells (b) Non-orthogonal cells

Figure 31: Comparison of orthogonal cells and non-orthogonal cells

Non-orthogonality is required to take into consideration as it increases the error of the calculations, especially at locations with high gradients. This can also cause an impact on the stability of the simulation or slower convergence (H. Xu 1999) [40]. OpenFOAM consists of built in graduate schemes for correcting non-orthogonality. The proper graduate scheme will be applied based on the non-orthogonality of the mesh which is

determined through the "checkMesh" command. If the non-orthogonality angle is higher 70 degrees, it is far too high and it is required to improve the mesh. The non-orthogonality can be reduced by applying mesh smoothing.

Another aspect of importance is awareness of numerical viscosity. Numerical viscosity is an effect caused by the error that is introduced when discretisating the equations that are solved by the CFD program. The error is dependant on the time step and size of the mesh cells. Improving the spatial resolution of the numerical grid can help reduce numerical viscosity.

Lastly the Courant number will be discussed. The Courant number represents the ratio of the distance information travels in one timestep ($u\Delta t$) to the spatial resolution (Δx). It quantifies how far a signal travels relative to the grid space in a single timestep and is shown in the formula below.

$$Co = \frac{u\Delta t}{\Delta x}$$

The Courant number is crucial for ensuring numerical stability, which is achieved when the Courant number is less than or equal to 1. When the Courant number exceeds 1, it implies that information is propagating across more than one grid cell per timestep. This can lead to numerical instability, where errors accumulate and the solution diverges from the physical behavior of the system (S. Hickel 2022) [16].

By keeping the Courant number below 1, each grid cell is traversed by at most one characteristic length during each timestep, ensuring that the solution evolves in a stable manner and accurately captures the physics of the system.

All the mentioned information in this paragraph will be used in order to create a stable simulation, when a problem occurs caused by the aforementioned occurrences, then the fitted solution will be applied on it.

4.3.2 Boundary conditions

For a CFD simulation certain boundary conditions and initial values are required in order to run the simulation. Based off of these conditions, the variables will develop till the simulation is ended or a steady state is reached.

Based on the geometry shown in figure 29d, a mesh has been created. The outline of the mesh has the construction shown in figure 32. The junction of the pipe is normally located as close to the draghead as possible. This has been visualised back in figure 28. However, in the simulations the junction will be placed at the center instead because stability is much higher here as it will prevent the boundary condition of the inlet affecting the junction by forcing a situation that is either inaccurate or unrealistic. Additionally, the distance allows the flow to develop, which makes it possible to better distinguish the effect that different variables have on the separation efficiency. From a production standpoint it is not problematic to place the junction further up the pipeline as long as it is located in the lower pipe, which limits the complexity of the system.

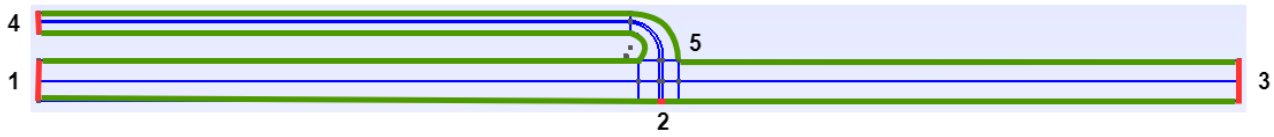

Figure 32: Mesh and the boundary conditions

The mesh consist of 6 different surfaces which are shown in figure 32. These locations have been marked with a red or green line. The name and function of each boundary has been explained in table 4.

Number	Boundary	Function
1	Inlet	Introduces a mixture of fluid and particles
2	Jet	Pushes sediment upwards
3	Outlet	Delivers coarse particles to the hopper
4	Filter Outlet	Releases fine particles to the seabed
5	Wall	Contains everything inside the system
6	Empty	Condition to turn 3D simulation into 2D

Table 4: Description for the boundary conditions

These boundaries will have the following conditions applied to them to achieve their function: The inlet will have a fixed concentration, velocity and a constant pressure is applied by allow no pressure gradient to occur here. This way the interested concentration and velocity can be realised at the inlet and the pressure will be calculated by OpenFOAM itself. The same will be done at the jet as this behaves as an inlet as well. For the outlets the opposite is done, no concentration and velocity is forced here and instead the pressure is given. Applying a fixed variable on a location is called a Dirichlet condition. And when a constant value is applied, then it is called a Neumann condition. At the wall there is a no slip condition, this is a zero velocity condition. Additionally the k-epsilon turbulence is modelled here which speeds up the simulation time compared to solving it normally. This is done by calculating the turbulence near the wall with a continuous formula instead of solving it through discretisation, thus this variables is not dependant of the fineness of the mesh which reduces the computational load. And the boundary "empty" has the empty condition. Since OpenFOAM only works with 3D geometries, this is a requirement to create a 2D simulation with a 3D geometry.

For the driftFluxFoam solver with the k-epsilon turbulence model the following variables are required to run a simulation: Velocity, pressure, volume fraction of the sediment, turbulent kinetic energy and the turbulence dissipation rate. Which are described as u, v, α, k and ϵ respectively in OpenFOAM. Whilst the velocity, pressure and alpha can be directly determined, k and ϵ need to be calculated. Since the system is in a smooth duct, the following equations can be used (D.Frolez 2012) [11]:

$$l = 0.07D$$
$$I = 0.16Re^{-1/8}$$
$$k = \frac{3}{2}(uI)^2$$
$$c_\mu = 0.09$$
$$\epsilon = \frac{c_\mu^{3/4} k^{3/2}}{l}$$

And the conditions used for each boundary are shown in table 5.

Boundary	α	u	p	k	ϵ
Inlet	Dirichlet	Dirichlet	Neumann	Dirichlet	Dirichlet
Jet	Dirichlet	Dirichlet	Neumann	Dirichlet	Dirichlet
Outlet	Neumann	Neumann	Dirichlet	Neumann	Neumann
Filter Outlet	Neumann	Neumann	Dirichlet	Neumann	Neumann
Wall	Neumann	Dirichlet (noSlip)	Neumann	WallFunction	Wallfunction
Empty	Empty	Empty	Empty	Empty	Empty

Table 5: Boundary Conditions

The table shows the type of boundary condition is used but not their numerical value. The numerical values that will be used on the boundary condition itself will be determined and explained in the configuration analysis.

4.3.3 Mesh structure

The mesh generation was executed using the GMSH tool, which is chosen for its compatibility with OpenFOAM. In figure 33 the whole mesh is visualised and it can be seen that this is very fine for the whole mesh. Thus it is required to zoom in in order to examine the mesh effectively. The relevant area is the junction, where the separation process occurs and the inlet, where the mixture is introduced. These are focused on in the next page.

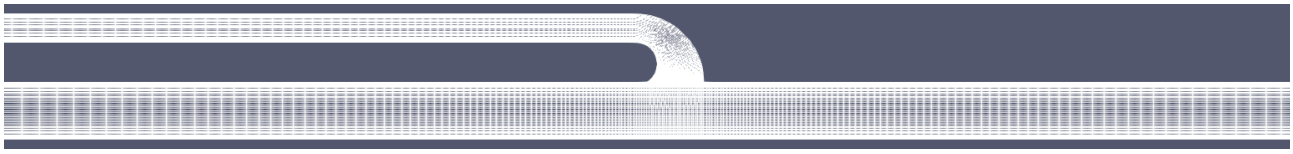

Figure 33: Whole geometry divided in grids

Firstly the inlet will be focused. In figure 34 the inlet can be seen on the left side. From this image two things can be noticed. First of all, the mesh starts off large at the center and as it reaches the walls it reduces

in height. This is implemented as a response to the high velocity gradient near the walls. The cause of the high gradient arises from the wall having a velocity of zero, thus the fluid velocity reduces as it nears the walls, which requires a finer mesh to determine this more accurately.

Figure 34: Mesh of the inlet

The second phenomenon that occurs is the increase in the mesh's grid length as it nears the inlet. This phenomenon applies for the inlet, outlet and filter outlet. This is implemented due to these locations having a simple geometry and low or no gradients in its output variables. This makes it unnecessary to have a fine mesh and allows the simulation to require less computational power whilst having a negligible loss of accuracy.

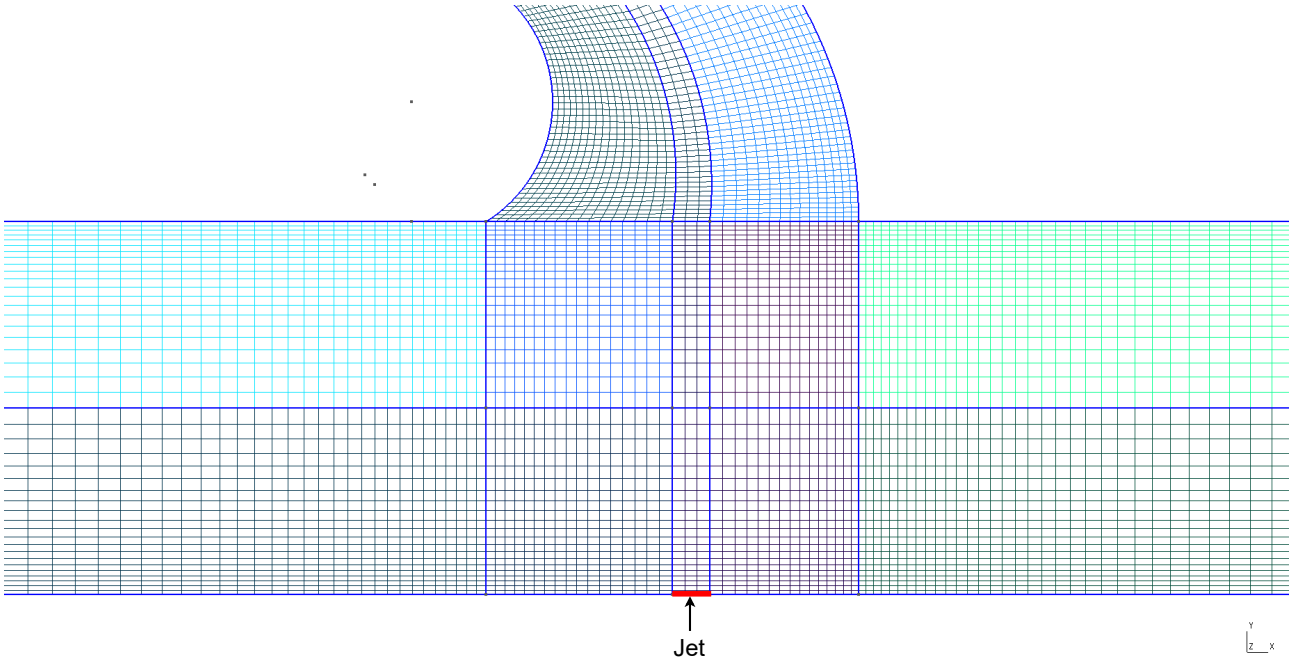

Figure 35: Mesh of the pipe junction

The pipe junction is the most complex area of the system. Here the jet is introduced and the pipe is split in two. For this reason a lot of effects occur around this area which need to be accurately simulated through the use of a fine mesh. For this location the following are taken into account. Firstly, as mentioned before, the mesh is required to be fine in order to correctly simulate the effect of fluctuations. Secondly, using structured meshes to create a geometry with bends has a challenge, which is that a coarse mesh is unable to replicate a bend well and will instead give a pointy geometry. A fine mesh is required here which will smoothen the points, which will make the mesh resemble a circle far better. A bend will cause the grid cells to "bend" in an angle, which causes non-orthogonality. This non-orthogonality has been reduced using two methods. Firstly, the bend radius has been lightly increased. And secondly, the grid cells have been made finer in order to divide the non-orthogonality over more cells, causing many cells to have a low non-orthogonality instead of a few cells to have a high non-orthogonality.

4.4 Convergence study

A convergence study will be conducted where two things will be determined. Firstly, the system will be checked whether it has reached steady state. And secondly the difference in the output of the variables will be checked when adjusting the timestep and grid size.

Steady state means that the flow is no longer time dependent and will give the same value at every timestep. Steady state is checked by reviewing an output value and observing the change over time. This will be checked at the two outlets, which can be found in figure 32 at number 3 and 4. These locations are chosen as the flow is developed and they do not directly determine the volume flow with their boundary conditions.

For this research it is not necessary to determine the actual steady state, instead it will be checked how close the system is to reaching steady state. Waiting for the system to reach steady state would take an impractical amount of time, thus a compromise is made by looking at the moment when the simulation sufficiently reaches steady state. For this research, if the difference in volume flow after one second is smaller than 0.1%, then the error will be neglected and the system will be considered sufficiently steady state. Once it is confirmed that a system sufficiently approaches steady state, the timestep and mesh size will be tested on convergence. These variables will be increased with a factor of at least two. For this convergence study the goal is to sufficiently converge the output values whilst keeping the simulation time at around a few hours. If the simulation time cannot be reduced to the preferred time, then other measures could be taken such as the usage of fractional factorial design of experiments.

Below in figure 36 and 38 the volume flow and concentration over time are shown. The development of these variables becomes nearly horizontal at an early stage. Thus to better visualise the development of the volume flow and concentration, the derivative of these graphs are made which is shown in figure 37 and 39. It should be noted that the derivatives start at T=10s to filter out the high values at the start. In the tables 6 and 7 the difference between timestep 100s and 99s, 50s, and 30s are shown. The difference between the two timesteps is calculated with the following formula:

$$\Delta \dot{Q}_{2,1} = \frac{\dot{Q}_2 - \dot{Q}_1}{\dot{Q}_2} * 100\%$$

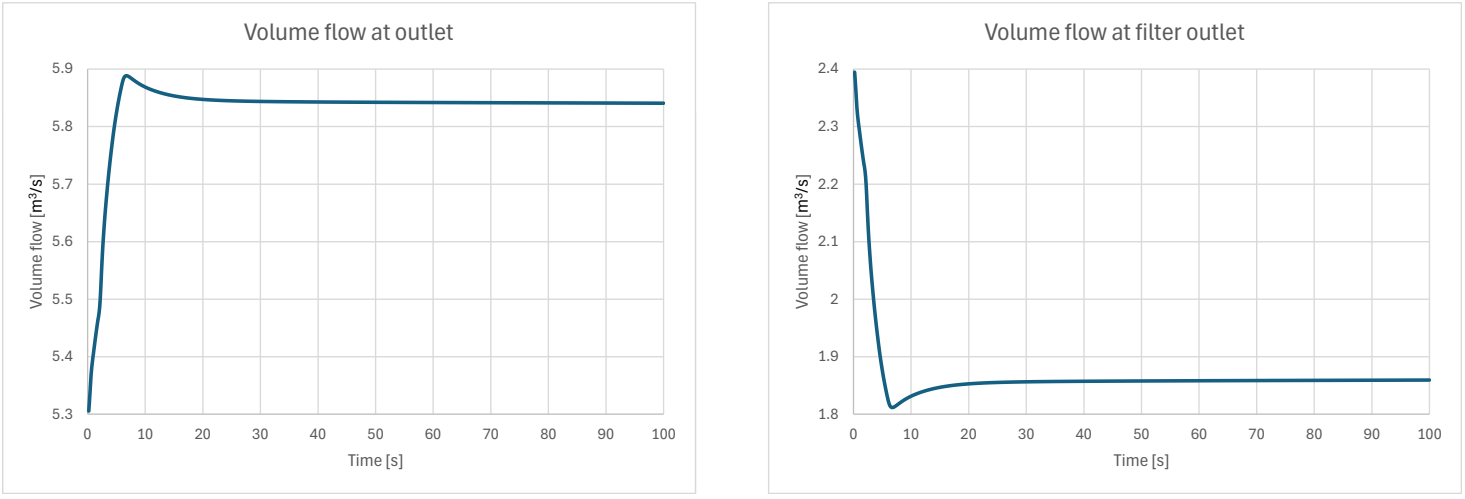

(a) (b)

Figure 36: Volume flow over time for both outlets

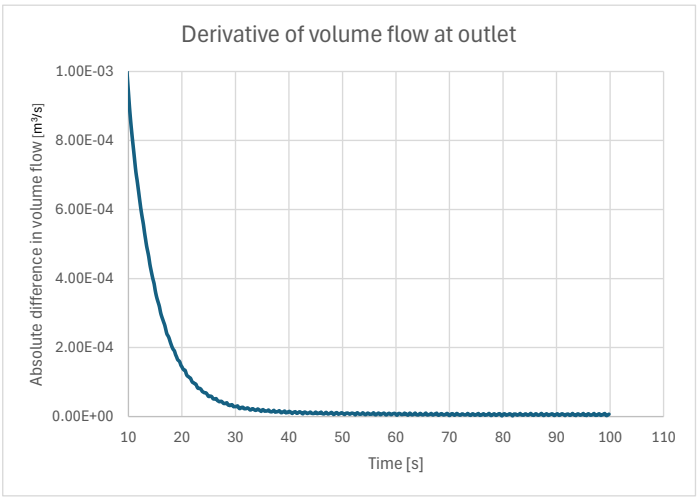

(a)

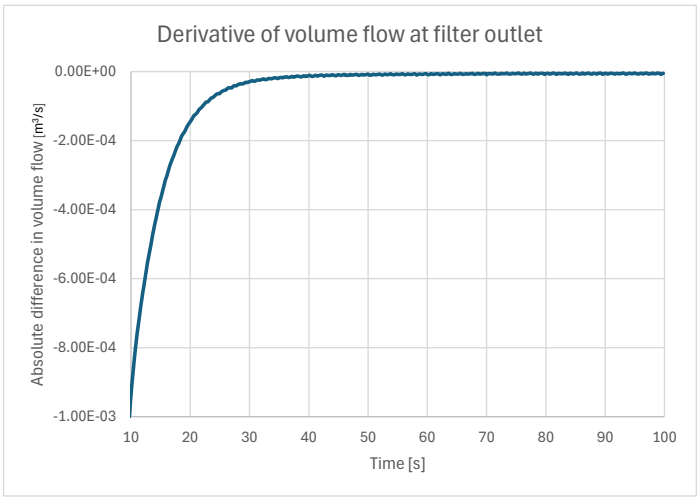

(b)

Figure 37: Derivative of the volume flow over time for both outlets

Location	Outlet	Filter outlet
$\Delta\dot{Q}_{T100,T99}$	-4.79e-4 %	2.69e-4 %
$\Delta\dot{Q}_{T100,T50}$	-2.74e-2 %	8.64e-2 %
$\Delta\dot{Q}_{T100,T30}$	-5.26e-2 %	0.165 %

Table 6: Outlets volume flow time comparisons

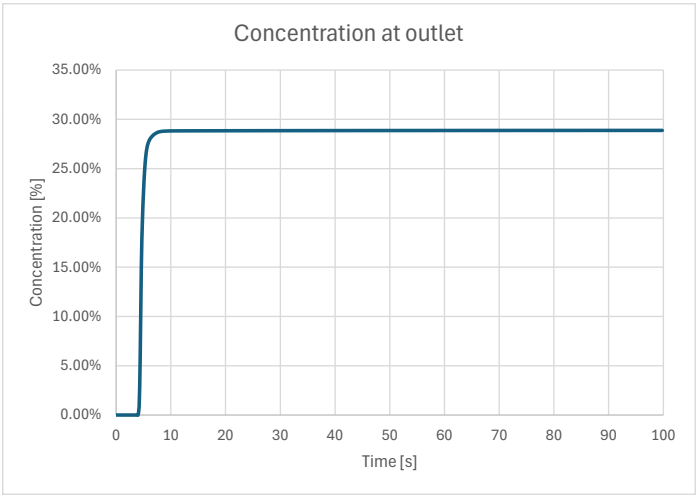

(a)

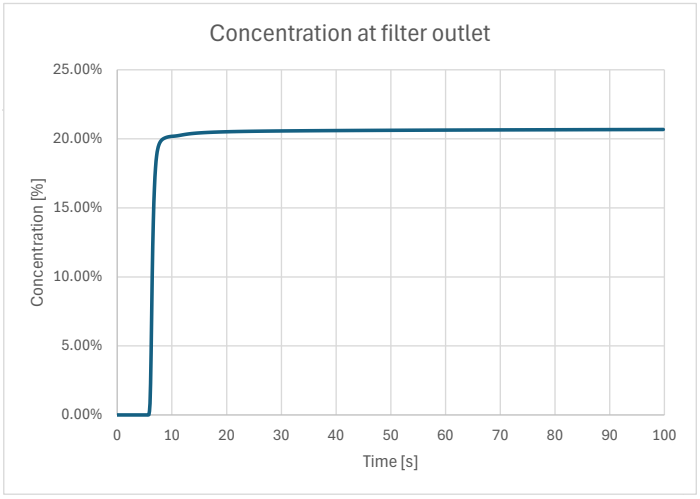

(b)

Figure 38: Solids concentration over time for both outlets

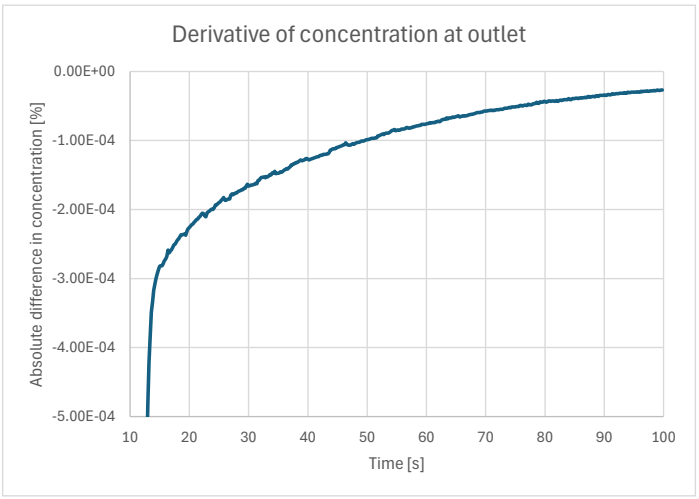

(a)

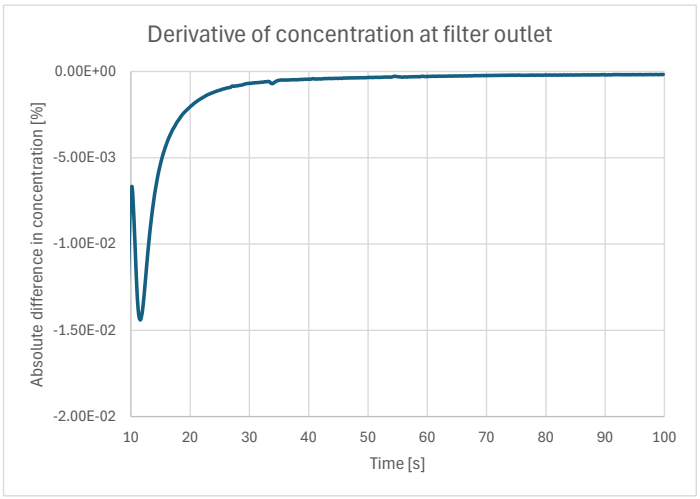

(b)

Figure 39: Derivative of solids concentration over time for both outlets

Location	Outlet	Filter outlet
$\Delta c_{T100,T99}$	4.50e-4 %	3.82e-3 %
$\Delta c_{T100,T50}$	4.60e-2 %	2.85e-2 %
$\Delta c_{T100,T30}$	8.89e-2 %	0.517 %

Table 7: Outlets solids concentration time comparisons

The tables 6 and 7 show that the difference between the two timesteps is low enough to consider the situation to be steady state.

The simulation are almost converged at 30 seconds, and are sufficiently converged at 50s as the difference in output values between 100s and 50s is less than 0.1%. Additionally, it can be seen that there is a peak near 30 seconds in figure 36a and 36b, meaning that this situation reached steady state very recently. The risk of different configurations not being in steady state at time timestep is high. Thus as a safety measurement the simulations will be run till 50 seconds.

Next the convergence of the timestep and mesh size will be tested through the following method. The mesh size and timestep will be reduced with a factor of approximately two. As smoothening of the grid is of importance, an exact factor of two will not be strived for. If the results of the higher resolution simulations strongly differ from the base simulation, additional refinement will be applied until the output values converge. In the steady state test the simulation reaches steady state far before the timestep of 100. Thus the output values in the convergence test will be compared on timestep 30, 50 and 100. In the convergence test firstly the timestep size, the amount of mesh cells and the simulation time will be noted. And then the output values are compared with each other. Since massflow is of importance, this will be checked by splitting it into two variables which is consists of, volume flow and concentration.

In table 8 the difference in timestep, amount of cells in the mesh and the required time for each simulation is shown. In this test the timestep and mesh size was reduced by a factor of around 2. It can be seen that the timestep has been reduced in the fine mesh. This is because the Courant number would get above one if the timestep was not reduced.

During the test also a simulation time bigger than 5e-4s has been tried. But this causes the Courant number to slowly increase to a value above 1. This creates instabilities and the simulation is unable to continue shortly after. Thus no values above 5e-4s are used for the timestep.

In table 9 the difference in percentage is calculated between the base simulation and the adapted version with the formula below. The formula shows it for the volume flow $\dot{Q}$ however, this formula can also be used for concentration by changing the $\dot{Q}$ into c.

Variable	Base simulation	Small timestep	Fine mesh
Timestep size [s]	5e-4	2e-4	1e-4
Amount of cells in mesh [-]	12882	12882	27618
Simulation time [s]	3284	7848	39192

Table 8: Characteristics of base simulation and improved versions

$$\Delta\dot{Q} = \frac{\dot{Q}_{base,version} - \dot{Q}_{improved,version}}{\dot{Q}_{base,version}}$$

Variable	Base & small timestep	Base & fine mesh
$\Delta\dot{Q}_{outlet}$	-0.112 %	-0.044 %
Δc_{outlet}	0.021 %	-0.225 %
$\Delta\dot{Q}_{Filteroutlet}$	0.353 %	0.139 %
$\Delta c_{Filteroutlet}$	-0.187 %	3.008 %

Table 9: Difference in output variables between base simulation and improved versions

The results show a good convergence for the base simulation as the output data generally changes with a percentage lower than 1%. However, when comparing the base and fine mesh results, it can be seen that the difference in concentration at the filter outlet is relatively high. Since the solids concentration has a direct effect on the conservation of mass, a research will be done on the conservation of mass between the two situations. From this research the impact of this error will be determined. The conservation of mass will be calculated with the following formula.

$$\dot{M} = uA\rho_m$$

$$\rho_m = \alpha_s\rho_s + \alpha_f\rho_f$$

Where u is the velocity, A is the area and ρ_m is the mixture density. The mixture density is calculated with the concentration and density of the fluid and solids. All these values can be found in the simulation, however the flow is not homogeneous. The concentration and velocity change over the height of the pipe. For this reason it is required to multiply the local values with each other and not the average values over the boundary. In figure 40 this phenomenon is visualised through the velocity and concentration profile respectively over the pipe height in the outlet for the base simulation.

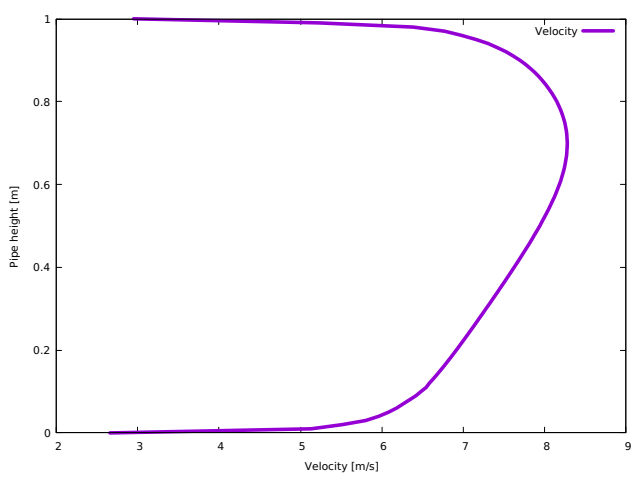

(a) Velocity profile of the outlet

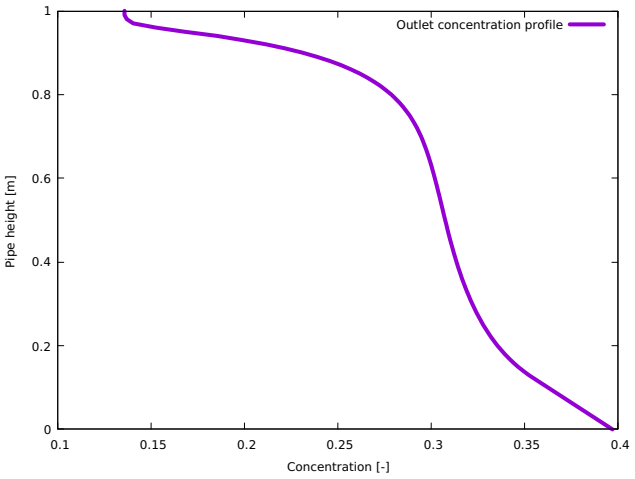

(b) Concentration profile of the outlet

Figure 40: Outlet velocity and concentration profiles

In these images it is noted that the velocity is higher as the concentration decreases, which is to be expected as the sediment is heavier than the fluid. This leads to an increase of the weight of the local mixture as the concentration increases.

To test the convergence of the base and fine simulations, the conservation of mass is calculated by using the following formula.

$$\Delta\dot{M} = \frac{\dot{M}_{inlet} + \dot{M}_{jet} - \dot{M}_{outlet} - \dot{M}_{filterOutlet}}{\dot{M}_{inlet} + \dot{M}_{jet}}$$

Here the data is obtained at the pipes entrances and exists. These are shown for the base and fine simulations in table 10.

	Base	**Fine**
$\Delta\dot{M}$	0.50%	0.19%

Table 10: Conservation of mass for the base and fine mesh simulation

The table above shows an error of 0.5% for the massflow, which is acceptably low for this research. The finer simulation gives an error of 0.19%, which is lower but takes over 11 hours to simulate whilst the base simulation takes 1 to 3 hours. In the next section, 4.5, it will be shown that there will be 54 simulations done in total, 11 hours per simulation would lead to almost a month of simulation time. In order to balance simulation time and massflow error, the base simulation will be taken as the error is below 1%. The massflow error will be tracked for all configurations to determine whether these remain in an acceptable range. Thus the base simulation will be used instead of the fine mesh simulation. And this will be run till 50 seconds in order to sufficiently reach steady state.

4.5 Configuration analysis

The goal of the simulations is to determine the effectiveness of the separator, which is realised by analysing the following three output data. Firstly, the amount of fines that are separated from the system. Secondly, the percentage of coarse particles that are contained in the system. And lastly, the pump energy. When the required pump energy increases, so does the financial cost of this concept. These output data are affected by the following. The flow field, the pipe geometry, characteristics and the properties of the fluid and sediment. Fixed properties such as the density of the fluid or particles are not considered as they remain constant in dredging practise. Thus the system is affected by the following variables:

Flow field components

- Inlet velocity
- Jet velocity
- Jet location
- Jet width

Pipe geometry and characteristics

- Pipe diameter
- Radius of the bend
- Location of the pipe junction
- Shape of the pipe bend
- Pipe angle
- Pipe wall roughness

Sediment characteristics

- Sediment size
- Sediment size distribution

This list will be condensed to variables which have the highest impact that can be adjusted during operation or are of importance to determine the separation efficiency of the system.

Anything that affects the pipe geometry and material is not considered as the focus is on operational parameters. After removing the aforementioned variables, the following remains.

- Inlet velocity
- Jet velocity
- Jet location
- Sediment size
- Sediment concentration
- Pipe angle

The reason why these variables stayed is because of the following. The inlet and jet velocity directly affect the drag forces on the particles and can make this more dominant than the inertial forces, which is the mechanism that determines the cutoff diameter. The jet location at the junction changes when the particles are pushed up, but this also has an influence on the percentage of fluid which leaves through the filter. The sediment size determines the inertia of the particle, which determines how strongly the particles resist the flow. The sediment concentration affects the flow profile as it affects the density of the mixture increases and the particle hindreded settling velocity. And lastly the pipe angle will change the angle of gravity, reducing the settling velocity further.

Whilst these variables are of high importance, the jet location and pipe angle will not be used. The reason for this is because modifying these conditions causes instabilities to the system. When the jet location is moved, the local increase of pressure will be moved as well. In extreme cases this causes the filter outlet to function as an inlet and introduce water into the system.

As for the pipe angle, this causes instabilities at the filter outlet which makes it clog in an unnatural manner, which is shown in figure 41. In this figure the red colour shows a high concentration of particles. Near the filter outlet the concentration increases steeply which is likely caused by the forced boundary condition at this location.

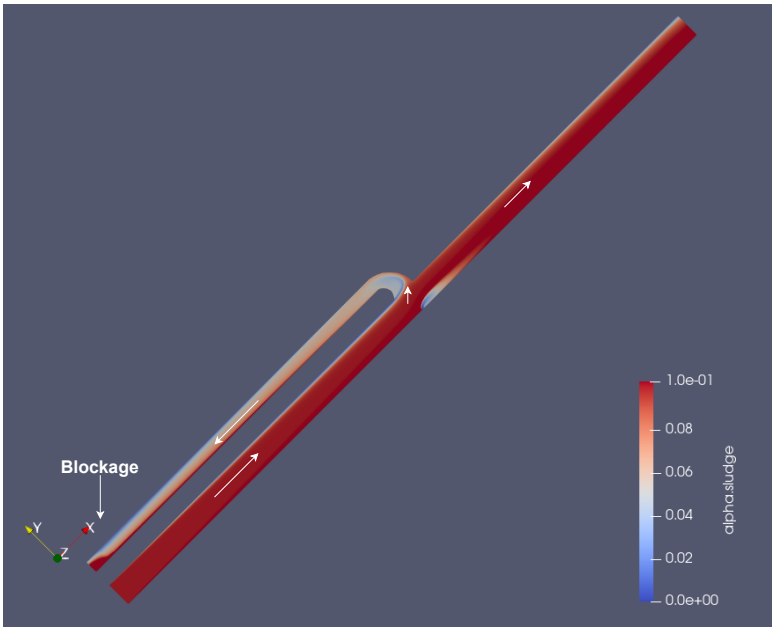

Figure 41: Concentration profile of pipe visualising the clogging at filter outlet

However, when the pipe is on a 0 degree angle the instabilities do not occur. Thus it is likely that the instabilities occur when the boundary condition is at an angle with gravity. Therefore the research will be done with a pipe angle of 0 degree.

If these problems had not occurred, then simulating 3 levels for each variables would lead to $6^3 = 216$ simulations. Gathering data for all these configurations would lead to an extremely long simulation time, which would necessitate reducing the number of configurations. Due to the excessive number of variables, the decision

was made to proceed with the functioning variables.

Thus the remaining variables are the following.

- Inlet velocity
- Jet velocity
- Sediment size
- Sediment concentration

The remaining variables will be split into two or three levels which are tested. The velocity at the inlet and jet and sediment size have a strong, direct effect on the separation efficiency. For this reason three levels will be checked during the design of experiments. These levels will have a base value with a maximum and minimum. These three values will be based on either two things, firstly, whether they are realistic values. And secondly whether they are of interest for this research. For the inlet and jet velocity a base value of 7 m/s is used which is realistic in dredging applications. For a low value and high value 5m/s and 9 m/s are chosen respectively. As for the sediment size a base value of 6mm is chosen as that is the cutoff diameter for this research. The low and high value are 0.125mm and 32mm respectively. Since the seabed contains sand and gravel, the minimum and maximum values for fine sand and coarse gravel are used. As for the sediment concentration, whilst this has a visible effect on the results, it is not as dominant as the other three. For this reason only two values are used, 10% and 30%. The reason for these two values is because they are realistic low and high values in dredging applications.

Value	Inlet velocity [m/s]	Jet velocity [m/s]	Sediment size [mm]	Sediment concentration [%]
Low	5	5	0.125	10%
Medium	7	7	6	-
High	9	9	32	30%

Table 11: Input variables and their values

For this experiment it is of importance to obtain as much data as possible in order to accurately define the effect of each input variable. The relatively short simulation time in combination with the total amount of configurations makes it possible to simulate all possible configurations in an acceptable time frame. For this reason a Full-factorial screening design will be conducted.

Thus the following full factorial set has been made in table 12.

Run	Inlet Velocity	Jet Velocity	Sediment Size	Sediment Concentration
1	Low	Low	Fine	Low
2	Low	Low	Fine	High
3	Low	Low	Medium	Low
4	Low	Low	Medium	High
5	Low	Low	Coarse	Low
6	Low	Low	Coarse	High
7	Low	Medium	Fine	Low
8	Low	Medium	Fine	High
9	Low	Medium	Medium	Low
10	Low	Medium	Medium	High
11	Low	Medium	Coarse	Low
12	Low	Medium	Coarse	High
13	Low	High	Fine	Low
14	Low	High	Fine	High
15	Low	High	Medium	Low
16	Low	High	Medium	High
17	Low	High	Coarse	Low
18	Low	High	Coarse	High
19	Medium	Low	Fine	Low
20	Medium	Low	Fine	High
21	Medium	Low	Medium	Low
22	Medium	Low	Medium	High
23	Medium	Low	Coarse	Low
24	Medium	Low	Coarse	High
25	Medium	Medium	Fine	Low
26	Medium	Medium	Fine	High
27	Medium	Medium	Medium	Low
28	Medium	Medium	Medium	High
29	Medium	Medium	Coarse	Low
30	Medium	Medium	Coarse	High
31	Medium	High	Fine	Low
32	Medium	High	Fine	High
33	Medium	High	Medium	Low
34	Medium	High	Medium	High
35	Medium	High	Coarse	Low
36	Medium	High	Coarse	High
37	High	Low	Fine	Low
38	High	Low	Fine	High
39	High	Low	Medium	Low
40	High	Low	Medium	High
41	High	Low	Coarse	Low
42	High	Low	Coarse	High
43	High	Medium	Fine	Low
44	High	Medium	Fine	High
45	High	Medium	Medium	Low
46	High	Medium	Medium	High
47	High	Medium	Coarse	Low
48	High	Medium	Coarse	High
49	High	High	Fine	Low
50	High	High	Fine	High
51	High	High	Medium	Low
52	High	High	Medium	High
53	High	High	Coarse	Low
54	High	High	Coarse	High

Table 12: Design of experiments setup

4.6 Massflow error check

The error in massflow has been obtained for each configuration in order to trust the results. In figure 42 this has been visualised.

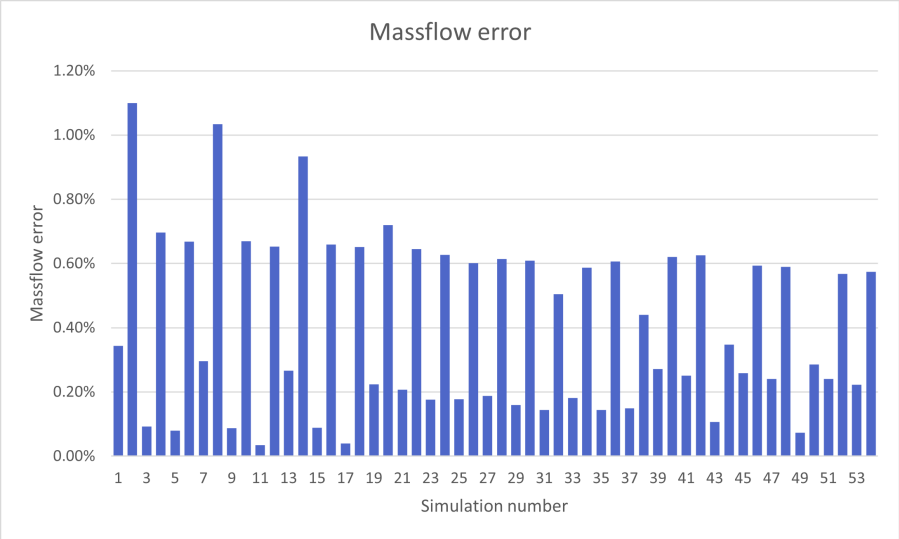

Figure 42: Massflow error for every simulation

This shows that generally the error is below 1% except for simulation 2 and 8. These configurations slightly exceed the requirement, in the results below it will be determined if these configurations are of interest. If these configurations have a low separation efficiency and are not of interest, then no improvement will be applied on its accuracy. If the accuracy is of importance, then the fineness of the mesh will be increased.

Additionally when looking at the figure a trend is noticed where the error increases by approximately 3 times between even and uneven numbers. All even numbers have a concentration of 30% whilst the uneven numbers have a concentration of 10%. This means that the error is directly related to the concentration. Overall the massflow error fluctuates between 0.2% and 0.6%, which is below 1%. Thus the error is in an acceptable range.

5 Results

The result of the simulation is shown in table 13 below. The result consists of the inlet pressure, jet pressure and the particle containment. The particle containment is shown for fine, medium and coarse particles, which is coloured in red, yellow and green respectively. These data are presented as they serve a purpose in determining the efficiency of each configuration. The inlet and jet pressure are required to determine the required pump power, and the particle containment determines the separation efficiency. The pressure is directly gathered from the inlet and jet boundary. And the particle containment is calculated by dividing the solids flow from the outlet with the inlet.

Run	Inlet pressure [Pa]	Jet pressure [Pa]	Particle Contained
1	1137.199	7532.924	91.68%
2	3080.765	9343.494	87.21%
3	1654.348	7065.432	100.00%
4	2033.391	10259.440	100.00%
5	1486.667	9114.429	100.00%
6	1767.696	10014.630	100.00%
7	2654.087	7808.799	87.81%
8	4313.136	9714.996	82.98%
9	3289.169	10323.270	100.00%
10	3543.768	10554.260	99.99%
11	3240.052	10033.650	100.00%
12	3364.308	10650.730	100.00%
13	4214.191	7588.824	84.35%
14	5743.630	9038.605	79.24%
15	4954.217	10703.270	100.00%
16	5293.077	10684.430	99.89%
17	4929.791	10583.580	100.00%
18	5113.275	10821.710	100.00%
19	-758.803	7076.295	88.40%
20	287.185	8448.440	83.69%
21	115.293	9566.845	100.00%
22	428.479	9506.792	100.00%
23	-25.181	8995.872	100.00%
24	75.547	9032.769	100.00%
25	1310.426	7629.056	85.37%
26	2164.814	8934.172	80.49%
27	2242.413	10869.050	100.00%
28	2362.890	10531.950	100.00%
29	2089.126	10229.830	100.00%
30	2032.825	10167.530	100.00%
31	3490.643	7688.306	82.77%
32	4385.125	9020.146	77.85%
33	4462.433	11402.720	100.00%
34	4429.140	10533.830	99.97%
35	4381.149	11122.290	100.00%
36	4149.038	10319.710	100.00%
37	-3728.094	6399.141	86.72%
38	-4085.155	7576.222	82.38%
39	-2269.760	9630.954	100.00%
40	-2388.618	8884.690	99.99%
41	-2516.522	8832.847	100.00%
42	-2488.454	7924.142	100.00%
43	-1240.433	7555.107	83.95%
44	-1517.726	8540.610	79.76%
45	178.731	11508.380	100.00%
46	124.873	9736.632	99.96%
47	-91.758	10961.010	100.00%
48	-431.211	9505.616	100.00%
49	1506.420	8040.623	81.69%
50	1425.193	9395.339	77.71%
51	2909.090	13036.860	99.99%
52	2594.564	10820.410	99.84%
53	2646.954	12608.220	100.00%
54	2088.403	10323.210	100.00%

Table 13: Output variables of each simulation

Table 13 shows negative values for the inlet pressure, which should not be possible. This phenomenon could not be solved and thus is left out of the research. More information about this can be found in appendix B.

Whilst this phenomenon makes the inlet pressure values questionable, it has been noticed that the pressure does not get negative values for an inlet velocity of $5m/s$. Thus the influence of each input variable on the pressure is analysed for simulation 1 to 18. This is of interest as the pressure gradient is indirectly related to the required pump power.

Contour plots are made to visualise the effect of input variables. The contour plots are figure 43, 44 and 45 where the figures have a jet velocity of $5m/s$, $7m/s$ and $9m/s$ respectively.

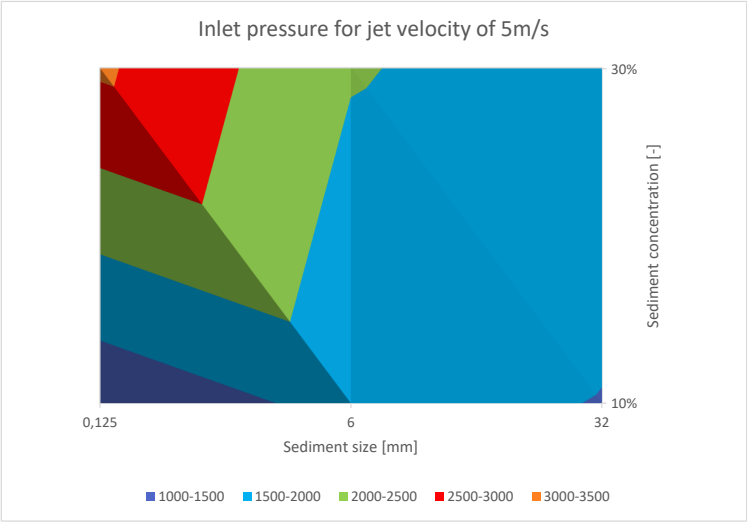

Figure 43: Contour plot of inlet pressure with jet velocity of 5m/s

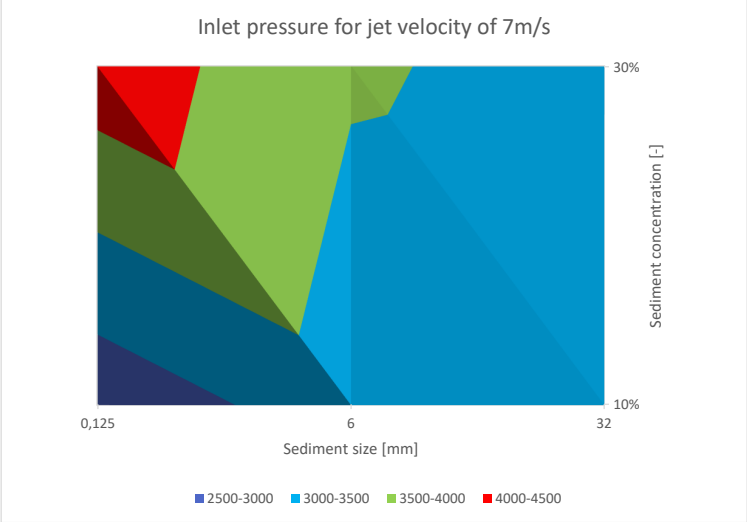

Figure 44: Contour plot of inlet pressure with jet velocity of 7m/s

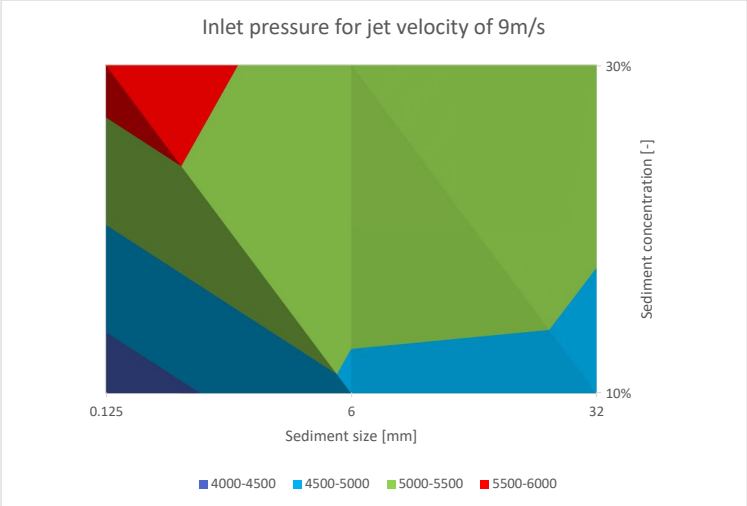

Figure 45: Contour plot of inlet pressure with jet velocity of 9m/s

From these figures it is observed that increasing the jet velocity causes a strong increase of inlet pressure. This makes sense as the jet moves perpendicular to the inlet flow, thus becoming an obstacle for it. The obstacle caused by the jet locally "reduces" the pipe diameter. Increasing in the sediment size causes a reduction of the inlet pressure. This effect is the strongest at high particles concentration. Since it was expected that the pressure would increase as the sediment size increases, additional observations have been made. In order to investigate the reason causing this, simulation 2 and 6 will be visualised. These simulations have a fine and course particles respectively with a high particle concentration. A difference can be found in the streamlines of the simulations. In figure 46 and 47 it can be seen that an increase in sediment size can also result in a reduction of recirculation at the junction. The recirculation is an obstacle that causes the filter pipe to have a "smaller" entry, which leads to higher pressure requirements for the jet in order to retain the same velocity. Since simulation 6 has a smaller recirculation, the required pressure is lower here.

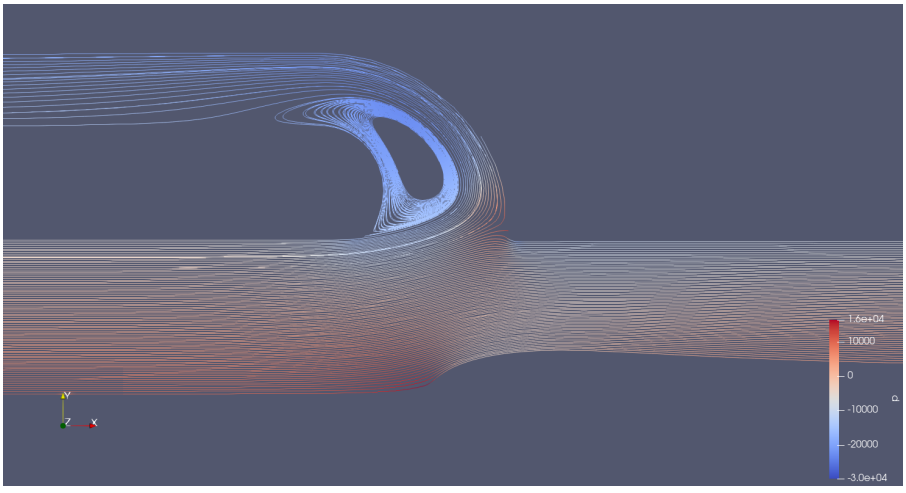

Figure 46: Streamline at junction of simulation 2 which has fine sediment

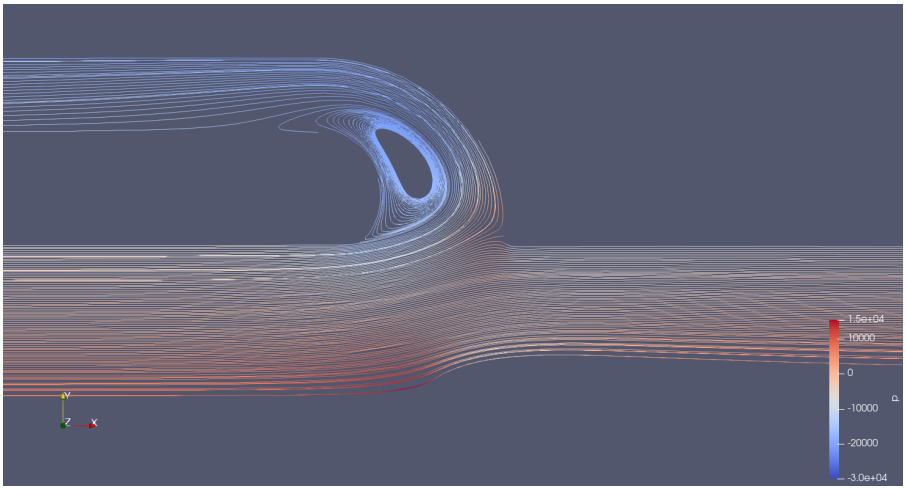

Figure 47: Streamline at junction of simulation 6 which has coarse sediment

Additionally, the concentration affects the pressure mostly when there is fine sediment. This can be explained since an increase in concentration causes the mixture density of the fluid to increase. However, coarse particles do not cause a strong increase of pressure at higher concentration because they settle and create a moving bed. This leads to the mixture above the bed to mostly consists of water. Figures 48 and 49 show the concentration profile for fine and coarse particles respectively. This shows that the coarse particle cause a far less homogeneous flow profile than the fine particles.

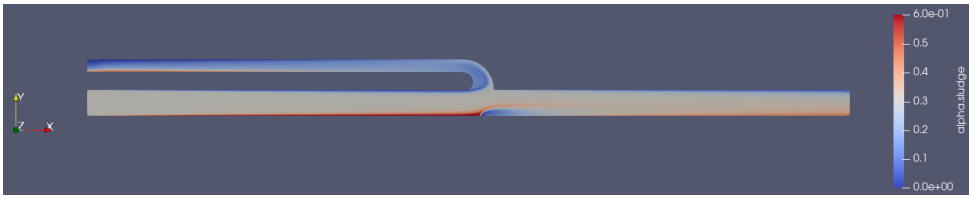

Figure 48: Concentration profile of simulation 2, which has fine particles

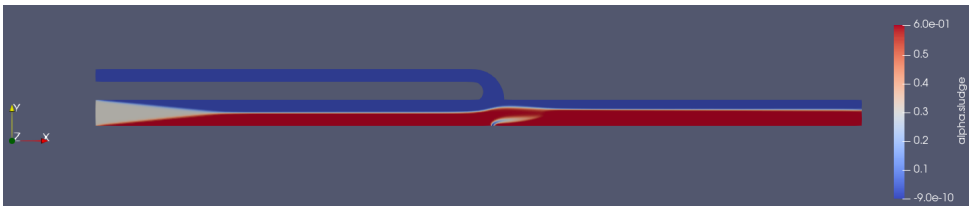

Figure 49: Concentration profile of simulation 6, which has coarse particles

From this analysis it can be seen that the behaviour of the inlet pressure does behave as expected for a low inlet velocity. This shows that in this range the values are trustworthy and further analysis between input variables and pressure is appropriate.

A linear fitting of the data is created with Matlabs "fitlm" function. Through the function the following are done. Firstly, the data is visually plotted with a fitted line which aids in the determination whether the line approximates the data. Secondly the R-squared value can be gained. This will numerically show how much the linear line overlaps with the given data. The value of R^2 can be between 1 and 0, where the line overlaps the data accurately for $R^2 = 1$, and it does not overlap it accurately for $R^2 = 0$. Secondly the p-value is given. This will reveal how relevant each input variable is on the output data. The lower the p-value is for a certain variable, the higher the impact that variable has. In this research a variable is considered essential if the p-value is below 0.05.

The linear fitting is done for the inlet and jet pressure. The input variables are the jet velocity, sediment size and sediment concentration. Plotting the inlet pressure over the jet velocity, sediment size and concentration individually in figures 50, 51 and 52 reveals the following.

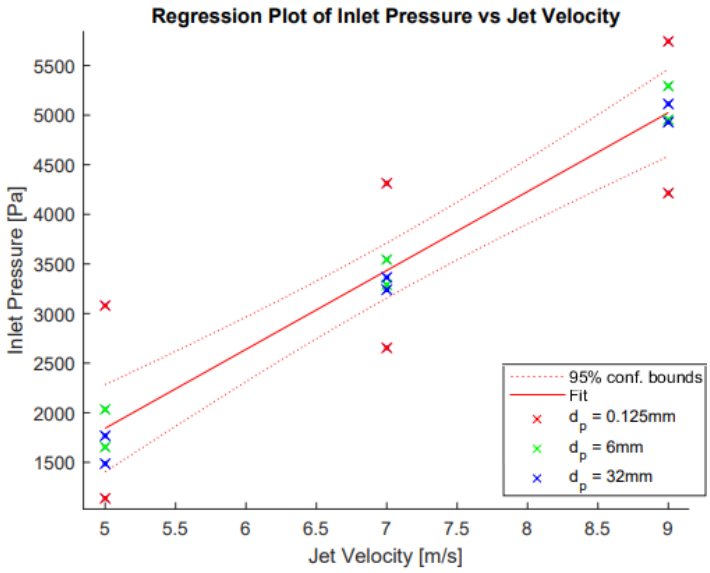

Figure 50: Regression line of inlet pressure over jet velocity

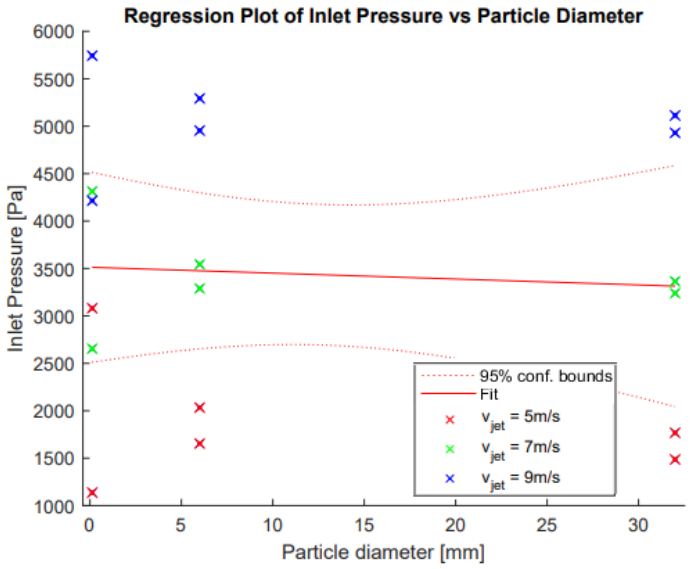

Figure 51: Regression line of inlet pressure over sediment size

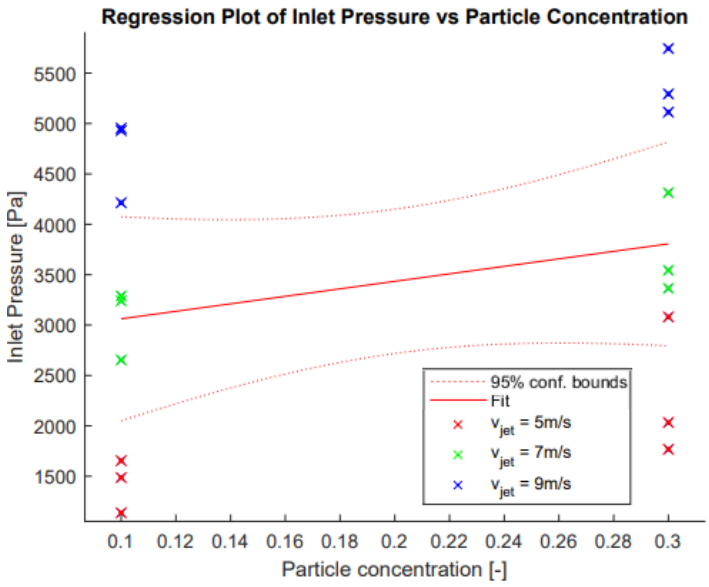

Figure 52: Regression line of inlet pressure over sediment concentration

Each figure shows the inlet pressure for different jet velocities, particle diameter and concentration. The data points have different colours to distinguish the effect of multiple input variables. These regression lines show the relation between each input variable on the inlet pressure. The effectiveness of each input variable is determined by the steepness of the regression line, as a steep line is strongly affected by said variable. However, many of data points far away from the regression line, thus a multi regression line is made with the following linear regression model:

$$y = \beta_0 + \beta_1 v_{jet} + \beta_2 d_p + \beta_3 c_p + \epsilon$$

Where y is the output data, β_0 is the coefficient for the constant term, which represents the output value if all the input values are set to zero. β_n is the coefficient for the input variables, which is the value the output data increases with if the input variable increases by one. And lastly ϵ is the error of the fitted line with the data. From the regression model the following equation is created with its coefficient and p-value shown in table 14.

$$p_{inlet} = -2798.2 + 795.34 v_{jet} - 6.2059 d_p + 3718.5 c_p + \epsilon$$

Variable	Coefficient	pValue
β_0	-2798.2	3.8379e-05
v_{jet}	795.34	2.0603e-09
d_p	-6.2059	0.38717
c_p	3718.5	0.0017284

Table 14: Regression coefficients and statistics for the inlet pressure

It can be seen here that the p-value for the coefficient, v_{jet} and c_p is lower than 0.05. This means that the relation between these values and the inlet pressure is significant and will be used in the formula in order to create the finalised formula. The new regression equation and table can be found below:

$$p_{inlet} = -2877.2 + 795.34 v_{jet} + 3718.5 c_p + \epsilon$$

This regression equation has a R^2 value of 0.93, which proves that the line has a good fitting. This is also visualised in figure 53.

Variable	Coefficient	pValue
β_0	-2877	1.6357e-05
v_{jet}	795.34	7.8428e-10
c_p	3718.5	0.0014571

Table 15: Adjusted regression coefficients and statistics for the inlet pressure

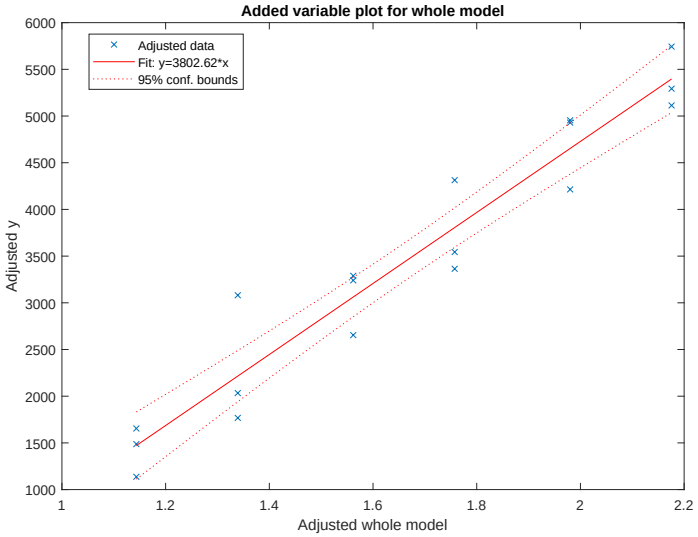

Figure 53: Comparison of inlet pressure with regression line

The same is applied for the jet pressure and the following formula and table is created.

$$p_{jet} = 7840.5 + 5737.8c_p + 6.2769v_{jet}d_p + \epsilon$$

Variable	Estimate	pValue
β_0	7840.5	2.7642e-10
c_p	5737.8	0.021314
$v_{jet}d_p$	6.2769	0.01193

Table 16: Regression coefficients and statistics for jet pressure

This regression equation has a R^2 value of 0.496, which is relatively low. However, when looking at the plot in figure 54 it can be seen that the regression line follows the data generally except for a few outliers.

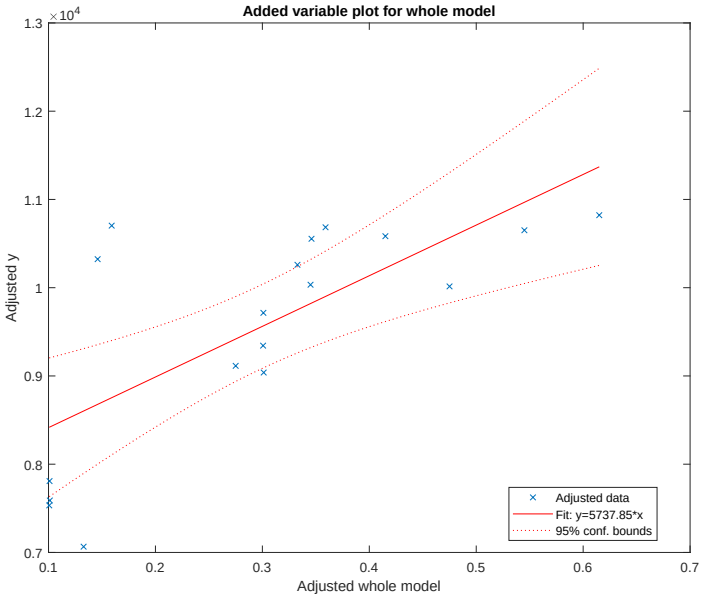

Figure 54: Comparison of jet pressure with regression line

From this data it can be summarised that the inlet pressure is mostly affected by the jet velocity and particle concentration, whilst the jet pressure is mostly affected by the particle concentration and the interaction of jet velocity with the particle size.

Next the relationship between input variable and particle containment will be made for all 54 simulations. The effect of each input variable will first be visualised individually through the use of column diagrams. The diagrams will have sets of columns where each set of columns will have the exact same input values, except for one variable where a low, medium or high value is filled in. The height of each diagram shows the percentage of particles that are contained in the system. The diagrams showing the effect of inlet velocity, jet velocity, sediment size and concentration are visualised in figure 55, 56, 57 and 58 respectively.

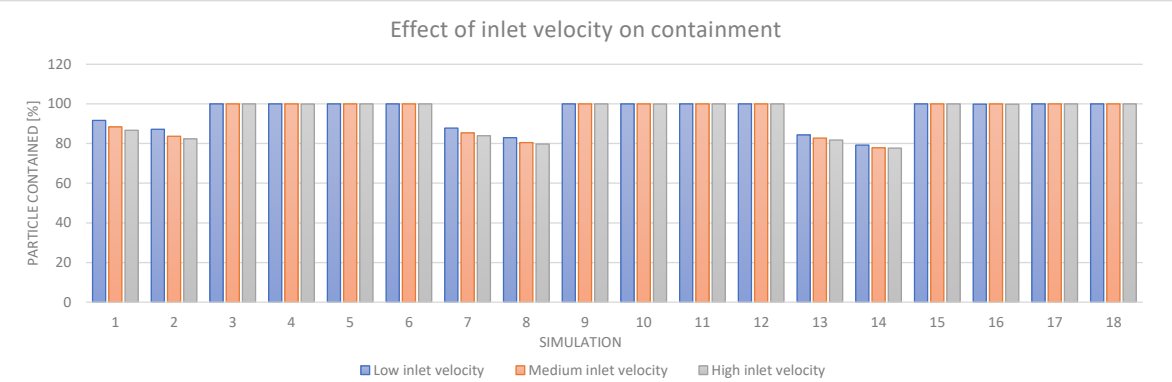

Figure 55: Percentage of particle contained based on inlet velocity

Figure 55 shows a reduction in particle containment with an increase in inlet velocity. Two phenomenon take place when increasing the inlet velocity, firstly, a higher percentage of fluid leaves through the outlet. Since the fluid drags the particles, more fluid leaving through the outlet causes the amount of contained particles to increase. Secondly, the particles move faster and reach the junction faster, resulting in less settling of the particles. Thus the particles are at a higher height when reaching the junction, which increases the amount of particles that are pushed up and separated. Since the particle containment decreases as the inlet velocity increases, it means that the second phenomenon has a more dominant effect than the first one. Furthermore, the reduction of particle containment is not linearly correlated with the inlet velocity as some cases give nearly

the same containment for medium and high inlet velocities. This is likely caused by the two phenomena working against each other.

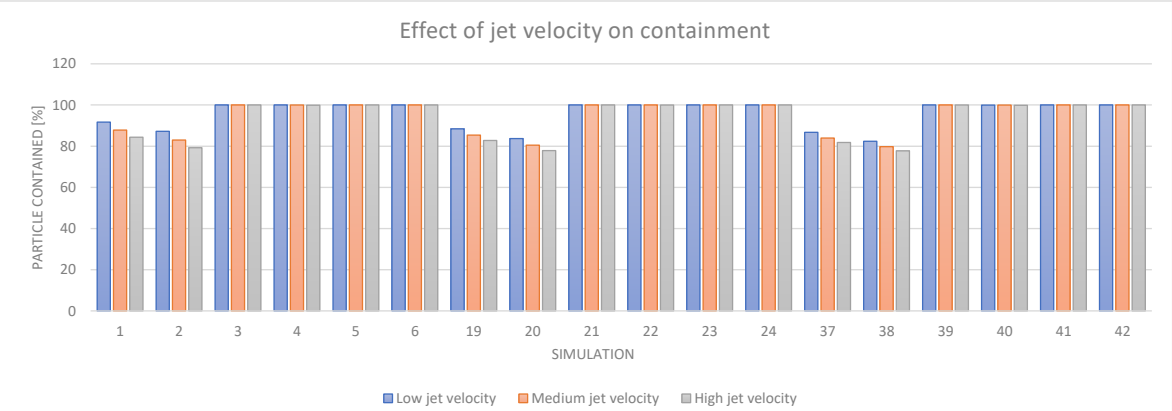

Figure 56: Percentage of particle contained based on jet velocity

In figure 56 the relation between jet velocity and particle containment is shown to be very straightforward. As the velocity of the jet increases, more particles are pushed up and released through the filter outlet. Unlike the inlet velocity, an increase in jet velocity seems to be linearly correlated with a reduction in particle containment.

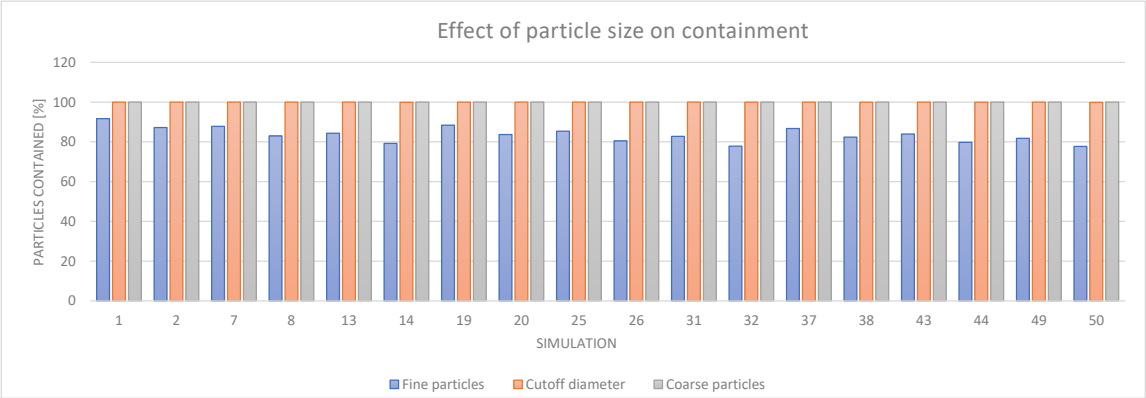

Figure 57: Percentage of particle contained based on sediment size

The figure 57 shows a strong increase in containment for larger particles sizes. The increase in settling velocity plays a strong role in this, which brings particles at a lower height when reaching the junction. The lower a particle is located in the junction, the more power is required from the jet in order to push it up to the filter. Additionally, the larger particles are less drag dominated and more inertia dominated. which reduces the influence of the flow on the particle.

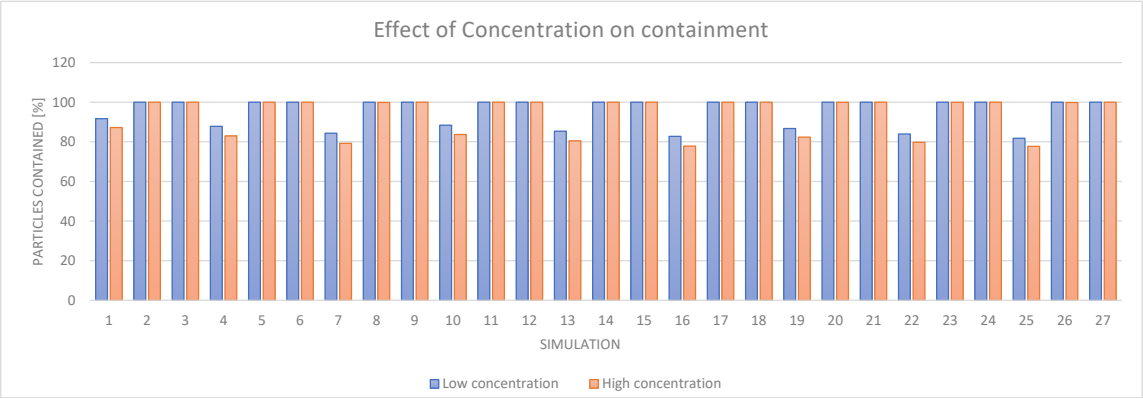

Figure 58: Percentage of particle contained based on sediment concentration

Lastly, figure 58 shows a reduction of containment with higher concentrations. This is caused by the effect of hindered particle settling velocity. As the particle settles less, it is easier for it to be pushed into the filter by the jet.

It was also noticed that in the paper of A. Pukkella et al (2019)[28] that an increase in concentration also reduced the particle containment in the bend separator. Which is expected to be caused by the particle-particle interaction with the increasing concentration.

Now that the effect of the individual input variables are clear, these will be combined in order to create two contour plots which summarise the effect of the input variables. Particles of the size 6 and 32mm, which is the cutoff diameter and coarse particle size respectively, always have a containment of 100% and thus are not included in the contour plot, this can be seen in figure 57. Thus the contour plots will visualise the particle containment based on the inlet, jet velocity and concentration. Figure 59a shows the contour plot for a concentration of 10% and figure 59b show this for a concentration of 30%. From the contour plot it is seen that the jet velocity has the highest impact on the particle containment, thus the jet velocity is the strongest operational parameter which affects the effectivity of the separation process.

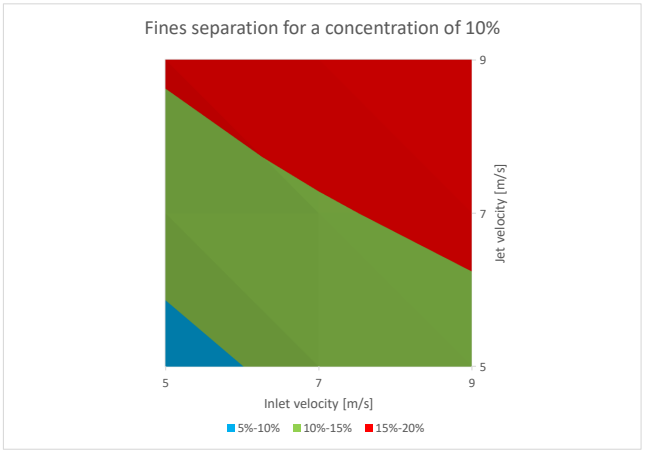

(a) Fines separation with concentration of 10%

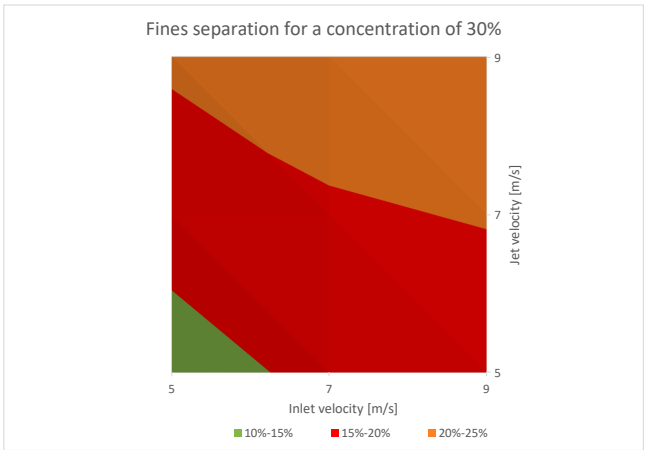

(b) Fines separation with concentration of 30%

Figure 59: Contour plot of the percentage of fines separated

In figure 55 it was expected to gain an increase in sediment containment as the inlet velocity increases. The reason for this expectation is because the percentage of fluid that leaves through the outlet would be increased. And since the fluid carries particles it was expected that the particle containment would be increased. Thus figure 60 is created which visualises the percentage of the flow passing through the outlet based on the inlet velocity.

This is calculated with the following formula.

$$Q_{OutletRatio} = \frac{\dot{Q}_{outlet}}{\dot{Q}_{inlet} + \dot{Q}_{jet}}$$

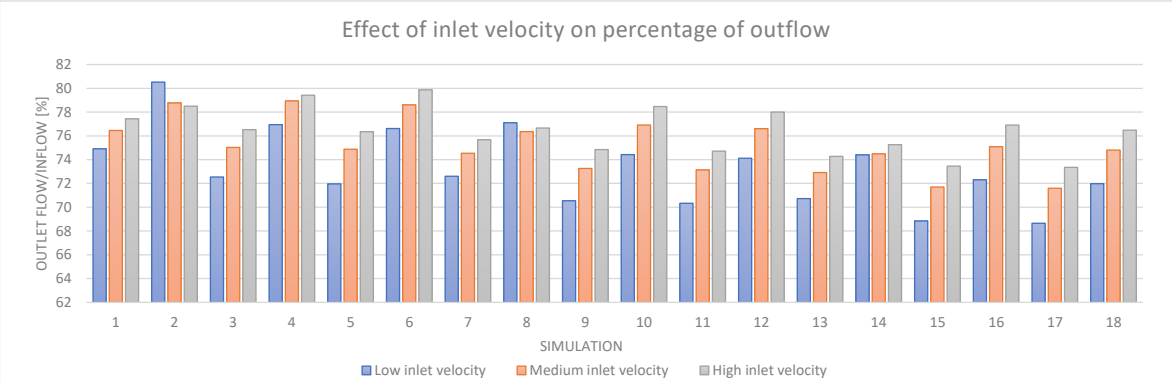

Figure 60: Percentage of inflow that is released in the outlet based on the inlet velocity

Increasing the inlet velocity from low to high results in an average flow increase of approximately 3.1% at the outlet. This is a relatively small increase for almost doubling the inlet velocity, which explains the limited influence of this phenomenon.

Next the influence of the jet velocity on the percentage of fluid which leaves thorugh the outlet has been visualised in figure 61.

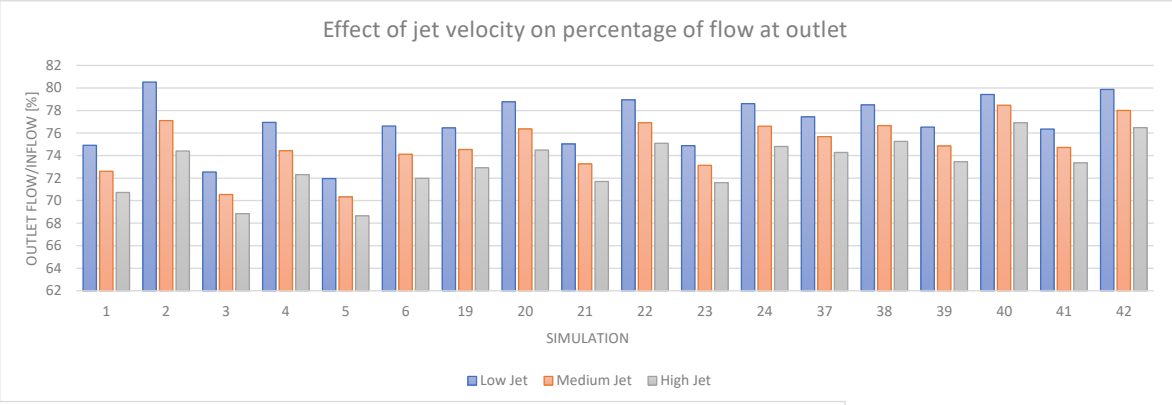

Figure 61: Percentage of inflow that is released in the outlet based on the jet velocity

Here it can be seen that the jet velocity has a stronger effect on the percentage of flow through the outlet, whilst the diameter of the jet is 10 times smaller than that of the outlet and thus has a relatively low volume flow. The average decrease in the ratio between the outlet and inlet volume flow is 3.7%. When the outlet flow percentage needs to be adapted, a change in the jet velocity or ratio between jet and inlet velocity can be used.

This effect is further visualised through the use of ink. This is achieved by adding sediment which has no settling velocity and a neutral density. Meaning that its density is equal to that of the fluid. Because of this, the sediment will follow the fluids streamlines, making it behave like ink. Through the use of ink at the inlet, it is possible to visually track the flow from here, making it possible to visualise the fluid distribution throughout the flow. This research will be done for the configuration with the highest potential, which is configuration 50 as this has the least fines containment, which is shown in table 13. The inlet and jet velocity of the configuration will be adjusted in order to see the effects on the flow field. In the figure 62 below the pipeline is shown where the concentration is visualised. The colour of the ink is red and the colour of the fluid is blue, thus the redder an

area is, the more ink it has. Since the ink is introduced from the inlet, all red areas consist of purely or majorily fluid from the inlet. In the figures below the two extreme conditions are visualised by using the minimum and maximum velocity for the inlet and jet. The first figure includes an inlet velocity of 5 m/s and a jet velocity of 9 m/s. The second figure has an inlet velocity of 9 m/s and a jet velocity of 5m/s.

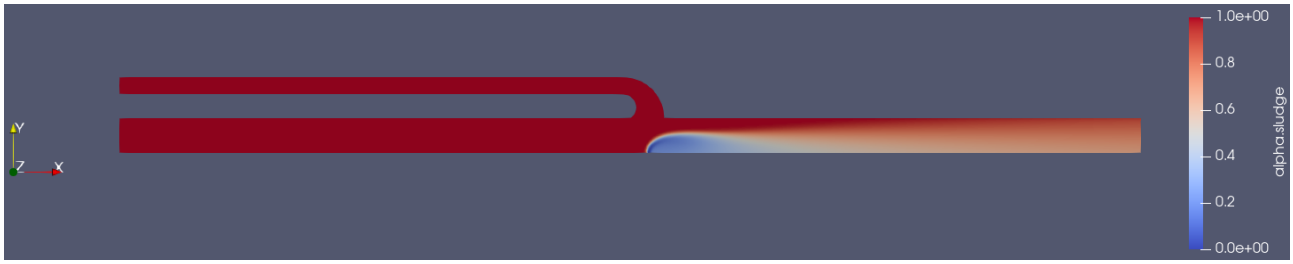

(a) Ink with inlet velocity of 5 m/s, jet velocity of 9 m/s

(b) Ink with inlet velocity of 9 m/s, jet velocity of 5 m/s

Figure 62: Pipe with red ink introduced at the inlet

These figures reveal that the percentage of ink is 100% everywhere except between the jet and outlet. This implies that the water from the jet is solely directed towards the outlet as the jet water only thins out the concentration in this area. This is not surprising as the flow from the inlet is pushing the fluid from the jet towards the outlet. Especially since the inlet opening is 10 times larger than the jet opening, thus the volume flow is larger. This leads to the flow of the inlet dominating the flow from the jet, causing it to bend towards the outlet.

The flow has also been visualised using streamlines to further proof this. First streamlines originating from the inlet have been visualised in figure 63, and in figure 64 it has been visualised for the flow from the jet. Here the velocity profile is shown of the pipe with white lines visualising the streamline from either the inlet or jet.

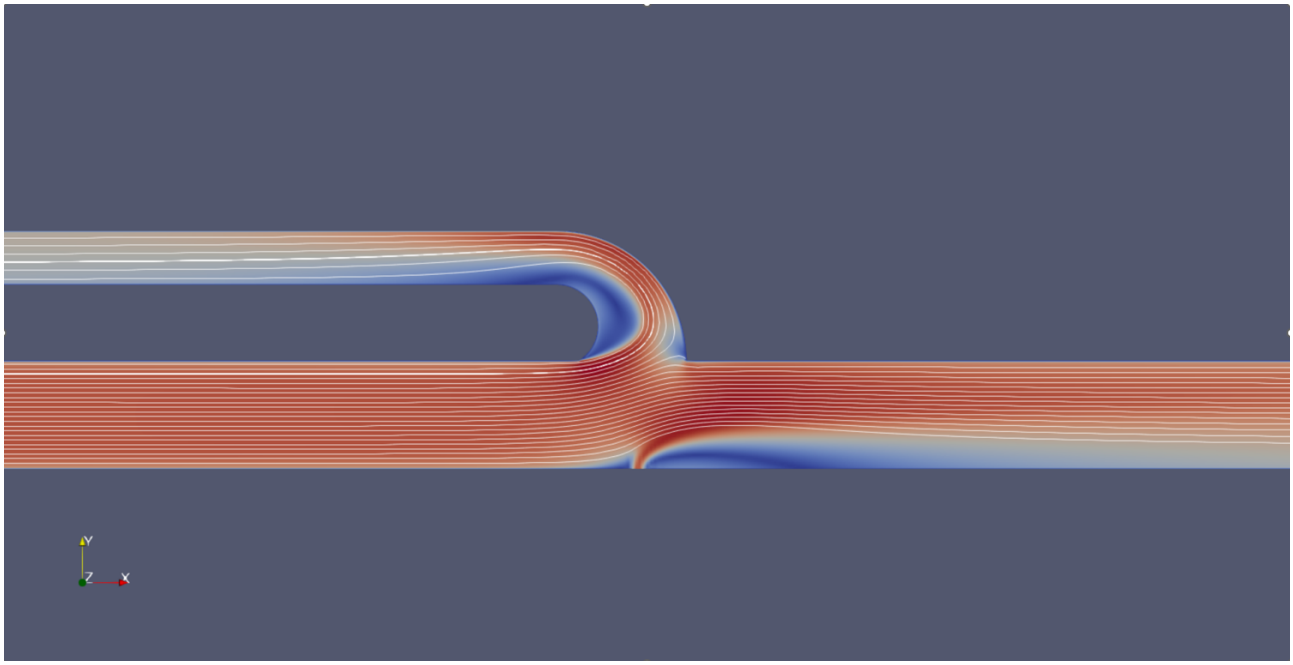

Figure 63: Flow with streamline of the fluid from the inlet

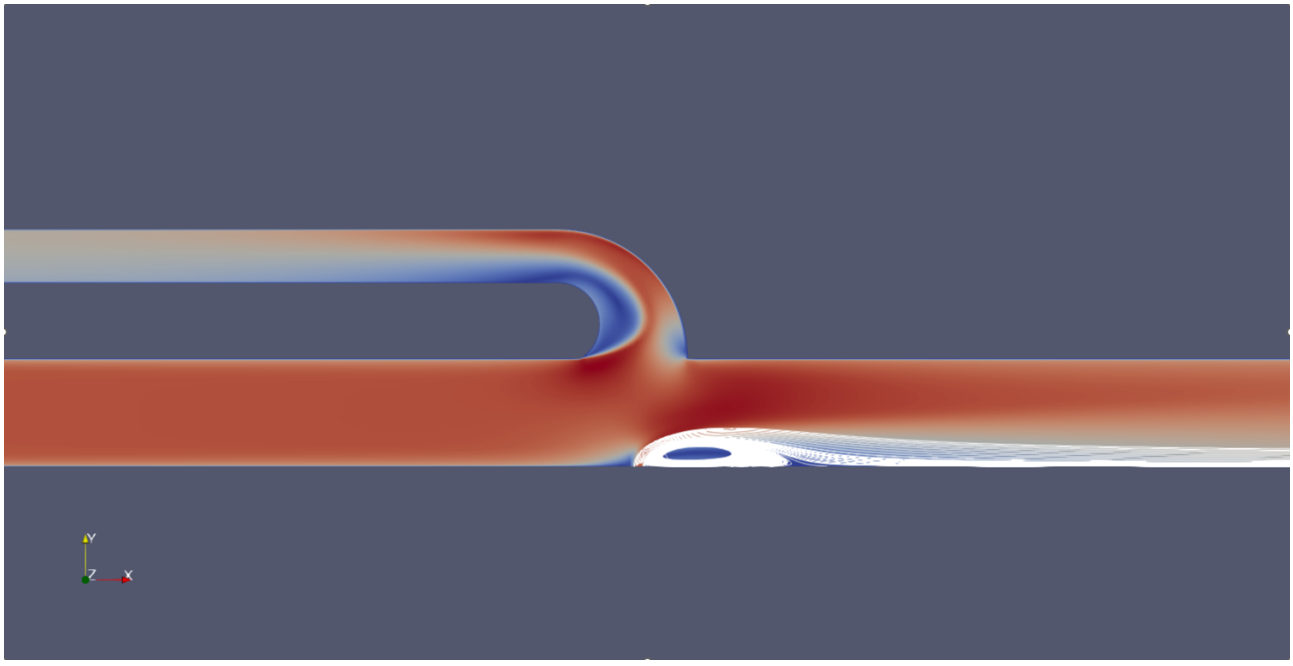

Figure 64: Flow with streamline of the fluid from the jet

These figures visualise that the streamlines of the jet do bend sharply towards the outlet. Additionally, it shows that the streamlines at the filter outlet purely originate from the inlet, and the streamlines at the outlet consists of those originating from both the inlet and jet.

Figures 62a and 62b show that an increase in jet velocity reduces the concentration at the outlet. This implies that the fluid from the jet replaces the ink. Therefore, the excess fluid from the inlet must seek an alternative path, which is the filter outlet. Therefore, increasing the jet velocity leads to an increase in fluid velocity at the filter outlet. This is verified in figure 65 which visualises the volume flow at the filter outlet with increasing inlet and jet velocities.

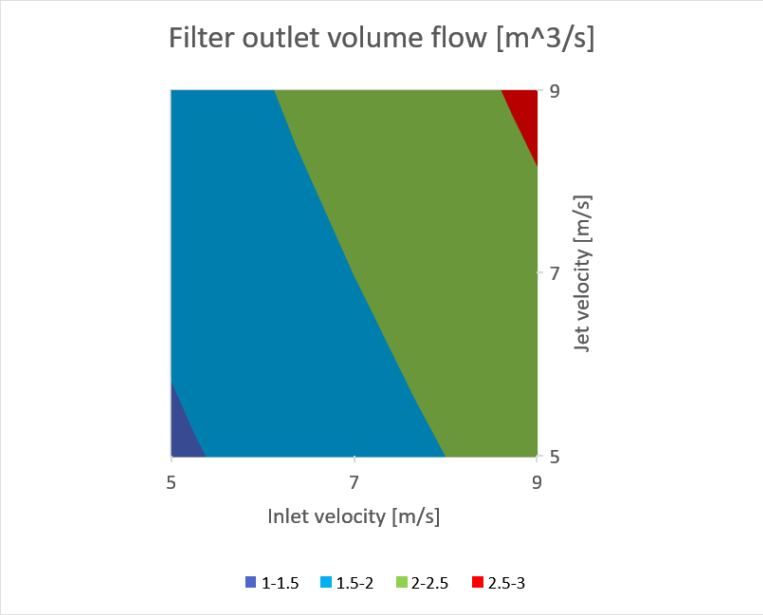

Figure 65: Volume flow of filter outlet based on inlet and jet velocity

Additionally the same data has been visualised for the outlet in figure 66.

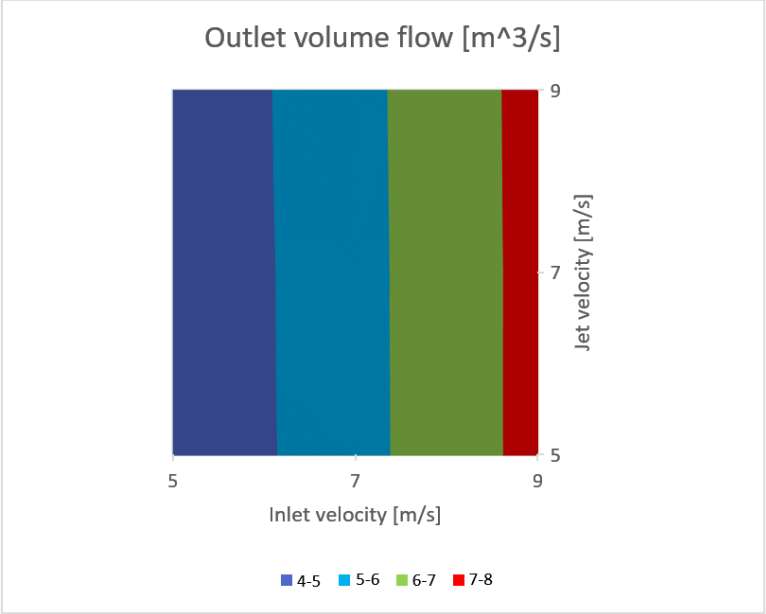

Figure 66: Volume flow of outlet based on inlet and jet velocity

This reveals that the jet velocity does not increase the outlet volume flow. This is in line with the anticipated outcome as it was predicted that the fluid from the jet replaces the ink from the inlet, which leads to a constant volume flow.

Lastly the percentage of the inlet massflow in the outlet is shown with figure 67. This is calculated by taking the difference between the inlet and filter outlet massflow and dividing it with the outlet massflow as shown in the formula below.

$$\dot{M}_{ratio} = \frac{\dot{M}_{inlet} - \dot{M}_{filter,outlet}}{\dot{M}_{outlet}}$$

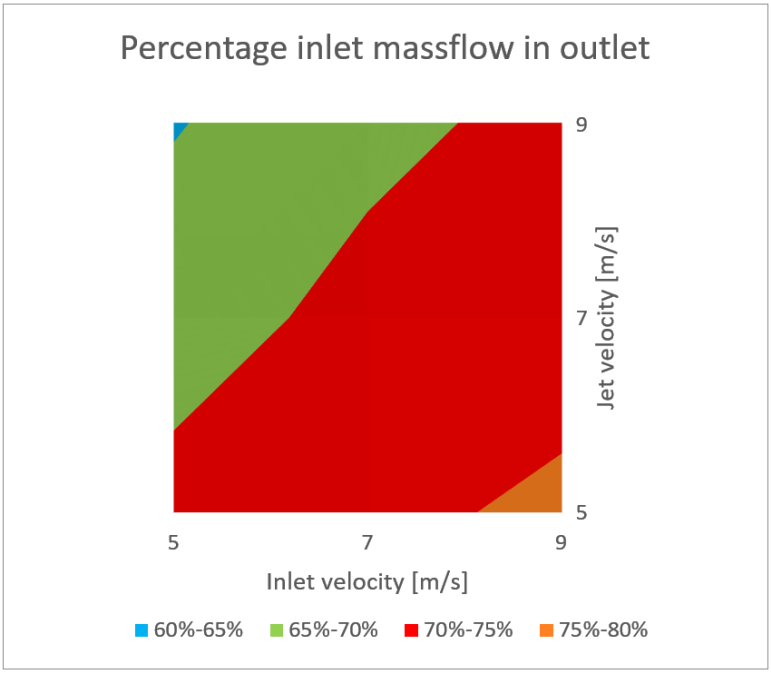

Figure 67: Percentage of inlet that goes to the outlet

This figure reveals that the percentage of the inlet going through the outlet increases with higher inlet velocities and lower jet velocities. Which was also established in figure 61 which showed a decrease in the ratio of inlet flow in the outlet for every configuration when the jet velocity is increased.

Another noticeable occurrence is the concentration profile where the inlet and jet velocity are equal. These all look identical and thus this is tested by examining the concentration at the outlet for these conditions. The concentration is observed instead of the massflow to exclude the effect of the velocity. By checking the concentration it is possible to see whether the absolute value of the flow has a significant effect on the spread of the ink. This is shown in table 17 below.

Inlet and jet velocity [m/s]	Outlet concentration
5	26.20 %
7	26.19 %
9	26.17 %

Table 17: Outlet concentration at different inlet and jet velocities

The difference between the highest and lowest value is $(\frac{0.2619803}{0.2617483} - 1) * 100\% = 0.088\%$, which happens when almost doubling the absolute velocity. This difference in concentration is extremely low, thus it can be concluded that the distribution of the fluid and the flow field are near equal when the inlet and jet velocity are equal.

In figure 57 it has been observed that there is a relatively high containment of particles. Particles of the size of 6 mm and above have a containment near 100%. This means that at that magnitude, increasing the particle size from 6 mm to a higher diameter will have negligible improvements on the containment. The reason for this would be that the cutoff diameter of the system is smaller than 6 mm. Additionally the containment for particles of a size of 0mm have been simulated, which reveals the theoretical minimum containment of particles. These particles have no settling velocity and result in 70% not being separated from the system. With this additional data a graph has been created which visualises the relation between particle containment and particle size in figure 68. Here the maximum, average and minimum particle containment for each particle size has been visualised. The dots show the result for the simulation and the lines shows a linear interpolation between these dots.

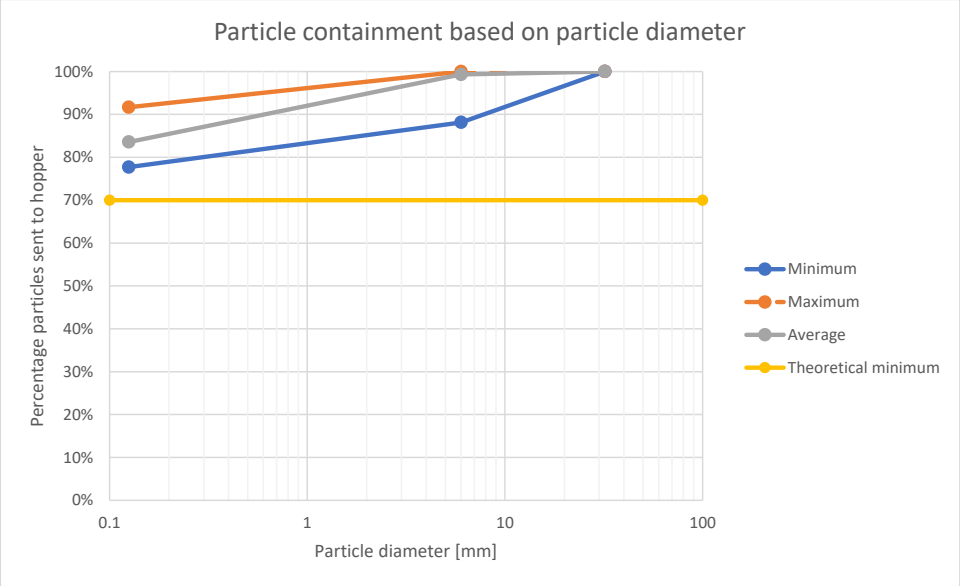

Figure 68: Particle containment over particle diameter

The results are not pleasing as the system cannot filter more than 30% of the fines in its current state. And the cutoff diameter of the system is smaller than 6 mm, which is lower than desired. This is an issue as the majority of the seabed in gravel deposits is fine. Up to 80% of the seabed can consists of fine sediment. Since the majority of the sediment is fine, it would be more beneficial to have a cutoff diameter higher than 6 mm than having it below. If the cutoff diameter is above 6 mm, then most fines will be filtered from the system and some of the coarse particles will as well. However, if the cutoff diameter is smaller than 6 mm then many fines will still stay in the system and be pumped to the ship.

In order to increase the cutoff diameter, the following actions can be taken. The recirculation at the junction can be reduced to increase the percentage of the flow going through the filter. There is a recirculation that covers over half of the filter pipe at the junction as shown in figures 46, 47 and 63. If this were to be reduced, the flow through the filter would be substantially increased. This will increase the cutoff diameter as the drag force upwards will be increased, and this will reduce the containment of particles as well. One of the reason why such a large recirculation occurs is because the flow needs to make an abrupt turn, thus making the bend radius larger could give the flow more time and space to turn. This can also be solved by increasing the jet velocity, which aids in bending the flow upwards.

A second option is to place the junction at an earlier location of the pipe. In the results above it has been observed that giving particles less time to settle will result in a lower containment of particles. This is great since the initial plan is to have the junction as close to the draghead as possible, but in the simulations this was placed far more behind in order to ensure stability. However, it should be noted that placing the junction too close to the draghead could lead to the cutoff diameter becoming too large, thus a balance should be sought for the location of the junction. Currently the junction is 15 meters away from the draghead and it would interesting to see how the system would react if this is reduced to 10 meters or 5 meters, however this also increases the risk of instabilities occuring as it nears the boundary condition of the inlet. As seen in figure 49, the coarse sediment takes around 5 meters to settle down whilst figure 48 shows that most of the fines have not settled yet at that distance. An additional benefit of moving the separation system closer to the draghead is that the unwanted fines will be separated from the system earlier, which reduces the energy requirements of the system. Furthermore, the length of the return flow pipe is reduced. When the pipe length is reduced, then so is the frictional resistance caused by the pipe. Thus the pump will be able to operate using less power. If the cutoff diameter can be increased to 6mm with these improvements, then the majority of the fines would be removed from the system, whilst losing a small fraction of the coarse sediment.

6 Discussion

6.1 Results analysis

Before comparing the results of each configuration, it is of importance to discuss the reason to use a separator inside the pipeline. The goal of this separation method is to improve the system by reducing or removing the following issues.

1. When dredging gravel the system pumps unwanted sand. The energy used to pump the sand is a waste as this is returned to the seabed.
2. The fine sand is returned to the seabed by dropping it off the ship. The fines are not directly released on the seabed and thus becomes a suspension cloud which sink slowly to the seabed.
3. In order to separate the gravel from the sand, a large sieve installation is required. This reduces the already limited space on board and also adds extra steps to the collection of gravel which is time consuming.

Each of the aforementioned issue can be broken down into a variable that can be checked.

1. The unwanted sand add weight to the slurry, making the pumps require more energy than when transporting pure coarse sediment. Removal of the fine sediment will reduce the strain on the pump and reduce the required pressure. Contrary to the fine sand, gravel needs to be retained in the system. The less gravel leaves the system, the more favourable it is. Thus the variable that will be checked is the percentage of fines that are removed and the percentage of coarse gravel that is retained.
   (a) However, high jet velocities in this system lead to high pump power requirements, thus limiting this is of interest.
2. A secondary pipe has been added which directs the separated fine sediment to the seabed. An increase of fines released through the secondary pipe will aid in lessening the environmental impact.
3. Similarly, the size of the sieve installation depends on the supply of fines. If this is reduced then the size of the installations can be reduced to retain more space on the ship.

For the decision of the best configuration the percentage of coarse particles contained and the percentage of fines removed will be reviewed. The pressure increase of the inlet and jet will not be reviewed as these did not provide realistic values.

All configuration with coarse particle have a particle containment of near 100%, thus these values are not compared with each other. However, the configurations with fine sediment do show fluctuation of their values based on its input values. In table 18 five configurations with the most filtered of fines are shown.

Run	Inlet Velocity	Jet Velocity	Sediment Size	Sediment Concentration	Particle separated
50	High	High	Fine	High	22.29%
32	Medium	High	Fine	High	22.15%
14	Low	High	Fine	High	20.76%
44	High	Medium	Fine	High	20.24%
26	Medium	Medium	Fine	High	19.51%

Table 18: Five configurations with the most fines separated

Upon examination it has been revealed that configuration 50 has the highest fines separation where 22.29% of the fines are separated from the system. Furthermore it is observed that the other 4 results have high similarities in their configuration. Firstly, the sediment concentration is always high, thus the sediment concentration is a dominant contributor in particle containment. Secondly, the jet velocity is frequently high, and sometimes medium. Therefore the jet velocity has a relatively high impact on particle containment as well. In all 54 configurations there are six configurations with a high jet velocity with fines, and three of these condition are in the top 5 of the best configurations. Lastly the inlet velocity is the only input parameter that has all three levels from low to high. The average of these is slightly above medium, thus a higher velocity does help with particle containment, but it is a minor factor compared to the rest.

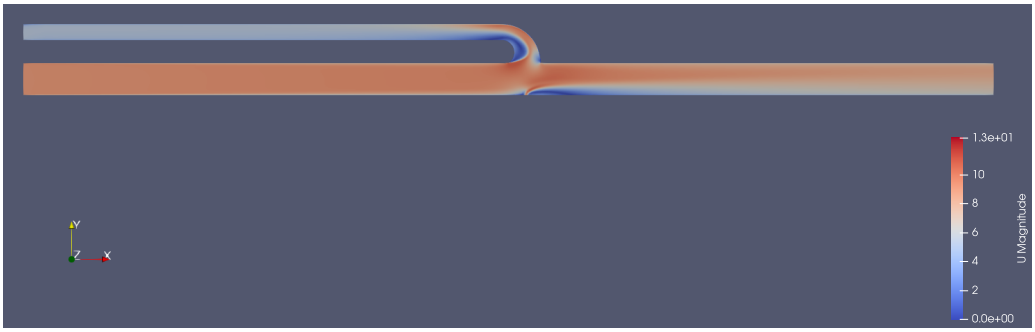

(a) Flow velocity throughout the pipe

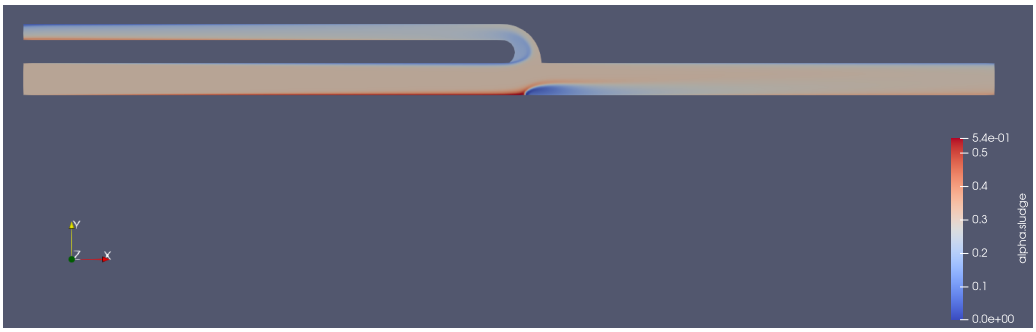

(b) Solids concentration throughout the pipe

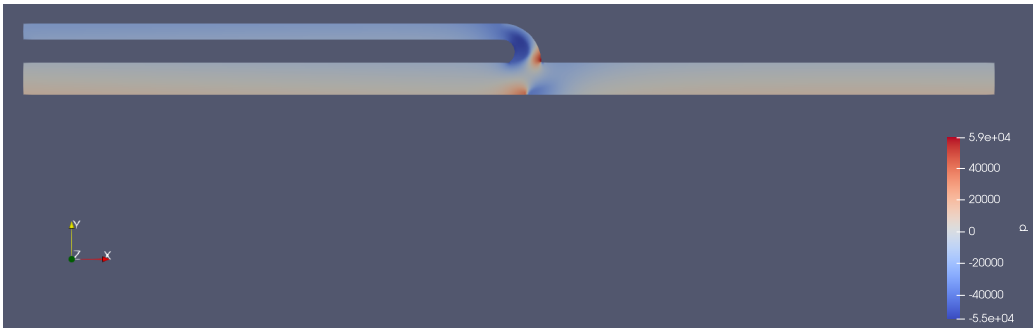

(c) Pressure throughout the pipe

Figure 69: Conditions throughout the pipe for configuration 50

In figure 69 the velocity, concentration and pressure throughout the pipe is shown for simulation 50, which is the best configuration. Here the development of the output data is smooth which confirms that the refinement of the simulation is sufficient. No unnatural effects occur at the junction that would be caused if this was located too close to the boundary conditions. The blue area near the junction in figure 69a is a recirculation that occurs because the flow is not able to closely follow the bend, this phenomenon has been visualised closely in figure 46 and 47.

For the solids concentration, which is shown in figure 69b, a red line starts to form at the bottom of the pipe. The solids settle at this area, causing the increased concentration. This figure clearly visualises the benefit of the jet as it pushes all the sediment up, enhancing the separation of the particles. This was also predicted during the multi-criteria analysis of the concepts done during the literature research. Here it was told that the jet would push particles away from the pipe, thus reducing the wear on the bottom of the pipe.

Lastly the pressure field throughout the pipe can be seen in 69c. There are two points of high pressure gradients. Firstly at the jet the pressure increases strongly. This occurs due to the jet acting as an obstacle for the main flow, which bends the flow direction at this location. Secondly, a very low pressure can be found just above the junction. Normally this is great as the flow goes from high to low pressure, thus causing the fluid to be sucked up into the pipe. But this location also has recirculation, thus blocking the opening partially.

6.2 System improvement

As the separation efficiency is below the desired results, improvements for the system will be discussed which increase the performance. Based on the results two phenomena are observed which reduce the separation efficiency. These phenomena are the recirculation at the junction and the settling of particles. The influence of these phenomena is reduced by increasing the jet velocity. The jet pushes the flow upwards, which aids the flow with following the pipes bend. And increasing the jet velocity also pushes the particles higher, thus allowing particles located low in the junction to be pushed up to the return pipe. The jet velocity will be increased to 20 and 40 m/s to test whether the systems performance will be improved significantly.

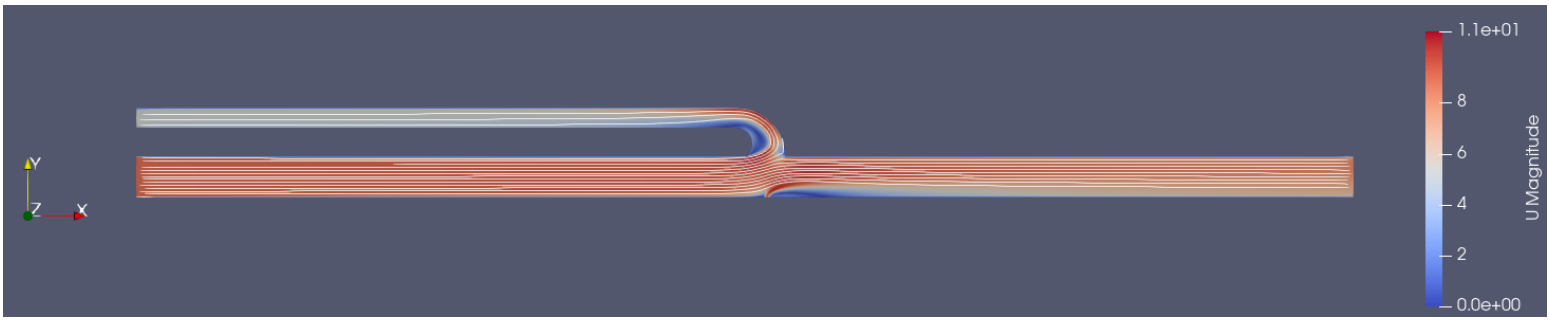

(a) Flow velocity throughout the pipe with jet velocity of 9 m/s

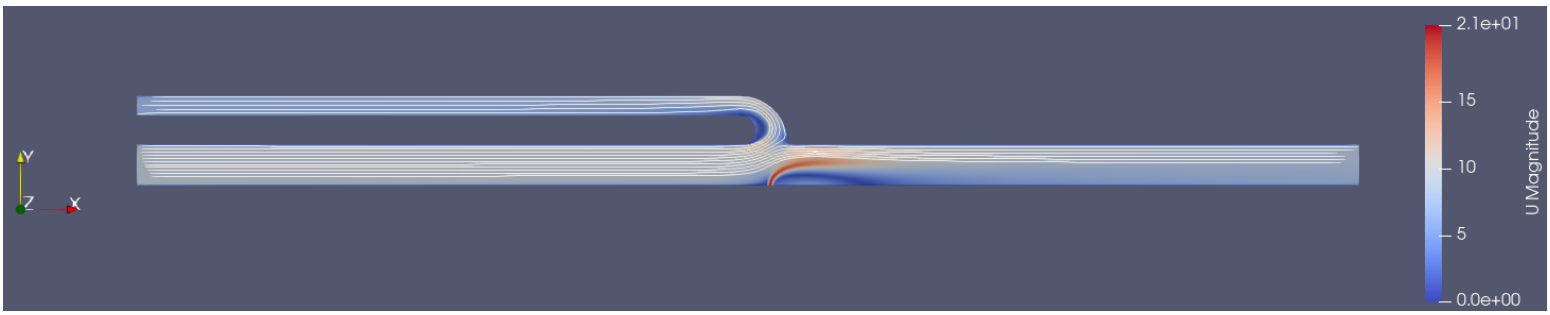

(b) Flow velocity throughout the pipe with jet velocity of 20 m/s

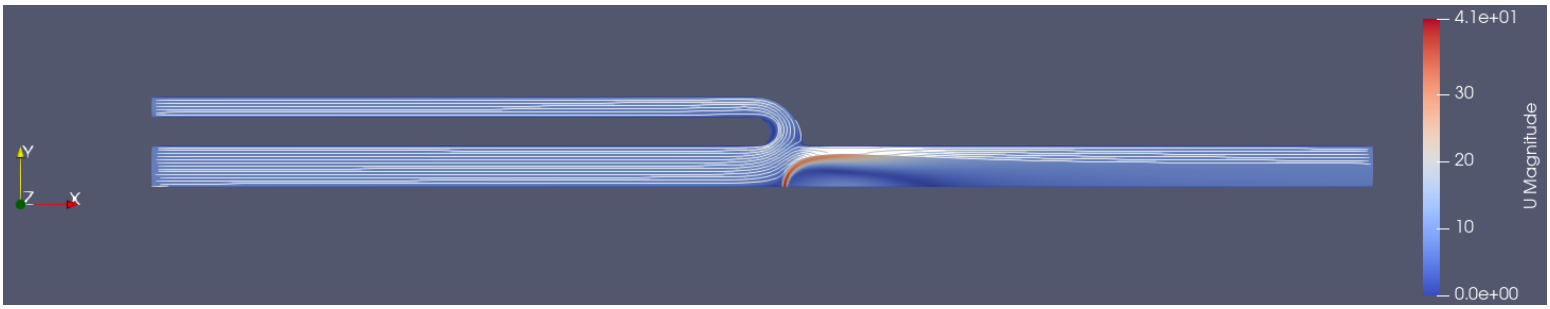

(c) Flow velocity throughout the pipe with jet velocity of 40 m/s

Figure 70: Velocity profile throughout pipe with increasing jet velocity

In figure 70 the velocity profile and streamlines are visualised for a jet velocity of 9, 20 and 40m/s respectively. In these figures it is observed that more of flow from the inlet will be pushed up towards the retour pipe. When the jet velocity is increased to 40m/s the recirculation is strongly reduced.

The effect on the separation efficiency for these cases is visualised in figure 71 where the containment for different particles sizes is illustrated.

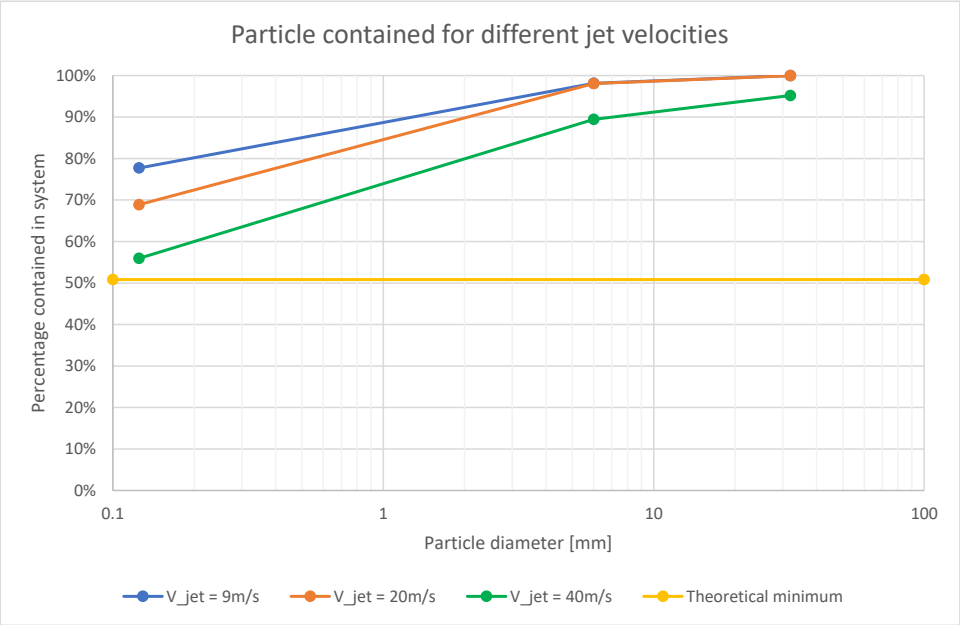

Figure 71: Particle separation for jet velocities of 9, 20 and 40 m/s

In figure 71 it can be seen that the increase in jet velocity eventually leads to a particle filtration of 50%, which is a satisfying result. It can also be seen in the figure that the jet velocity has a stronger impact on the separation of fines than the coarse particles. This leads to a high containment of coarser particles, which is a desired result.

However, in figure 70c it is observed that the jet is a large obstruction to the flow going to the outlet, which possibly reduces the outlet velocity. This has a risk of becoming too low to transport coarse particles, however figure 72 shows that the outlet velocity still increases when the jet velocity increases.

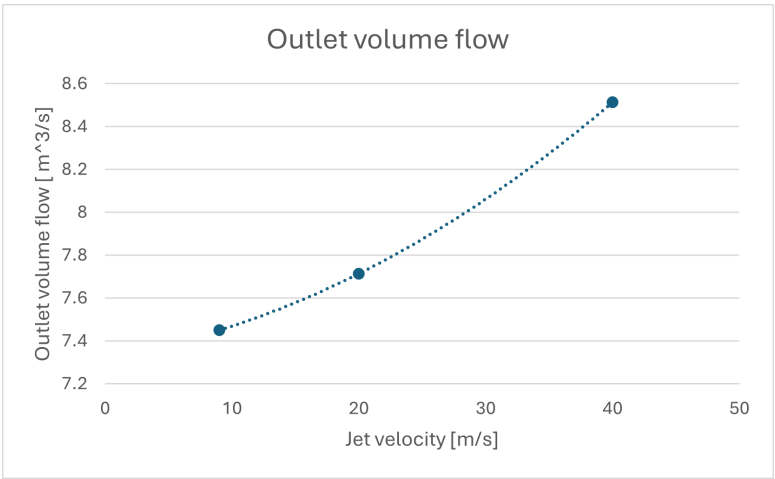

Figure 72: Outlet volume flow for jet velocities of 9, 20 and 40 m/s

Another improvement of the system can be realised by performing simulations on an angled pipe. Currently the research is done with a horizontal pipe. Here the gravity force is in the opposite direction of the jet force, thus hindering the separation process. When the pipe is at an angle, the gravity force will also be at an angle relative to the pipeline. This will reduce its hindrance against the separation process and make it possible for more sediment to be separated. In the most extreme case the pipe would be in a vertical position, where the gravitational force is parallel with the pipe, thus no longer pushing the particles away from the filter opening.

This effect is visualised in figure 73.

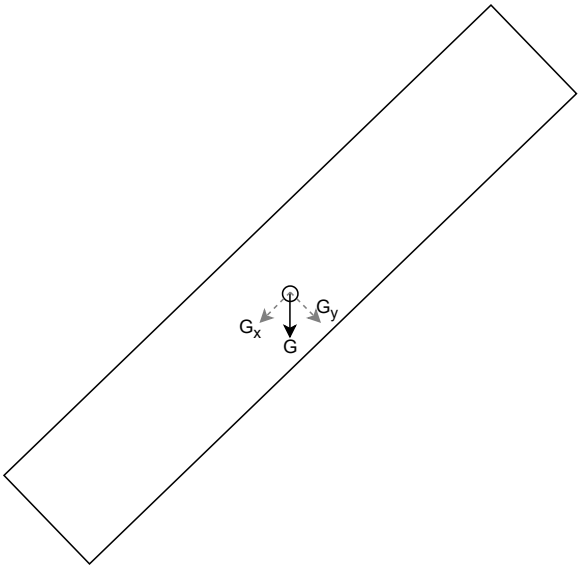

Figure 73: Effect of an angle on gravity

Since placing the pipe on an angle is both beneficial for the separation process and also closer to the situation in reality, it is interesting to simulate this effect. However, when trying this the simulation ended up becoming unstable. However, this can be solved with the following methods. The problem occurs at the end of the filter outlet, where the sediment piles up and quickly clogs. A possible cause for this issue is the fact that the filter outlet is at an angle with the gravity. This is expected since simulating the pipe at an angle of 0 or 90 degrees, has no issues. Thus bending the pipe right before the filter outlet to make it horizontal could possibly solve this issue. The original and adjusted bend pipe has been shown in figure 74.

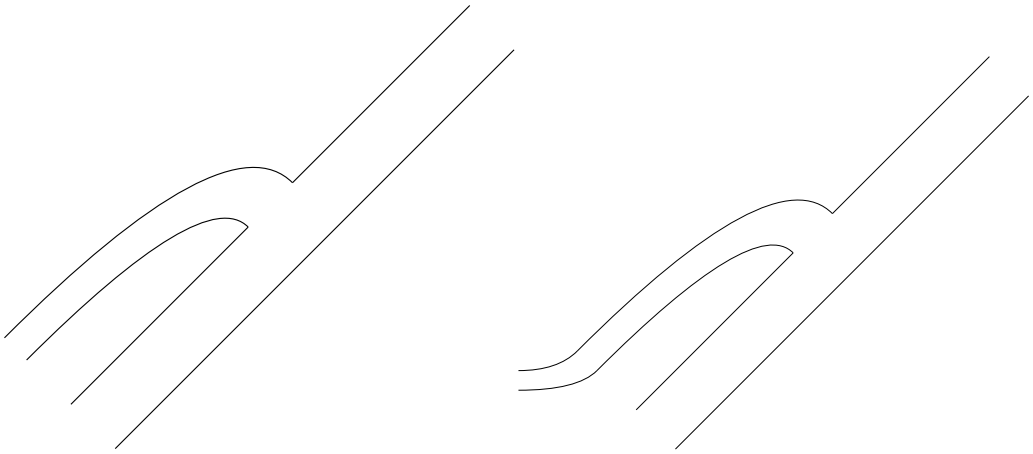

(a) Original pipe geometry

(b) Adjusted pipe geometry

Figure 74: Modification of pipe geometry

Bending the outlet to make it horizontal will mean that it is parallel to the seabed. However, dredging ships work with different sea depths, meaning that the pipes angle is not always the same. Therefore the outlet will not always be perfectly horizontal and face up or down at times. This is shown in figure 75.

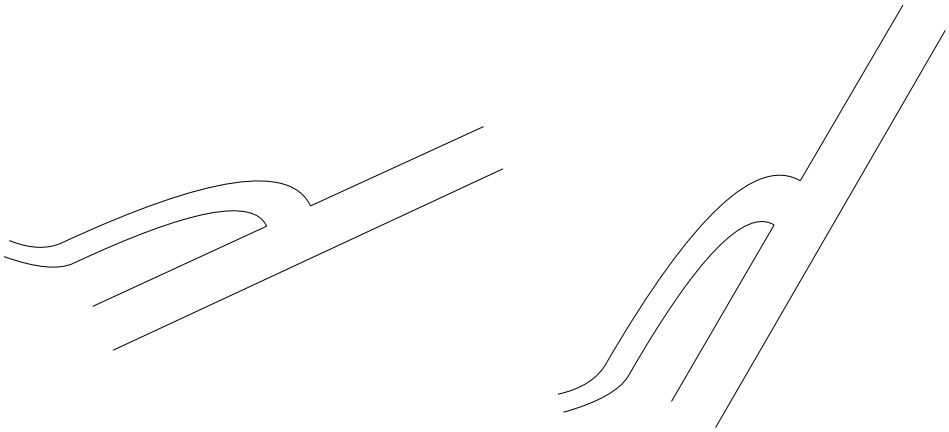

(a) Pipe with a small angle, causing the filter outlet to face upwards

(b) Pipe with a big angle, causing the filter outlet to face downwards

Figure 75: Adjusted pipe on two non-ideal angles

Therefore the pipe will not always release the fines perfectly horizontal. However in chapter 3.4 it was already mentioned that a flexible or partially flexible pipe could be used that is placed on the draghead. In order to make the exit parallel to the seabed, a visor, which is also used in the draghead, is required to change the angle of the flexible pipe to make this parallel to the seabed.

Another possible way to solve this is by cutting the filter outlet parallel to gravity. This would be simpler than the previous method as a bend is no longer required. This is easier to achieve but does not have the benefit of the first suggestion. Furthermore, if the pipe is cut at an angle, then the structured grid would be affected by this, causing it to become highly non-orthogonal. Thus to solve this, an unstructured grid should be used. In figure 76a, the pipes original situation is shown, which has perfect orthogonality. And figure 76b shows how the structured mesh adepts to cutting the pipe at an angle, which shows that the cells are non-orthogonal.

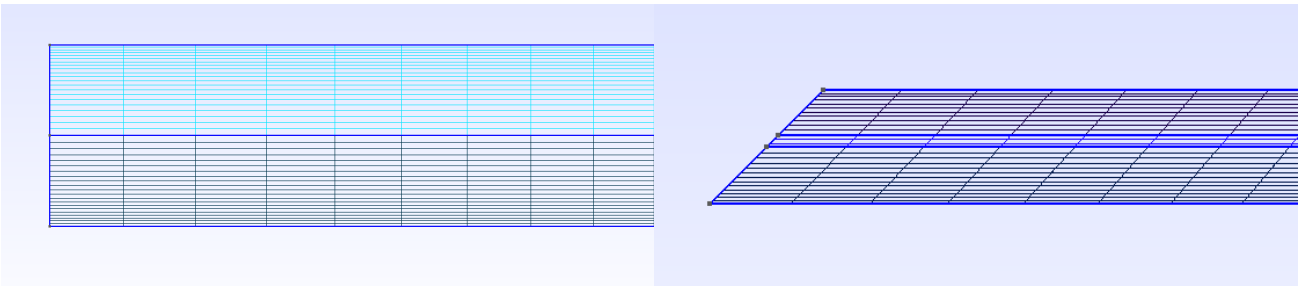

(a) Original filter outlet

(b) Adjusted filter outlet

Figure 76: Modification of filter outlet

And the last way to make an angled pipeline is by removing boundary condition at the filter outlet. Instead extend the geometry to include a portion of the open water which the fluid moves to when it leaves the pipeline. The additional benefit of this is the possibility to see the general behaviour of the sediment leaving the system and determine effects such as the travel distance based on the impulse. With this data a sensitivity analysis could be performed which shows the behaviour of the sediment plume based on the input variables. An interesting effect would be to apply a diffusor which increases the pipes diameter at the end. This reduces the impulse of the particles by reducing the flow velocity.

Lastly it should be mentioned that a the 2D simulation lacks certain aspects that can be gained through 3D simulations. For example the turbulent fluid behaviour 3D geometries. Additionally, in the 2D geometry the jet only causes a velocity upwards. But with 3D geometries the jet also causes recirculation in the 3rd dimension. The recirculation in the 3rd dimension has been visualised in figure 77.

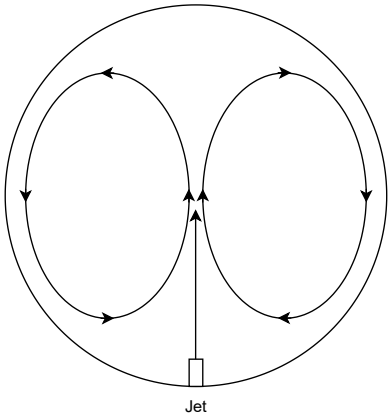

Figure 77: Effect of jet in 3D pipe

Thus 3D simulations add additional data which cannot be obtained through 2D simulations.

7 Conclusion and recommendations

The goal of this research is to determine whether underwater separation of fine and coarse sediment is possible with gravel dredging ships. Through the literature research the mechanism of dredging ships were investigated and it was decided that underwater separation could be done with a flow separator. The flow separator has been investigated further through simulations, which showed that around 22% of the unwanted sediment could be removed from the system. The most dominant operational contributor for the separation efficiency is the jet velocity, however this acts as an obstacle for the flow to the ship, thus increasing the systems power requirement. Improving the separation efficiency by further increasing the jet velocity increased the separation of sediment up to 50%, which makes this concept satisfactory. Since the underwater separation method still retains a high percentage of fine particles, the on board sieve installation will still be required. To further increase the concept potential it is recommended to do future research on certain aspects.

Firstly, the influence of the jet location, pipe angle and the location of the junction are relevant to expand data about the efficiency and stability of the system. Coarse particles travel a distance of around 5 meter before being fully settled, thus the junction could be placed near here to improve the amount of fines being separated whilst retaining most coarse particles. The large recirculation reduces the flow through the filter outlet which indirectly affects the separation effectivity. Research on different geometries for the bend on the recirculation and separation efficiency are of interest as the recirculation acts as an obstruction, which increases the power requirement of the system.

Secondly, research on the cause for negative pressure would be of interest. When this is solved it is possible to calculate the required pump power for the inlet and jet. With this information an energy consumption analysis can be executed.

By improving the aforementioned points, the system will have enough separation of fines, thus the focus should shift towards releasing fines in the least environmentally impacting way. The influence on this by the input variables should be analysed and mechanisms that can limit the impact.

Lastly a 3D simulation of the system would of interest as 3D turbulence effects can be included. Additional effects can be monitored such as the recirculation that occurs by the jet, which can be obtained through the data in a 3D LES simulation.

8 Appendix A

As mentioned in section “Approach”, a simple geometry will be created first for the simulation, which is then made more complex throughout multiple steps. When simulating the geometries shown in figure 29, the following concentration profiles can be seen.

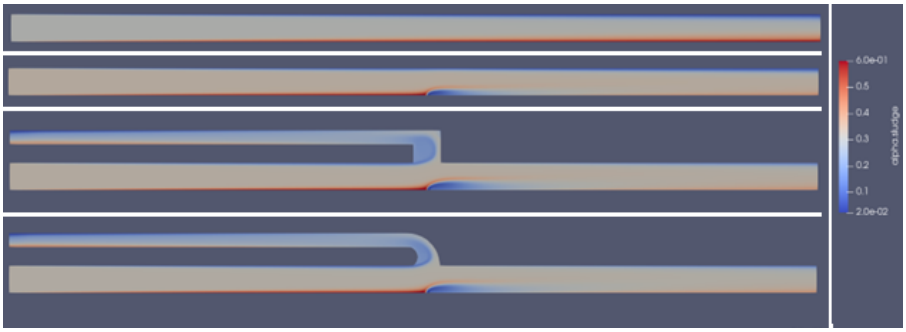

Figure 78: Effect of increasing complexity of geometry changes

In figure 78 the sediment concentration is visualised and the red colour stands of 60% particle concentration and blue stands of 0% particle concentration. These figures visualise a straight pipe, a straight pipe with a jet, a pipe with a jet and squared retour pipe and a pipe with a jet and a bend retour pipe respectively.

The first figure shows that the concentration of particle starts to increase at the bottom. The 2nd figure, which has a jet shows that this will be push the sediment up from the ground. When the second pipe is added the jet is able to push higher before it bends horizontally. And making the junction curved instead of straight reduces the size of the recirculation that occurs at the junction.

9 Appendix B

After running a high set of simulations a problem was noticed. Although the pressure seemed realistic at the first set of simulations, after a certain point certain configurations were giving a negative pressure at the inlet, which is impossible. When checking both the absolute value of the pressure and the pressure difference between the inlet and outlet the resulting answer was still unrealistic. What is interesting about this case is the fact that, other than the pressure, all other output variables have a realistic value. This applies for both the development of the output variables through the system and flow directions such as streamlines. The given values are also of a realistic magnitude.

Improvements such as time step reduction, mesh size refinement and using different numerical schemes did not solve this occurrence. Simulation 38, which has the most negative pressure, has been tested with a finer mesh. The amount of grid cells was doubled, but the pressure remained negative. The inlet pressure remained negative even when lowering the jet velocity or when the jet was completely removed from the system. What is also unnatural is that the inlet pressure decreases as the inlet velocity is increased. But also that the flow was moving from a low pressure to a high one. Since the simulation has no issues with the other output variables, combined with the fact that no cause could be found for the problem in the given time, it has been decided to no longer use the output data of pressure for the decision of the best configuration.

References

1. Barone, D., Loth, E., and Snyder, P. (2015). Efficiency of an inertial particle separator. *Journal of Propulsion and Power*, 31:997–1002.

2. Barone, D., Loth, E., and Snyder, P. (2017). Influence of particle size on inertial particle separator efficiency. *Powder Technology*, 318:177–185.

3. Bojdo, N., Filippone, A., and Uk, N. (2012). A comparative study of helicopter engine air particle separation technologies.

4. Burt, T. and Fletcher, C. (1999). Feasibility of decontainating dredged material.

5. Camuffo, D. (2019). *Microclimate and Atmospheric Variables*, pages 3–14. Elsevier.

6. Cheng, Y., Zhao, N., Zhang, K., and Wei, W. (2021). Research on the plume stability of air bubble curtains under low transverse flow velocity environment in dredging engineering. *Ocean Engineering*, 232.

7. Cuming, H. and Council, A. R. (1955). The secondary flow in curved pipes.

8. Dziubak, T., Bąkała, L., Karczewski, M., and Tomaszewski, M. (2020). Numerical research on vortex tube separator for special vehicle engine inlet air filter. *Separation and Purification Technology*, 237.

9. Filippone, A. (2017). Conceptual and preliminary design of a hybrid dust filter for helicopter engines.

10. Filippone, A. and Bojdo, N. (2010). Turboshaft engine air particle separation.

11. Florez-Orrego, D., Arias, W., Lopez, D., and Velasquez, H. (2012). *Experimental and CFD study of a single phase cone-shaped helical coiled heat exchanger: an empirical correlation.*

12. Gao, H., Guo, L., and Zhang, X. (2002). Liquid-solid separation phenomena of two-phase turbulent flow in curved pipes.

13. Goeree, J. (2018). Drift-flux modeling of hyper-concentrated solid-liquid flows in dredging applications.

14. Gupta, A. and Yan, D. (2016). *Mineral Processing Design and Operations*, pages 421–469. Elsevier.

15. Heibel, D., Mitch, A., and Wolff, M. (1994). Coordinating the feasibility of a dredged material separation system using hydrocyclones for the maintenance dredging operation at canaveral harbor, florida. proceedings of the second international conference on dredging and dredged material placement. In *American Society of Civil Engineers.*, volume 44.

16. Hickel, S. (2022). Lecture title: 05_rans.

17. Holzinger, G. (2020). Openfoam a little user-manual.

18. Hydrocyclone (24-02-2022). in *Wikipedia* https://en.wikipedia.org/wiki/Hydrocyclone.

19. Idrissi, B. E., Éric Loranger, Lanouette, R., Bousquet, J. P., and Martinez, M. (2019). Dewatering parameters in a screw press and their influence on the screw press outputs. *Chemical Engineering Research and Design*, 152:300–308.

20. Inertia (23-05-2022). in *Wikipedia* https://en.wikipedia.org/wiki/Inertia.

21. K., M. (2018). Design of a screw press for dewatering of cattle dung slurry.

22. Kim, N. H., Pham, V. S., Hwang, J. H., Won, N. I., Ha, H. K., Im, J., and Kim, Y. (2018). Effects of seasonal variations on sediment-plume streaks from dredging operations. *Marine Pollution Bulletin*, 129:26–34. doi:10.1016/j.marpolbul.2018.02.014.

23. Lyons, G. A., Cathcart, A., Frost, J. P., Wills, M., Johnston, C., Ramsey, R., and Smyth, B. (2021). Review of two mechanical separation technologies for the sustainable management of agricultural phosphorus in nutrient-vulnerable zones. doi:10.3390/agronomy11050836.

24. Muhammadu, M. M. and Hamzah, E. (2013). Jurnal teknologi effect of flow pattern at pipe bends on corrosion behaviour of low carbon steek and its challenges. 63:2180–3722.

25. Müller, A. and Martins, I. (2022). Recycling of building materials generation-processing-utilization.

26. Nieuwboer, B. J. (2022). Modelling spillage in rotating cutter suction heads a combined finite volume and discrete element model.

27. Pretorius, C. F. (2012). A review of vortex grit basin design. volume 9, pages 5715–5734. Water Environment Federation.

28. Pukkella, A. K., Vysyaraju, R., and Subramanian, S. (2019a). Enhanced gravity particle classifier: Experiments with 3d printed device and computational fluid dynamics simulations. *AIChE Journal*, 65.

29. Pukkella, A. K., Vysyaraju, R., and Subramanian, S. (2019b). Experimental investigation of novel enhanced gravity closed spiral classifier. *Transactions of the Indian Institute of Metals*, 72:2239–2248.

30. Qincy (n.d.). *Trailing Suction Hopper Dredger*. retrieved 10-06-2022 from https://confluence.qps.nl/qinsy/latest/en/trailing-suction-hopper-dredger-tshd-object-definitions-54878709.html.

31. Razavi-Alavi, S. A., Lay, E. N., and Makhmali, Z. S. A. (2018). A cfd study of industrial double-cyclone in hdpe drying process. *Emerging Science Journal*, 2:31–38. doi:10.28991/esj–2018–01125.

32. Rhee, C. V. (2016). Lecture title: The trailing suction hopper dredger [powerpoint].

33. Rhee, C. V. (2018). Dredging processes ii, lecture notes.

34. Shapiro, M. and Galperin, V. (2005). Air classification of solid particles: A review. In *Chemical Engineering and Processing: Process Intensification*, volume 44, pages 279–285.

35. Sparks, T. and Chase, G. (2016). A.

36. Dredge drag head (2018). Wikiwand. Retrieved from *Wikiwand* https://www.wikiwand.com/en/Dredge_drag_head.

37. Vlasblom, W. J. (2007). Introduction to dredging equipment. *Chapter 2 Trailing suction hopper dredger*.

38. Wahl, T. L. (2001). Hydraulic performance of coanda-effect screens.

39. Wahl, T. L. (2003). Design guidance for coanda-effect screens.

40. Xu, H. and Zhang, C. (1999). International journal for numerical methods in fluids study of the effect of the non-orthogonality for non-staggered grids-the results.